Metal Adduction in Mass Spectrometric Analyses of Carbohydrates and Glycoconjugates

Darren T. Gass, Ana V. Quintero, Jacob B. Hatvany, and Elyssia S. Gallagher*

Department of Chemistry and Biochemistry, Baylor University

*Corresponding author:

Elyssia S. Gallagher

elyssia gallagher@baylor.edu

One Bear Place #97348, Waco, Texas 76798

Telephone: (254) 710-2783

ESG ORCID: 0000-0002-5411-7285

Short title:

MS of Metal-Adducted Carbohydrates

Keywords:

carbohydrates, mass spectrometry, metal ions, glycoconjugates, glycan

Contents

I.	Abstract	3
II.	Introduction	4
III.	Ionization of Carbohydrates	7
A.	Electrospray Ionization (ESI)	7
B.	Matrix-Assisted Laser Desorption Ionization (MALDI)	14
IV.	Ion Mobility	17
A.	Principles of Ion Mobility	17
В.	Gas-Phase Structures of Carbohydrate-Metal Adducts	20
C.	IMS Analysis of Carbohydrate-Metal Adducts	21
D.	IMS with High Resolving Power	28
V.	Fragmentation of Carbohydrates	33
A.	Collision Induced Dissociation	34
В.	Electron Fragmentation	46
C.	Photon Fragmentation Methods	58
D.	Gas-Phase IR Spectroscopy	62
E.	Charge Transfer Dissociation	68
F.	Tandem Fragmentation Methods	72
G.	Fragmentation and IRMPD/cryogenic IR Spectroscopy	75
VI.	IMS Coupled with Fragmentation	76
VII.	Hydrogen/deuterium exchange mass spectrometry	82
VIII.	Conclusion	86
IX.	Abbreviation List	88
Χ.	Acknowledgements	94
ΧI	References	94

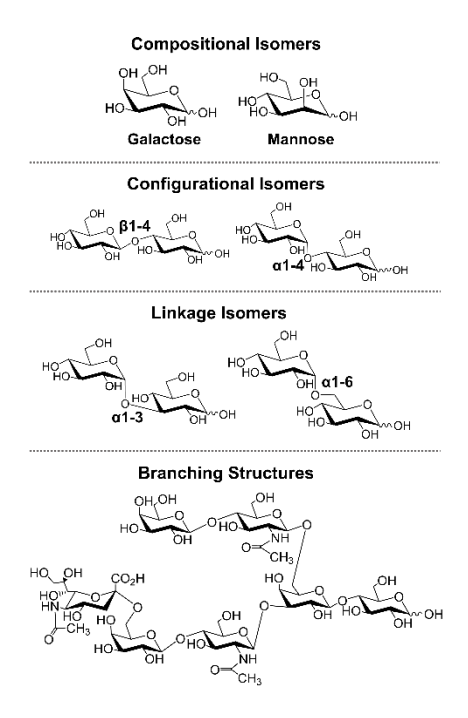
I. Abstract

Glycans, carbohydrates, and glycoconjugates are involved in many crucial biological processes, such as disease development, immune responses, and cell-cell recognition. Glycans and carbohydrates are known for the large number of isomeric features associated with their structures, making analysis challenging compared with other biomolecules. Mass spectrometry has become the primary method of structural characterization for carbohydrates, glycans, and glycoconjugates. Metal adduction is especially important for the mass spectrometric analysis of carbohydrates and glycans. Metal-ion adduction to carbohydrates and glycoconjugates affects ion formation and the three-dimensional, gas-phase structures. Herein, we discuss how metal-ion adduction impacts ionization, ion mobility, ion activation and dissociation, and hydrogen/deuterium exchange for carbohydrates and glycoconjugates. We also compare the use of different metals for these various techniques and highlight the value in using metals as charge carriers for these analyses. Finally, we provide recommendations for selecting a metal for analysis of carbohydrate adducts and describe areas for continued research.

II. Introduction

Glycans, which are polymers of monosaccharides, are involved in cellular signaling (Bucior et al., 2004), immune response (Le Pendu et al., 2014), and disease progression (Dube & Bertozzi, 2005; Varki et al., 2015; Kailemia et al., 2017). Glycans are often attached to proteins or lipids, forming glycoconjugates; though oligosaccharides also exist in biological systems as metabolites and human milk oligosaccharides (HMOs). Glycans and oligosaccharides result from enzymatic reactions; therefore, the structures are heterogeneous with compositional, anomeric configurational, and linkage isomers, contributing to the formation of diverse branched structures (Bertozzi & Rabuka, 2009), as shown in Figure 1. Theoretically, ~10¹² possible mammalian glycan structures have been predicted (Laine, 1994). This diversity of potential structures, combined with isomeric features, makes the structural analysis of glycans challenging. Yet, analytical methods are necessary to correlate glycan structures with their biological functions.

Figure 1. Structural features of carbohydrates.



Biomolecular protein structures have been characterized using nuclear magnetic resonance (NMR), X-ray crystallography, and mass spectrometry (MS) (Wormald et al., 2002; Kleckner & Foster, 2011). NMR and X-ray crystallography have substantial limitations for glycan analysis. NMR requires large quantities of pure samples, making the analysis of heterogeneous glycans challenging (Vliegenthart et al., 1983; Bubb, 2003; Rondeau et al., 2003). Additionally, glycosidic bonds are flexible, which limits the use of crystallization. Therefore, MS has become a prevalent method for glycan analysis (Kailemia et al., 2014; Grabarics et al., 2021). MS methods require significantly reduced sample quantities (micromolar to nanomolar concentrations) compared to NMR and X-ray crystallography (Mechref & Novotny, 2002). Additionally, because MS monitors the mass-to-charge (*m/z*) ratio of analytes, heterogeneous structures with different numbers of monosaccharides can be distinguished by differences in *m/z*, while isomers can be characterized with tandem methods, including ion mobility spectrometry (IMS)-MS and tandem MS (MS/MS) (Grabarics et al., 2021; Peng et al., (accepted for publication)).

Gas-phase ions are detected in MS; thus, ions must be generated in the instrument source. Neutral carbohydrates contain hydroxyls but lack acidic or basic functional groups. Some glycans and glycoconjugates, including glycolipids, proteoglycans, and acidic HMOs, ionize in negative-ion mode through proton loss in acidic functional groups (Zaia, 2005; Chao & McLuckey, 2021; Peterson & Nagy, 2021). Yet, the ionization efficiency for protonated, neutral carbohydrates is low (Harvey, 2000). Metal-ion adduction, in which oxygen atoms in carbohydrate hydroxyls coordinate to metal ions, improves ionization efficiency in positive-ion mode (Harvey, 2000; Harvey, 2001). For metal-carbohydrate adducts, the charge is localized to the metal, which is distinct from protonation or deprotonation, where the charge can migrate throughout the gas-phase

structure (Zhang & Brodbelt, 2004; Struwe et al., 2016; Mucha et al., 2018; Liyanage et al., 2019). Furthermore, the three-dimensional structures formed by coordination are unique to the metal and carbohydrate, which has been valuable for characterizing carbohydrate structures. Na⁺ is ubiquitous and readily observed as an adduct with carbohydrates, even when Na⁺ salts are not added to the sample. Other metal ions have also been used to form carbohydrate adducts for MS analyses. Table 1 lists the physical properties of these metals, including charge, ionic radius, charge density, ionization energies, and electron configuration. In this review, we will examine the utility of metal-ion adduction for MS analyses of carbohydrates and glycoconjugates and compare the effects of different metal ions.

Table 1. Metals used for carbohydrate ionization and their physical properties.

Element	Charge (Q) ^a	Ionic Radius (R) ^b	Charge Density (Q/R ³) ^c	First Ionization Energy (kJ/mol) ^d	Second Ionization Energy (kJ/mol) ^d	Electron Configuration
Н	1.00	-	-	1310	-	-
Li	1.00	0.090	1370	520	7300	[He]
Na	1.00	0.116	640	496	4560	[Ne]
K	1.00	0.152	285	419	3050	[Ar]
Rb	1.00	0.166	219	403	2600	[Kr]
Cs	1.00	0.181	169	376	2230	[Xe]
Mg	2.00	0.086	3140	738	1450	[Ne]
Ca	2.00	0.114	1350	590	1150	[Ar]
Ba	2.00	0.149	605	503	965	[Xe]
Al	3.00	0.0675	9750	578	1820	[Ne]
Cr	3.00	0.0755	6970	653	1590	$[Ar]3d^3$
Mn	2.00	0.097	2190	717	1509	[Ar]3d ⁵
Fe	2.00/3.00	0.092/0.0785	2570/6200	763	1560	$[Ar]3d^{6}/[Ar]3d^{5}$
Co	2.00	0.0885	2890	760	1650	[Ar]3d ⁷
Ni	2.00	0.0830	3500	737	1750	[Ar]3d ⁸
Cu	1.00/2.00	0.0910/0.0870	1330/3040	746	1960	$[Ar]3d^{10}/[Ar]3d^{9}$
Zn	2.00	0.0880	2940	906	1730	[Ar]3d ¹⁰
Cd	2.00	0.109	1540	868	1630	[Kr]3d ¹⁰
Ag	1.00	0.129	476	731	2070	[Kr]3d ¹⁰
La	3.00	0.117	1870	538	1070	[Xe]

^aQ in 1.6x10⁻¹⁹ C. ^b R in nm (Shannon, 1976). ^c Q/R³ in 1.6x10⁻¹⁹ C/nm³. ^d (Haynes et al., 2016)

III. Ionization of Carbohydrates

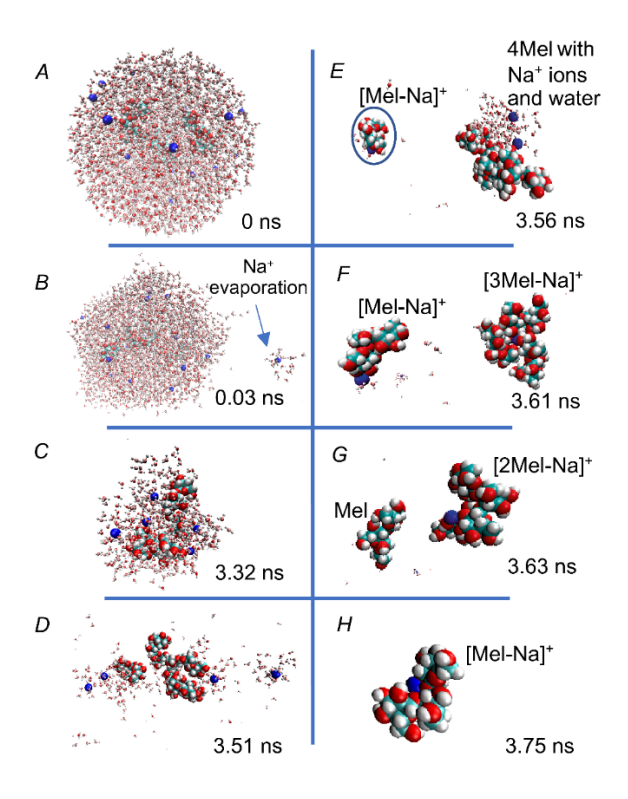
Electrospray ionization (ESI) (Yamashita & Fenn, 1984) and matrix-assisted laser desorption ionization (MALDI) (Karas et al., 1985; Tanaka et al., 1988) are common for MS analyses of carbohydrates. Both methods are soft ionization techniques that can be combined with tandem methods for isomer identification (Zaia, 2004). In ESI, ions form as analytes transition from solution to the gas phase. This enables ESI to be readily coupled with liquid chromatography (LC), allowing for carbohydrate separations in the liquid phase before ionization (Kohler & Leary, 1995; Kawasaki et al., 1999). Alternatively, in MALDI, ions are formed under vacuum from a solid, organic matrix. MALDI has been used to rapidly screen samples, allowing for high throughput analysis of carbohydrates (Drake et al., 2018). In positive-ion mode, both MALDI and ESI result in the formation of metal-adducted and protonated carbohydrate ions.

A. Electrospray Ionization (ESI)

ESI is one of the primary methods for creating gas-phase, metal-adducted carbohydrates (Zaia, 2004; Grabarics et al., 2021). In ESI, a potential is applied to a liquid exiting a capillary, resulting in the formation of a Taylor cone and the release of charged droplets. As solvent evaporates, charge builds up in the droplets. When the charge density overcomes the solvent surface tension, at the Rayleigh limit (Lord Rayleigh, 1882), each droplet fissions into smaller, highly charged droplets. These processes of evaporation and fission repeat until nanodroplets form, with analyte ionization occurring from nanodroplets (Konermann et al., 2013). Many carbohydrates do not contain basic or acidic functional groups; thus, rather than acquiring or losing protons during ESI, neutral carbohydrates coordinate to metal ions.

Molecular dynamics (MD) simulations have predicted that Na⁺-adducted carbohydrates ionize by the charged residue model (CRM) (Calixte et al., 2020). In the CRM, solvent evaporates to dryness, causing residual charges in the drying droplets to adduct to the analyte (Konermann et al., 2013). As shown in Figure 2A-C, hydrogen bonding between carbohydrate hydroxyls and aqueous solvent causes carbohydrates to be retained in the droplet center. If multiple carbohydrates are present in the droplets, clusters of Na⁺ ions and carbohydrates form as the solvent continues to evaporate (Figure 2C). However, these clusters break apart, primarily releasing adducts with a single carbohydrate and a single Na⁺ (Figure 2D-F). These simulations correlate well with experimental results, in which a single carbohydrate and single Na⁺ are the most abundant ion, though structures with one Na⁺ and either two or three carbohydrates were observed at lower signal magnitude.

Figure 2. Timepoint images of an MD simulation showing release of a model trisaccharide, melezitose (Mel) from an aqueous droplet. (A) Initial aqueous droplet (3 nm radius) with 5 trisaccharides, water molecules, and 18 Na⁺. (B) As solvent evaporates, Na⁺ is ejected from the droplet. (C) As solvent evaporates, the trisaccharides remain in the droplet center, clustering with Na⁺ ions. (D-H) At low solvent density, individual Na⁺-trisaccharide adducts are released from the cluster. Na⁺ ions are in blue, hydrogens are white, oxygens are red, and carbons are cyan. [Color figure can be viewed at wileyonlinelibrary.com] Reprinted with permission from Calixte, E. I., *et. al.* Release of Carbohydrate-Metal Adducts from Electrospray Droplets: Insight into Glycan Ionization by Electrospray. *J. Phys. Chem. B*, 2020, 124, 3, 479-486. Copyright 2020 American Chemical Society.



Hydrogen bonding and carbohydrate localization are significant when comparing differences in ionization efficiency for carbohydrates sprayed from ESI versus nano-ESI. In ESI, larger droplets form, which undergo more cycles of evaporation and fission. Since charged droplets are released from the parent droplet surface, significant charge can be lost from the droplet prior to complete desolvation of the carbohydrate (Bahr et al., 1997). The charge loss reduces the potential for charge carriers to be retained in the late stage nanodroplets, minimizing the probability for carbohydrates to form ion adducts. In nano-ESI, smaller initial droplets form, which require fewer cycles of droplet evaporation and fission (Karas et al., 2000). Thus, the nanodroplets retain charges that can be adducted to the carbohydrate analytes as the droplets evaporate to dryness.

When performing MD simulations on Na⁺-adducted carbohydrates, ionized from binary solvent mixtures containing 25% or more water, the solvents were observed to demix during the simulation with the more volatile solvent (acetonitrile or methanol) moving to the droplet surface, while the carbohydrate remained solvated by water in the droplet center (Calixte et al., 2021). Ionization from these mixed solvent systems, showed that the CRM was still the dominant ionization mechanism. However, differences in the evaporative time (~40 ns) were observed as the percentage of the organic additive (acetonitrile or methanol) was increased from 0 to 99%. This difference in evaporative time was hypothesized to be the reason for increased ionization efficiency of carbohydrates. Evaporation of the more volatile solvent results in smaller aqueous droplets, from which charge would be adducted to the retained carbohydrates before release into the gas phase.

Permethylation increases ionization efficiency of carbohydrates (Dell, 1990). MD simulations have indicated that the ionization mechanism for a permethylated trisaccharide is the ion evaporation method (IEM) (Calixte et al., 2020). In IEM, charged analytes are pushed out of the nanodroplet in small solvent clusters due to coulombic repulsion. The replacement of hydroxyl protons with methyls to form ethers causes carbohydrates to become more hydrophobic and migrate to the droplet surface, where ejection becomes energetically favorable in the presence of a metal ion. The gas-phase structures of permethylated carbohydrates are distinct from unmodified structures due to alterations in the inter- and intra-molecular hydrogen bonding networks in ESI droplets (Warnke et al., 2019; Calixte et al., 2020). In addition to increasing the ionization efficiency, permethylation locks the carbohydrate into a single anomeric configuration, preventing mutarotation at the reducing end when solvated during ESI (Warnke et al., 2019). Permethylation

also stabilizes sialic acid residues, which are labile and can be lost during some MS analyses (Nishikaze, 2019).

Metal adduction is more effective for carbohydrate ionization than protonation, but the choice of metal ion affects ionization efficiency. Ca^{2+} -carbohydrate adducts have yielded higher signal intensities than adducts with other metals (Harvey, 2001; Schaller-Duke et al., 2018). This is hypothesized to be due to the ionic radius of Ca^{2+} being ~0.10 nm (Table 1), which allows for the formation of a highly stabile complex as the carbohydrate coordinates to the ion immediately before release into the gas-phase (Angyal, 1989). Other group II metals, such as Mg^{2+} , yield higher signals for carbohydrate adducts than group I or transition metals (Harvey, 2001; Schaller-Duke et al., 2018); while divalent transition metals, such as Co^{2+} , Zn^{2+} , and Ni^{2+} , generate higher signals than trivalent ions of Fe^{3+} or Al^{3+} (Schaller-Duke et al., 2018). Thus, the signal intensity of carbohydrate-metal adducts decreases according to group II > divalent transition metals \geq group I > trivalent transition metals. Finally, the weak ion signals for protonated carbohydrates, compared to carbohydrate adducts of group I or group II metals, have limited the use of protonated carbohydrates for MS analysis (Harvey, 2005a).

The charge states of metal-adducted carbohydrates are dependent on the metal ion as well as the carbohydrate size. For example, it is challenging to form ions with charges greater than 2+ for pentasaccharides or smaller carbohydrates, though these charge states (≥ 2+) are required for several electron-based fragmentation techniques (Zubarev et al., 1998; Syka et al., 2004; Huang & Dodds, 2015a; Wong et al., 2022). For penta- and tetra-saccharides, a single monovalent or divalent metal ion can coordinate to the carbohydrate, generating either 1+ or 2+ carbohydrate ions, respectively. For carbohydrates with seven or more monosaccharide subunits, 2+ ions can form from either two monovalent metals or a single divalent metal. Charge states of 3+ or higher

are rarely achieved with metal adducts (Adamson & Håkansson, 2007; Zhao et al., 2008; Schaller-Duke et al., 2018). However, 3+ ions of maltoheptaose have been detected with two divalent metals and a complexed anion (Schaller-Duke et al., 2018). Finally, it is challenging to form multiply protonated carbohydrates due to the preference for coordinating metals (Harvey, 2001; Adamson & Håkansson, 2007).

Various carbohydrate-metal adducts have been detected in the gas-phase, including adducts containing one metal and one carbohydrate (Asam & Glish, 1997; Sible et al., 1997), two metals and two carbohydrates (Williams et al., 2010; Morrison et al., 2017a), one metal and two carbohydrates (Schaller-Duke et al., 2018), and one carbohydrate with a divalent metal and an anion (Sible et al., 1997; Xie et al., 2020; Xie et al., 2021). The number of monosaccharide subunits in the carbohydrate and the metal adduct influence the detected gas-phase ions. When examining a trisaccharide model system, increasing the molar ratio of sugar to metal in the sprayed solution increased the probability of detecting two sugars adducted to a single Na⁺ (Calixte et al., 2020). However, the primary detected species was still the adduct with one sugar and one Na⁺. For maltoheptaose, a heptasaccharide, the ion with the highest magnitude contained two Na⁺ adducted to a single sugar. However, maltotetraose and melezitose, a tetra- and tri-saccharide, respectively, formed adducts with a single sugar and a single Na⁺ at the highest magnitude. The difference in the number of adducted Na⁺ is hypothesized to be due to coulombic repulsion of the metal ions, preventing attachment of multiple metals to small carbohydrates. Additionally, MD simulations show that a single Na⁺ can coordinate with multiple monosaccharide subunits within a trisaccharide model system (Calixte et al., 2020). For divalent metals (Zn²⁺, Mg²⁺, Ca²⁺, and Co²⁺), maltoheptaose and maltotetraose formed adducts with one metal and one sugar at the highest signal intensity (Adamson & Håkansson, 2007; Schaller-Duke et al., 2018). Again, this could be related

to coulombic repulsion since the higher charge state could make the binding of a second metal, even on the larger sugar, less favorable. This difference between divalent and monovalent metal ions indicates that the metal properties, such as charge, are important to the number of ions that can coordinate to the carbohydrate when forming gas-phase structures (Adamson & Håkansson, 2007; Schaller-Duke et al., 2018).

Experimentally, there are several ways to generate metal-adducted carbohydrates. Metals can be added to the samples and sprayed with the carbohydrate (Asam & Glish, 1997; Harvey, 2000). It is common to add only a single metal to a sample because multiple metals cause competition during ionization, which disperses detected ion signal across several m/z. In addition, with certain metals, such as Li⁺ or K⁺, naturally occurring isotopic distributions can disperse ion signal over multiple m/z (Haynes et al., 2016). Alternatively, trace metals can form detectable adducts with carbohydrates (Bansal et al., 2020; Abikhodr et al., 2021). Thus, Na⁺ contamination can result in signal or competition when other metal ions are added to the sample. To form protonated carbohydrate ions, the addition of formic or acetic acid is required because without acid, metal contaminants outcompete protons (Harvey, 2000; Uppal et al., 2017; Mookherjee et al., 2018; Mookherjee et al., 2020). Metals such as Na+, K+, Li+, or Ag+ have also been sprayed through secondary ESI sprayers, with adduction occurring during droplet mixing in ESI (Swanson et al., 2017; DeBastiani et al., 2021). Metals can also be attached by ion/ion reactions in the gasphase (Chao & McLuckey, 2021; Chao & McLuckey, 2021). For these reactions, Na⁺ or Mg²⁺ are ionized in positive-ion mode while attached to ligands. Carbohydrates or glycoconjugates are ionized in negative-ion mode by deprotonating a hydroxyl or acidic functional group. Then, ion/ion reactions occur as the metal is transferred from a nitrogen-containing ligand to the hydroxyl oxygens in the carbohydrate. Gas-phase metal binding causes the loss of the ligand and shifts the charge state based on the charge of the metal.

Glycoconjugates can also form metal-adducted ions during ESI. Acidic glycoconjugates, such as glycosaminoglycans (GAGs), readily form deprotonated ions. Sulfate functional groups are highly acidic; thus, the charge state increases in relation to the number of sulfate functional groups in a GAG. Metal ions, including Na^+ , Ca^{2+} , Mn^{2+} , and K^+ , have been attached to GAG ions to improve the stability and prevent the loss of sulfate groups from ionization, though these adducts are often detected in negative-ion mode (Zaia & Costello, 2003; Leach et al., 2011; Liu & Håkansson, 2011; Leach et al., 2017). Metal adduction can form additional charge states, increasing the number of detected peaks and splitting the ion signal over multiple m/z (Wolff et al., 2008). Unlike work with neutral carbohydrates, metal-adducted GAGs lose a proton when adducting a metal. The Amster group has shown that for the addition of every Na^+ , a proton is lost from the detected ion, causing GAG anions with a charge state of -5 to be detected with either one Na^+ combined with the loss of six protons or three Na^+ with the loss of eight protons (Leach et al., 2017).

B. Matrix-Assisted Laser Desorption Ionization (MALDI)

MALDI is another method for ionizing carbohydrates. To utilize MALDI, the carbohydrate is first mixed with a matrix, such as 2,5-dihydroxybenzoic acid (DHB). Then, the mixture is spotted on a plate to dry, which allows for evaporation of the remaining solvent while under vacuum. The selected matrix can significantly affect the carbohydrate ionization efficiency and must be compatible with the carbohydrate and solvent to crystallize (Mohr et al., 1995). Then, under vacuum, a UV laser (commonly between 190 and 360 nm) or IR laser (2 to 11 μm) is used to ablate the carbohydrate-matrix mixture (Berkenkamp et al., 1997; Zenobi & Knochenmuss,

1998; Harvey, 1999). Ions are formed from the desorbed samples by attachment of H⁺ or group I metals to carbohydrates. Metal salts (micromolar to millimolar concentrations) can be added to the matrix solutions before crystallization (Börnsen et al., 1995; Cancilla et al., 1996; Lee et al., 2016). However, Na⁺ and K⁺ contaminants can also result in detectable ion signals (Börnsen et al., 1995; Morelle et al., 2004). The reader is referred to several other publications for MALDI details that are beyond the scope of this review (Zenobi & Knochenmuss, 1998; Harvey, 1999; Lai & Wang, 2017; Harvey, 2021).

Multiple distinct ionization mechanisms have been proposed for MALDI. The predominant mechanism is hypothesized to be the thermal proton/cation transfer model (Chu et al., 2014). This two-step mechanism hypothesizes that the laser melts the matrix through increased surface temperature, which causes both the metal salt and the carbohydrate to dissolve in the matrix. During desorption, the metal adducts to the carbohydrate before entering the mass analyzer of the MS. This theory suggests that close contact between the salt and matrix molecules improves the formation of metal-adducted carbohydrates (Lee et al., 2016). Alternatively, the chemical physics and chemical dynamics (CPCD) model is another potential ionization mechanism for MALDI (Knochenmuss, 2002; Knochenmuss, 2003). CPCD involves three steps, ablation, primary ionization, and secondary ionization. In primary ionization, photons cause the formation of bound electron-hole pairs in which the electrons pool, forming ion pairs with opposite charges from matrix molecules due to proton or electron transfer. During secondary ionization, ion/molecule and ion/ion reactions occur between the matrix and analyte. It is during this secondary ionization that a carbohydrate abstracts a metal from a salt or matrix ion to form a metal-adducted ion (Knochenmuss, 2016).

MALDI analysis of carbohydrates has focused on using group I metals to form singly charged adducts. Carbohydrate adducts with group II metals do not readily form by MALDI (Mohr et al., 1995). For maltoheptaose-metal adducts, the ion signal intensities for group 1 metals during MALDI are $Cs^+ > K^+ > Na^+ > Li^+$ (Börnsen et al., 1995; Mohr et al., 1995). However, for monosaccharide-metal adducts, the ion signal intensities are $Li^+ > Na^+ > K^+$ (Botek et al., 2001). This suggests differences in metal binding preference during MALDI based on the size of the carbohydrate and metal ion. Unlike ESI, in MALDI, a single metal adducts to a single, neutral carbohydrate regardless of the carbohydrates size (Nicolardi et al., 2021). The detection of a single species, one metal with one carbohydrate, simplifies spectral identification compared to the multiple adducts that can form during ESI (Stahl et al., 1991; Cancilla et al., 1996; Harvey, 1999). However, there have been cases with sialylated N-linked glycans and gangliosides in which two or three Na⁺ or K⁺ adduct to the glycan, while one or two protons are lost, forming singly charged ions, e.g. [M - H + 2Na/K]⁺ or [M - 2H + 3Na/K]⁺ (Harvey et al., 1999a). Forming protonated carbohydrates using MALDI is challenging due to the higher affinity for oxygens coordinating metals in the gas-phase instead of protons (Chen et al., 2016).

The ionization efficiency of metal-adducted carbohydrates is dependent on both the metal and the matrix in MALDI. The ionization efficiency for pentasaccharides and smaller carbohydrates adducted to Na⁺ have lower signals than larger carbohydrates when using DHB as the matrix. It is hypothesized that the differences in ionization efficiency are due to how the matrix affects metal adduction. 1,4-dihydroxynaphthalene-2-carboxylic acid (DHN) combined with Na⁺ adduction enhances ionization of carbohydrates with masses below 1000 Da (Naven & Harvey, 1996). However, the impact of matrix interactions on the ionization efficiency of metal adducts is not well understood at a mechanistic level. Permethylation and other derivatization methods can

be combined with MALDI to improve the signal intensity and provide additional stability of metal-carbohydrate/glycoconjugate adducts (Powell & Harvey, 1996; Okamoto et al., 1997; Morelle et al., 2004; Kang et al., 2005; Wuhrer et al., 2006).

IV. Ion Mobility

A. Principles of Ion Mobility

Ion mobility spectrometry (IMS) coupled to MS has become a valuable technique for analyzing glycans (Chen et al., 2018). Isomeric carbohydrates cannot be distinguished by MS alone since they have the same m/z; thus, IMS is a tool for distinguishing isomers based on their three-dimensional, gas-phase conformations. IMS is a gas-phase method that monitors the mobility of ions as they traverse through an inert buffer gas (e.g., N_2 or He) under an applied electric field. Differences in ion velocities cause ions to separate based on size, shape, and charge.

In drift tube-ion mobility spectrometry (DTIMS), a voltage (V) is applied to drive ions through a drift tube of length L, resulting in a uniform electric field (E) (Equation 1).

$$E = \frac{V}{L} \tag{1}$$

Ions migrate through the drift tube due to their charge and the applied field. However, the drift tube is filled with neutral gas molecules, resulting in collisions between the ions and buffer gas. These collisions result in drag forces that increase the time (t_a) for the ions to pass through the drift tube, affecting the ions' velocity (v_a) (Equation 2).

$$v_a = \frac{L}{t_a} \tag{2}$$

The ions' mobility (K) describes the movement of ions in the drift tube, based on the ions' v_a and the influence of E (Equation 3).

$$K = \frac{v_a}{E} \tag{3}$$

The buffer-gas number density (N) influences K because more buffer gas molecules increase the frictional drag force that ions experience as they move through the drift tube.

The time for an ion to pass through a drift tube, or the arrival time (t_a), is used to calculate K. Momentum transfer collisional cross sections (CCS, Ω) relate an ion's mobility to its three-dimensional size and shape. CCS values can be calculated from K values determined in DTIMS experiments using the low-field Mason-Schamp equation (Revercomb & Mason, 1975; Clowers et al., 2005; Marchand et al., 2017):

$$\Omega = \frac{3}{16} \frac{2\pi}{\mu k_B T}^{1/2} \frac{ze}{KN} \tag{4}$$

where z is the charge of the ion, e is the charge of an electron, k_b is the Boltzmann constant, T is the temperature of the buffer gas, μ is the reduced mass of the ion and buffer gas, and N is the buffer-gas number density.

In traveling wave-ion mobility spectrometry (TWIMS), a direct current (DC) voltage is applied to electrodes in a stacked ring ion guide, and a traveling wave is created by changing the magnitude of this applied voltage in set intervals (Shvartsburg & Smith, 2008; Dodds & Baker, 2019). The motion of the resulting traveling wave can be controlled by changing the wave velocity and height. The traveling wave pushes ions through a buffer gas-filled tube, resulting in ions with higher mobility "surfing" along the voltage wave, while ions with lower mobility "roll over the wave", causing separation (Shvartsburg & Smith, 2008; Richardson et al., 2018). Ions are separated based on mobility differences, where smaller, higher mobility ions travel faster and migrate out of the TWIMS cell earlier than larger, lower mobility ions. In addition, radio frequency (RF) voltages are used to confine and focus the ions traversing the TWIMS cell, enhancing ion

transmission. Compared to DTIMS, TWIMS platforms allow for ions to travel longer path lengths with lower voltages, though experimental parameters, such as wave height, wave velocity, and gas pressure, must be optimized to enhance ion separation (Dodds & Baker, 2019). K and CCS values cannot be directly calculated from arrival times (t_a) in TWIMS due to the changing electric field. Thus, in TWIMS, CCS is calculated after calibrating with standards of known CCS values (^{DT}CCS) (Gelb et al., 2014). To improve the accuracy of CCS measurements, it is important to utilize metal-adducted carbohydrate standards with similar charge states.

It has been suggested that both K and CCS values be reported for DTIMS experiments, and that TWIMS calibrations utilize K instead of CCS (Gabelica et al., 2019). These recommendations are suggested to minimize the uncertainty associated with DTIMS and TWIMS measurements, including the effects of nonuniform fields, E, and variations in the gas pressure and temperature (Gabelica et al., 2019). Nevertheless, new calibration methods to derive accurate CCS calculations and measured uncertainty with TWIMS devices have been reported (Edwards et al., 2021; Richardson et al., 2021).

In trapped ion mobility spectrometry (TIMS), stacked ring electrodes make up the TIMS analyzer, which includes the entrance funnel, TIMS tunnel, and exit funnel (Michelmann et al., 2015; Ridgeway et al., 2018). Each electrode is divided into quadrants and RF and DC voltages are applied to create an electric field that is directed opposite to the buffer gas moving across the length of the TIMS analyzer, holding ions stationary. The RF voltage applied to each quadrant of the ring electrodes is responsible for confining and focusing the ions into each section of the TIMS analyzer. The DC voltage applied to the electrodes results in ions being transported across the TIMS analyzer. In conjunction with the buffer gas, the electric field across the TIMS analyzer results in ions being accumulated and trapped. Decreasing the applied electric field results in ions

migrating out of the TIMS analyzer based on their K. Ions with a lower mobility migrate first while ions with higher mobility are retained in the tunnel, and subsequently separated. Similar to TWIMS, K values cannot be directly measured; therefore, CCS calculations require calibration with standards of known ^{DT}CCS .

B. Gas-Phase Structures of Carbohydrate-Metal Adducts

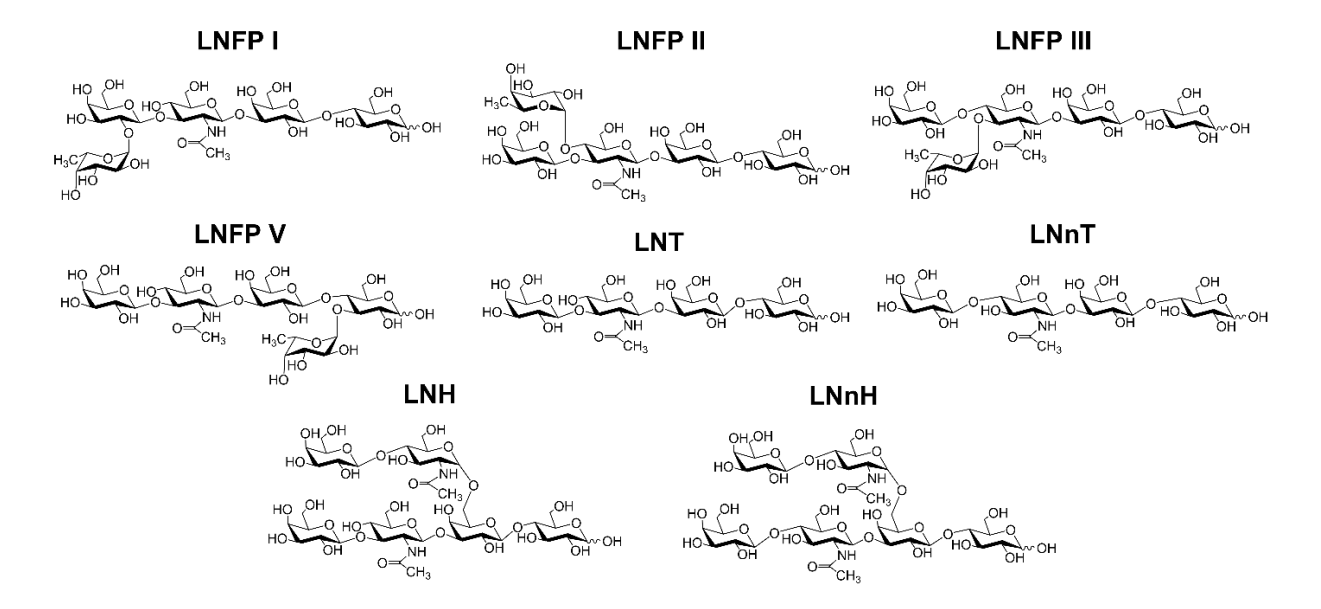
The three-dimensional structures of metal-adducted carbohydrates in the gas phase are dependent on the ionic radius of the metal, the coordination bond sites between the metal and carbohydrate oxygen atoms, and the intramolecular hydrogen bonds within the carbohydrate (Woods, 2018). The effects of structural features, such as glycosidic linkages, anomericity, and hydrogen-bond geometry, affect how carbohydrates coordinate metal ions (Gyurcsik & Nagy, 2000; Mucha et al., 2019; Calixte et al., 2020). Simulations of ESI predict that metal-adducted carbohydrates ionize via the charged residue model (Figure 2) (Calixte et al., 2020). For a trisaccharide model system, Na⁺ coordinates to the carbohydrate as the solvent in the droplet evaporates to dryness. Upon entering the gas phase, metal coordination and formation of intramolecular hydrogen bonds reduce the conformational freedom of the carbohydrate, limiting the number of gas-phase conformations compared to those observed in solution. Density functional theory (DFT) and other quantum chemical calculations have been used to examine Na⁺ binding to oxygen atoms in monosaccharide rings (e.g., xylose, arabinose, glucose, and galactose) (Heaton & Armentrout, 2008; Zheng et al., 2017). These calculations predicted that distinct oxygen atoms in each monosaccharide bind to Na⁺, changing the size of the sodiatedmonosaccharide structures. Similarly, Mg²⁺, Ca²⁺, Zn²⁺, and Cd²⁺ coordinate to different oxygen atoms in methyl \(\beta\)-xylopyranoside, resulting in different conformations (Fabian, 2007).

Different group I metals have been used to generate different three-dimensional gas-phase structures due to differences in binding interactions between the metals and oxygen atoms of carbohydrates. Though these studies focused on monosaccharides coordinating metals, similar gas-phase structural variations are expected for larger oligosaccharides based on both the carbohydrate structure and metal ion (Bythell et al., 2017; Rabus et al., 2017). These structural differences enable separation of isomeric carbohydrates during IMS due to differences in arrival times, CCS values, and mobility features in arrival time distributions (ATDs).

C. IMS Analysis of Carbohydrate-Metal Adducts

The gas-phase structures of carbohydrate-metal ion adducts are dependent on carbohydrate structure. Maltose, trehalose, melibiose, and sucrose are disaccharide isomers with α-linkages. Maltose and trehalose both contain two glucose units, melibiose is composed of a galactose and glucose, and sucrose is composed of a glucose and fructose. When adducted to the same metal, the arrival time for sucrose is less than that of trehalose (Huang & Dodds, 2013). Similarly for two pentasaccharide linkage isomers, when adducted to the same metal, the arrival time for lacto-*N*-fucopentaose (LNFP) V is less than that of LNFP I. The structural differences between LNFP V and LNFP I are shown in Figure 3.

Figure 3. Human milk oligosaccharide (HMO) structures, including Lacto-*N*-fucopentaose (LNFP I), Lacto-*N*-fucopentaose (LNFP II), Lacto-*N*-fucopentaose (LNFP III), Lacto-*N*-fucopentaose (LNFP V), Lacto-*N*-tetraose (LNT), Lacto-*N*-neotetraose (LNnT), Lacto-*N*-hexaose (LNH), and Lacto-*N*-neohexaose (LNnH).

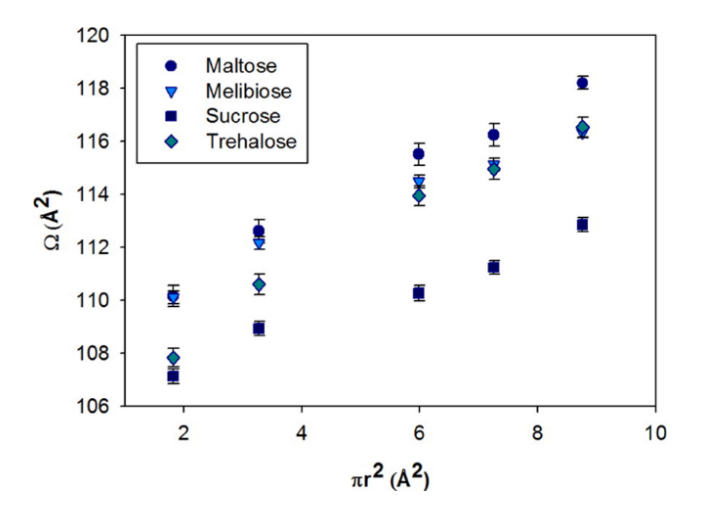


The ionic radius of the metal ion also has an effect on the gas-phase structure of carbohydrate-metal adducts. K*-adducted sucrose and trehalose had different arrival times, while Li*-adducted sucrose and trehalose had similar arrival times. (Huang & Dodds, 2013). Figure 4 shows that CCS values of disaccharide-metal adducts increase with increasing ionic radius (see Table 1) for group I metals (Huang & Dodds, 2013). Two pentasaccharide linkage isomers, LNFP I and II (Figure 3), were studied as Li*, Na*, K*, Rb*, and Cs* adducts (Fenn & McLean, 2011). Although an increase in CCS was observed between Li*-, Na*-, and K*-adducted LNFP I and II, an increase in CCS was not observed between the largest group I metals studied, Rb* and Cs*. Unlike the above trend for group I metal-adducted disaccharides, CCS values of group I metal-adducted pentasaccharides did not increase with increasing ionic radius. Linkage isomers, lacto-N-tetraose (LNT) and lacto-N-neotetraose (LNnT) (Figure 3) were analyzed by DTIMS as [M + Na]*, [M + K]*, and [M – H + Zn]*, where M is the HMO (Zheng et al., 2017). LNT and LNnT exhibited similar arrival times when adducted to Na*, though the arrival times for the two structures differed when adducted to K*. However, when LNT and LNnT were adducted to divalent Zn²* and

deprotonated, the arrival times for the two isomers differed more, yielding improved separation.

These results illustrate that though the metal ion affects the gas-phase structure of the carbohydrate adduct, the relationship between arrival time and metal ion radius is not linear or predictable.

Figure 4. Average CCS (Ω) for Li⁺-, Na⁺-, K⁺-, Rb⁺-, and Cs⁺-adducted disaccharides versus the cross-sectional area of the metal ion. Reprinted with permission from Huang, Y.; Dodds, E. D. Ion Mobility Studies of Carbohydrates as Group I Adducts: Isomer Specific Collisional Cross Section Dependence on Metal Ion Radius. *Anal. Chem.* 2013, 85, 20, 9728-9735. Copyright 2013 American Chemical Society.



In IMS, the gas-phase structures of carbohydrate-metal ion adducts are dependent on the combination of the metal ion, carbohydrate structure, and coordinate interactions. Figure 4 shows how the CCS is affected by the combination of the carbohydrate structure and the metal ion. For example, the CCS of melibiose and trehalose are distinct when adducted to Li⁺ or Na⁺ but similar when adducted to larger group I metal ions (Huang & Dodds, 2013). Additionally, apparent differences in CCS were observed between LNFP I and II when adducted to Li⁺, Na⁺, and Cs⁺, however the CCS for LNFP I and II were similar when adducted to either K⁺ or Rb⁺ (Fenn & McLean, 2011). These results demonstrate that CCS differences between LNFP I and II are a result

of both the size of the metal being bound to the isomer, as well as the coordinate interactions (Fenn & McLean, 2011). Thus, it is hypothesized that the carbohydrate size and its associated flexibility affect the carbohydrate coordination sites to the metal, resulting in different three-dimensional gasphase structures.

For some carbohydrate-metal adducts, multiple gas-phase structures can form, which are detected in IMS (Xie et al., 2020). Na⁺-adducted stachyose, a tetrasaccharide, yielded an ATD that indicates one dominant population of gas-phase structures was detected in IMS. However, K⁺- and Rb⁺-adducted stachyose resulted in broader ATDs with shoulders, indicating the presence of multiple gas-phase conformations. In comparison, isomaltotetraose, a compositional isomer of stachyose, generated ATDs with a single population of gas-phase structures when adducted to Na⁺, K⁺, and Rb⁺. Furthermore, compared to group I metal-adducted stachyose, isomaltotetraose adducted to the same metal had an earlier arrival time, indicating more compact metal-adducted, gas-phase structures (Xie et al., 2020).

Arrival times and CCS values are affected by the charge state of the carbohydrate-metal adduct. Carbohydrates, ranging from tri- to hexa-saccharides, and dimers of tetra- and penta-saccharides, were adducted to Na⁺ or Ca²⁺ and analyzed by DTIMS (Xie et al., 2020). Ca²⁺-adducted carbohydrates had faster arrival times and larger mobilities (*K*) than Na⁺-adducted carbohydrates. Arrival times of 270 carbohydrate-metal ion complexes were used to calculate CCS values (Equation 4) and determine IMS trends from the observed results (Xie et al., 2020). Group II metal-adducted carbohydrates, [M + group II]²⁺ and [2M + group II]²⁺, where M is the carbohydrate, had greater CCS values compared to group I metal-adducted carbohydrates [M + group I]⁺. This aligns with Equation 4, which shows that CCS is proportional to ion charge (*z*). Additionally, a wider range of CCS values resulted for [2M + group II]²⁺ complexes compared to

a smaller range of CCS values for [M + group II]²⁺ complexes. As previously described, the size of both the carbohydrate and the metal ion influences the gas-phase conformation of carbohydrate-metal adducts and affects the resulting arrival times and CCS values. In addition, we hypothesize that compared to a single carbohydrate coordinating a metal ion, when two carbohydrates coordinate a metal there are more potential gas-phase structures since the carbohydrates can take many different orientations while solvated during ESI, including different α and β anomeric forms at the reducing end, resulting in the formation of more gas-phase conformations and wider CCS distributions for [2M + group II]²⁺ complexes compared to [M + group III²⁺ complexes. Additionally, ESI conditions affect the formation of gas-phase carbohydrate-metal adducts (Calixte et al., 2021). Solvents affect intramolecular hydrogen bonding within carbohydrates during ESI, which can lead to differences in the structures of gasphase ions that cannot interconvert following solvent evaporation. All of these factors may affect the structures and associated CCS for the metal-adducted carbohydrate complexes. In comparison to the $[M + Na]^+$, $[M + K]^+$, and $[M - H + Zn]^+$ complexes of LNT and LNnT described above, further analysis on LNT and LNnT adducted to doubly sodiated cations, [M + 2Na]²⁺, resulted in the baseline separation of the isomers (Zheng et al., 2017). The order of their separation also differed when adducted to 2 Na⁺, with LNT migrating first, whereas with [M + K]⁺ and [M – H + Zn]⁺, LNnT migrated first (Zheng et al., 2017). These results illustrate that the charge state of the metal-adducted carbohydrate can affect the gas-phase structure of the carbohydrate-metal complex, allowing the carbohydrates to be separated based on arrival times and/or CCS values.

Transition metal complexes have also been used to analyze carbohydrates by IMS-MS (Gaye et al., 2016). Utilizing various combinations of carbohydrates (M) and metal ions with either

an amino acid (L-serine (L-Ser), L-asparagine (L-Asn)) or peptide (L-phenylalanine-glycine (L-Phe-Gly)), a dataset of CCS values was established to distinguish 16 isomeric monosaccharides. Based on a three-dimensional CCS plot for isomer adducts of $[M + L-Ser + H]^+$ (x-axis), $[M + L-Ser + H]^+$ Phe-Gly + H]⁺ (y-axis), and $[M + (L-Phe-Gly H) + Mn^{2+}]^+$ (z-axis), D-talose was not distinguished from D-idose and D-altrose. Further characterizations were conducted on D-talose, D-altrose, and D- and L-idose as adducts with either Mn²⁺ or Co²⁺ and either deprotonated Ser or Asn (Gaye et al., 2016). With $[M + (L-Ser - H) + Mn^{2+}]^+$, the CCS of the complexes of all monosaccharides were not distinguished. However, the D-talose complex could be distinguished from the other monosaccharides as [M + (L-Ser - H) + Co²⁺]⁺, indicating differences in the gas-phase conformations as a result of the different divalent cation. For $[M + (L-Asn - H) + Mn^{2+}]^+$ complexes, D-altrose was distinguished from D-idose and D-talose. Additionally, the [M + (L-Asn -H) + Co^{2+}] + complex enabled D-idose to be distinguished from D-talose and D-altrose. Although D- and L-idose were not distinguished from each other, it was apparent that unique CCS values resulted from forming complexes using Co²⁺ or Mn²⁺ with different amino acids, which enabled some monosaccharide isomers to be distinguished.

Ga-phase conformers of monosaccharide isomers adducted to transition metals were also investigated by DTIMS as [M+(L-Phe-Gly – H) + Mn²⁺]⁺ complexes, composed of a carbohydrate (M), deprotonated L-Phe-Gly peptide, and Mn²⁺ (Gaye et al., 2016). D-idose, L-idose, D-altrose, L-altrose, D-glucose, L-glucose, D-gulose, L-gulose, D-talose, L-talose, L-allose, and L-galactose were analyzed individually and one CCS mobility feature was observed for each isomer. Of all the D-enantiomers examined, two mobility features were observed for D-mannose, D-allose, and D-galactose, whereas among the examined L-enantiomers, only L-mannose had two features. Although D-mannose and L-mannose exhibited two mobility features and had similar CCS values,

the peak intensities of the two conformers differed, allowing the monosaccharides to be distinguished. In the carbohydrate complexes with deprotonated L-Phe-Gly, it was hypothesized that Mn²⁺ is at the center of the complex, forming three coordinate bonds with hydroxyl groups in the monosaccharide and three coordinate bonds within the deprotonated peptide (Gaye et al., 2016). Based on the conformational space of the trimeric complexes and the observed differences among the ATDs for the D- and L-monosaccharides, multiple gas-phase conformations were formed, allowing each monosaccharide to be distinguished from the others.

Carbohydrate adducts with both a metal cation (Ca²⁺ and Ba²⁺) and a halogen anion (Cl⁻, Br, and I) have also been used to distinguish isomeric pairs of oligosaccharides by TIMS (Xie et al., 2021). Adducts of [M + metal + halogen] with M as the oligosaccharide, have been used to analyze linkage isomers, stereoisomers, and structures with different monosaccharides. [M + Ca + Cl] complexes enabled separation of isomer pairs of malto- and isomalto-triose, -tetraose, pentaose, and -hexaose using low and high resolving power parameters, which varied the mobility and ramp settings for TIMS. With low resolving power settings, broad peaks were observed for [M + Ca + Cl] complexes of isomer pairs of malto- and isomalto-triose, -tetraose, -pentaose, and -hexaose, compared to the high resolving power settings. In addition, when using low resolving power settings, only minor separation was observed for [M + Ca + Cl]⁺ complexes of maltotriose and isomaltotriose. Using high resolving power settings, multiple peaks, representing multiple conformers, were observed for all maltose complexes of [M + Ca + Cl]⁺. Additionally, all conformers for malto-triose, -tetraose, -pentaose, and -hexaose complexes of [M + Ca + Cl]⁺, excluding the minor peaks of maltotriose, were baseline resolved from isomalto-triose, -tetraose, -pentaose, and -hexaose complexes. Because maltotetraose and stachyose could not be resolved as [M + Ca + Cl]⁺ complexes under high resolving power settings, the mobility distributions of maltotetraose and stachyose pairs were also studied as [M + Ca + X]⁺ and [M + Ba + X]⁺ complexes, where X represents a halogen anion (Cl⁻, Br⁻, or I⁻) (Xie et al., 2021). It was observed that the mobility differences between maltotetraose and stachyose complexes, [M + Ca + X]⁺, increased as the anion size increased from Cl to Br to I. In contrast, for maltotetraose and stachyose complexes of $[M + Ba + X]^+$, the mobility differences decreased with increasing anion size (Cl⁻ < Br⁻ < I⁻). Differences in the mobility distributions for maltotetraose and stachyose complexes, $[M + Ca + X]^+$ and $[M + Ba + X]^+$, differed based on the metal and halogen. Of all the complexes studied, $[M + Ca + I]^+$ and $[M + Ca + Br]^+$ were most effective in resolving various isomeric pairs of carbohydrates. From the twenty-one isomeric pairs consisting of tri-, tetra-, penta- and hexa-saccharides that differed in the monosaccharide unit composition, stereochemistry, and regiochemistry, twenty were able to be distinguished as $[M + Ca + I]^+$ and [M + Ca + Br]⁺ complexes, whereas twelve were baseline resolved when analyzed as [M + Ca + I⁺ complexes. These results indicate that adducting carbohydrates with both a metal cation and a halogen anion can change the gas-phase conformations of the carbohydrate, resulting in characteristic conformational features and the separation of isomer pairs.

D. IMS with High Resolving Power

Different IMS techniques yield different resolution (R) and resolving power (R_p) (Cumeras et al., 2015; Sans et al., 2018; Dodds & Baker, 2019). The R_p of a single peak is calculated from the ion's arrival time (t_a) and the peak width at half the maximum height (FWHM) (Equation 5) (Siems et al., 1994; Kanu et al., 2008; Dodds et al., 2017; Bohnhorst et al., 2020).

$$R_p = \frac{t_a}{FWHM} \tag{5}$$

DTIMS and TIMS instruments have lower resolving powers than TWIMS instruments, though new IMS platforms aim to further increase the resolving power (Michelmann et al., 2015; Dodds et al., 2017; Dodds & Baker, 2019; Hollerbach et al., 2020; May et al., 2021). Cyclic IMS (cIMS) and structures for lossless ion manipulations (SLIM) offer the ability to resolve multiple gas-phase conformations with extended path lengths compared to traditional IMS techniques. cIMS and SLIM platforms utilize printed circuit boards (PCBs), consisting of closely aligned RF and DC electrodes, that apply electric fields to manipulate ion movement (Tolmachev et al., 2014; Attah et al., 2019). TWIMS, operating at low voltages, is utilized in both cIMS and SLIM devices to separate ions based on mobility differences. Additionally, the RF electric fields enable ion transport over long distances without significant ion loss, providing effective ion transmission (Tolmachev et al., 2014).

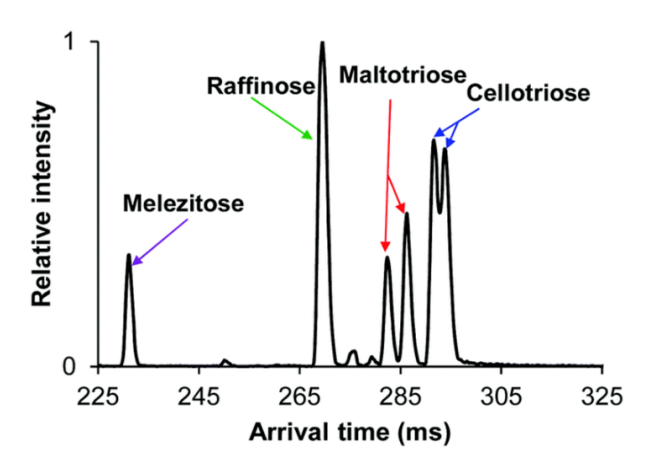
Both cIMS and SLIM enable increased resolving power compared to traditional IMS (DTIMS, TWIMS, TIMS) due to increased ion path lengths for separations. In cIMS instruments, the traveling waves move ions in a circular cell with a path length of 98 cm, though multipass separations can be performed to further increase the path length (Giles et al., 2019). Multipass separations can also be achieved with a TW-based SLIM serpentine ultralong path with extended routing (SUPER) device, with each pass through the device being 13.5 m (Deng et al., 2017). With SLIM SUPER, ions travel through the device in serpentine motions, making multiple turns around the PCB. Both cIMS and SLIM can suffer from "wrap-around" or "rollover" effects, where a faster ion laps a slower ion (Hollerbach et al., 2020). Multi-level SLIM devices can remove these effects. Thus, recent SLIM designs include elevators and escalators, allowing ions to traverse through multiple levels of the device, extending the path length to 43 m, and increasing the resolving power (Ibrahim et al., 2017; Hollerbach et al., 2020).

SLIM enabled resolution of Na⁺-adducted trisaccharide isomers, which could not be resolved by DTIMS. Four Na⁺-adducted trisaccharide isomers, including melezitose, raffinose, maltotriose, and isomaltotriose, were analyzed individually and separated from a mixture (May et al., 2021). Melezitose and raffinose are non-reducing carbohydrates that differ in one monosaccharide unit, linkages, and anomericity, while isomaltotriose and maltotriose are reducing carbohydrates with different linkages. In DTIMS, only melezitose could be resolved. The other three trisasccharides generated broad mobility peaks, preventing the carbohydrates from being resolved. However, with SLIM, narrower ATDs resulted. Melezitose and raffinose were fully resolved, and isomaltotriose and maltotriose were partially resolved. The SLIM experiments resulted in a higher resolving power (R_p of 297) compared to the DTIMS experiments (R_p of 56).

Metal adduction can lead to different gas-phase conformations, including those associated with different carbohydrate anomeric configurations. The SLIM SUPER platform, consisting of a 45 m path length, has been used to separate Na⁺-adducted isomers. For Na⁺-adducted trisaccharides, different numbers of peaks were detected for reducing versus non-reducing carbohydrates (Nagy et al., 2018). Figure 5 shows that single peaks were observed for non-reducing carbohydrates, melezitose and raffinose, while multiple peaks were observed for reducing carbohydrates, maltotriose and cellotriose. These additional mobility features are hypothesized to result from the anomeric configurations at the reducing end of the carbohydrates, generating different gas-phase conformations, which can be distinguished in IMS with sufficient resolving power. Na⁺-adducted pentasaccharide isomers, including linear cellopentaose, linear maltopentaose, and branched mannopentaose were separated in a SLIM device with a 13 m path length (Deng et al., 2016). Mannopentaose differs in both the monosaccharide composition and connectivity, compared to the stereoisomers cellopentaose and maltopentaose. The SLIM mobility

data showed multiple mobility peaks for the Na⁺-adducted carbohydrates that were not resolved by DTIMS, indicative of the anomeric configurations of the carbohydrates.

Figure 5. Separation of Na⁺-adducted trisaccharide isomers by cIMS. Republished with permission of Royal Society of Chemistry, from Nagy, G., *et. al.* Unraveling the isomeric heterogeneity of glycans: ion mobility separations in structures for lossless ion manipulations. *Chem. Comm.* 2018, 54, 83, 11701-11704; permission conveyed through Copyright Clearance Center, Inc.



SLIM was also utilized to distinguish various $[M + H]^+$ and $[M + K + H]^{2+}$ species of HMOs, resulting in different observed gas-phase conformations (Nagy et al., 2018). Protonated HMO isomers, LNT and LNnT, were resolved using a SLIM device with a 31.5 m path length. Four peaks were observed in the ATD of $[LNT + H]^+$, indicating that multiple conformations exist in the gas-phase. The conformational differences are hypothesized to be due to α and β anomers existing in the gas-phase and protons coordinating to different sites (Nagy et al., 2018). Lacto-*N*-hexaose (LNH) and lacto-*N*-neohexaose (LNnH), which are linkage isomers (Figure 3), were resolved as $[M + K + H]^{2+}$ ions after one pass (13.5 m) through a SLIM SUPER device, with arrival times of 0.140 s and 0.133 s, respectively. However, after nine passes (121.5 m), an additional,

unresolved conformational feature of LNnH was observed, indicating improved resolution for longer path length separations (Deng et al., 2017). [M + K + H]²⁺ complexes of lacto-*N*-fucopentaose isomers (linear LNFP I and branched LNFP II and III shown in Figure 3) were separated using SLIM SUPER with a 45 m path length. Due to the differences between the linear and branched HMO structures, their separation resulted in multiple mobility peaks in the ATDs, corresponding to multiple gas-phase conformations, potentially due to different K⁺ coordination sites (Nagy et al., 2018). In comparison to utilizing [M + H]⁺ complexes for separating LNT and LNnT, [M + K + H]²⁺ complexes of LNH and LNnH could be resolved at shorter path lengths (Deng et al., 2017), indicating that the metal addition provides enhanced separation. Additionally, depending on the HMO size and isomeric structural features, both [M + H]⁺ and [M + K + H]²⁺ HMO complexes result in multiple conformational features, indicating differences in gas-phase conformations.

cIMS has also been used to distinguish carbohydrate isomers of varying size using different metal adducts. A mixture of isomeric Na⁺-adducted pentasaccharides, including maltopentaose, cellopentaose, and branched mannopentaose, were separated in a cIMS device after three passes, approximately a 3 m path length (Giles et al., 2019). Na⁺-adducted isomeric di- and tri-saccharide HMO-core structures, including lactosamine, galactosyllactoses, fucosylated, and sialylated structures, were resolved on a cIMS platform with an extended path length of 40 m (Peterson & Nagy, 2021). Furthermore, as the path length was increased in increments from 10 m to 40 m, additional features were observed in the mobility data, highlighting the improvement in isomer resolution with increasing path length. Stereoisomeric pairs of maltose and cellobiose, as well as malto- and cello-triose, -tetraose, -pentaose, and -hexaose were adducted to group I metals (Li⁺, Na⁺, K⁺, Rb⁺, and Cs⁺) and analyzed by cIMS with a path length of up to 15 m (Williamson et al.,

2021). After separating each pair of metal-adducted stereoisomers and calculating the α/β anomeric ratios of the reducing end configuration, a trend was observed in the ATDs for the anomeric forms of the malto- and cello-stereoisomers. It was observed that the β cello-anomers had a higher mobility than the α cello-anomers, while the β -malto-anomers had a lower mobility than the α -malto anomers. It was hypothesized that multiple mobility peaks resulted from the α and β forms at the reducing end of the carbohydrates. Similar to lower resolving power IMS, separation of the stereoisomers was dependent on the carbohydrate and metal ion. For maltose and cellobiose, K^+ adducts yielded the best separation, while for malto- and cello-triose, Li^+ adducts resulted in the best separation. Additionally, the best separation was displayed for pairs of Li^+ and Li^+ and Li^+ adducts of malto- and cello-tetraose and malto- and cello-pentaose, respectively. However, a specific group I metal was not shown to separate pairs of malto- and cello-hexaose. Thus, there were no observed trends to correlate the size of the metal and ability to resolve pairs of maltose and cellobiose, malto- and cello-triose, -tetraose, -pentaose, and -hexaose and their anomeric forms.

V. Fragmentation of Carbohydrates

Tandem MS (MS/MS), which utilizes fragmentation, is valuable for analyzing isomeric species. During fragmentation, chemical bonds are broken in a manner dependent on the chemical structure of the precursor ion. Therefore, differences in gas-phase, isomer structures can be exploited to form diagnostic fragments with distinct m/z values and peak abundances. Fragmentation is deemed effective for sequencing structures based on the fragmentation efficiency, which is defined by the intensity of the precursor ion before and after fragmentation, as well as the ability to form unique fragments. However, a high fragmentation efficiency does not ensure the formation of diagnostic fragments. Scheme 1 shows carbohydrate fragments and the

associated Domon and Costello nomenclature (Domon & Costello, 1988). B/Y and C/Z fragments form from glycosidic-bond cleavages, while A/X fragments form from cleavages within rings. A, B, and C fragments retain the non-reducing end of the carbohydrate, while X, Y, and Z fragments retain the reducing end. The subscripted numbers identify the monosaccharide subunits retained in the fragment. For example, a B₁ fragment retains one monosaccharide subunit. Superscripts are used to describe the location of cross-ring cleavages for A/X fragments. As discussed in the ionization section of this review, many carbohydrate ions are formed as an adduct with a single charge carrier or metal ion. Therefore, detection is limited to fragments that maintain a charge. This is different than protein and peptide fragmentation, which may contain multiple protons, enabling detection of fragments on both sides of the cleaved bond. Additionally, the precursor ion signal intensity is important because higher precursor ion signals may enable the detection of low intensity fragments formed by less energetically favorable pathways.

Scheme 1. Modified from Domon & Costello, 1988

A. Collision Induced Dissociation

Collision-induced dissociation (CID) is an ion/molecule reaction in which an ionic species repeatedly collides with neutral gas molecules, such as helium, argon, or nitrogen (Jennings, 1968;

McLafferty & Schuddemage, 1969; McLafferty et al., 1973). These collisions increase the internal energy of the ions, causing dissociation of the carbohydrate bonds. Several related factors affect ion fragmentation by CID, including the efficiency of CID in converting kinetic energy into internal energy for the analyte ion, the amount and variability of the deposited energy, and the timeframe over which collisional activation occurs relative to the time required for unimolecular dissociation (McLuckey & Goeringer, 1997; Mitchell Wells & McLuckey, 2005). Additionally, the instrument must sample the reaction at a timescale appropriate to monitor dissociation (Mitchell Wells & McLuckey, 2005).

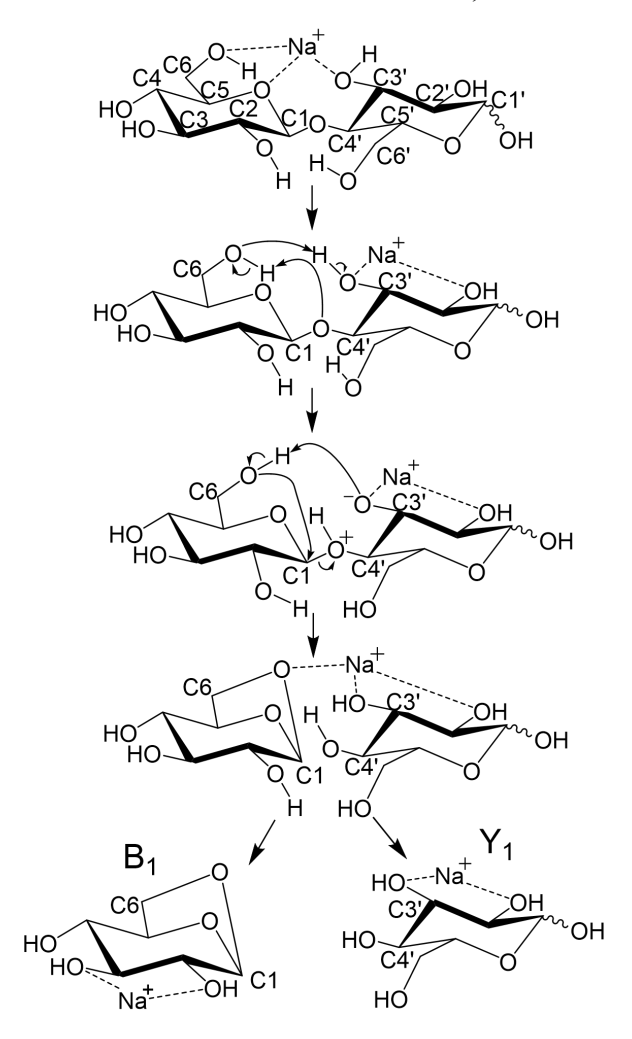
The fragmentation energy affects the product ions formed from metal-adducted and protonated carbohydrates. Single, high-energy collisions (>1 keV) form large numbers of crossring and glycosidic-bond cleavages for Na⁺ adducts (Spengler et al., 1994; Harvey et al., 1997). This is in contrast to low collision energies (<100 eV), which require multiple collisions since most of the collision energy is not converted into internal energy (Mitchell Wells & McLuckey, 2005). Low-energy CID is known to predominantly cleave glycosidic bonds; however, the extent of cross-ring cleavage is heavily influenced by the metal utilized to form the carbohydrate adduct (Sible et al., 1997; König & Leary, 1998; Harvey, 2001; Schaller-Duke et al., 2018). Because cross-ring cleavages are crucial for determining linkages, these fragments are vital for differentiating isomers (König & Leary, 1998).

Metal adduction alters the CID fragmentation mechanisms of carbohydrates compared to protonation (Harvey, 2000; Bythell et al., 2017). For protonated species, the detected CID fragments are primarily glycosidic-bond cleavages, with very few cross-ring cleavages (Harvey, 2000; Bythell et al., 2017; Castillo et al., 2021), though water loss is another major product (Bythell

et al., 2017). CID of protonated carbohydrates is also limited by inefficient ionization, making detection of low intensity fragments challenging.

For group I metal-adducted carbohydrates, fragmentation is proposed to occur by chargeremote fragmentation, in which the metal does not directly initiate dissociation; rather,
fragmentation is hypothesized to require a mobile proton (Bythell et al., 2017; Rabus et al., 2017).
Glycosidic-bond cleavage requires movement of a proton to the glycosidic bond. For Na⁺-adducted
cellobiose (Scheme 2), a proton migrates from the carbon-6 hydroxyl to the glycosidic bond. Then,
nucleophilic attack from the alkoxide on carbon-1 causes glycosidic-bond cleavage (Rabus et al.,
2017). Mechanisms for minor products have hypothesized that a proton attached to carbon-2 could
also migrate to the glycosidic oxygen to initiate bond dissociation (Bythell et al., 2017). The metal,
Na⁺ in Scheme 2, stabilizes hydroxyls during proton migration by coordinating multiple oxygens
during the dissociation reaction. This stability is not present for protonated carbohydrates, as the
proton is hypothesized to interact with one, or at most, two oxygens. Thus, the gas-phase structures
of metal-adducted carbohydrates influence CID fragmentation. This difference in stability is
fundamental to the fragmentation differences seen for metal-adducted compared to protonated
carbohydrates.

Scheme 2. Modified from Rabus et al., 2017



Cross-ring cleavages require that two bonds be broken in a carbohydrate ring, both of which require proton migration. For Na⁺-adducted carbohydrates, a proton is hypothesized to move from a hydroxyl to the oxygen in the monosaccharide ring. Scheme 3 shows the cross-ring cleavage of Na⁺-adducted gentiobiose to form ^{0,2}A₂. First, a proton migrates from the hydroxyl on carbon-1' to the oxygen in the monosaccharide ring, causing the glucose ring to open and form an aldehyde. A second proton then migrates from one of the remaining hydroxyls to the aldehyde, cleaving a carbon-carbon bond and resulting in a cross-ring cleavage. In Scheme 3, for the formation of the ^{0,2}A₂ fragment, a proton migrates from the carbon-2' hydroxyl to the aldehyde.

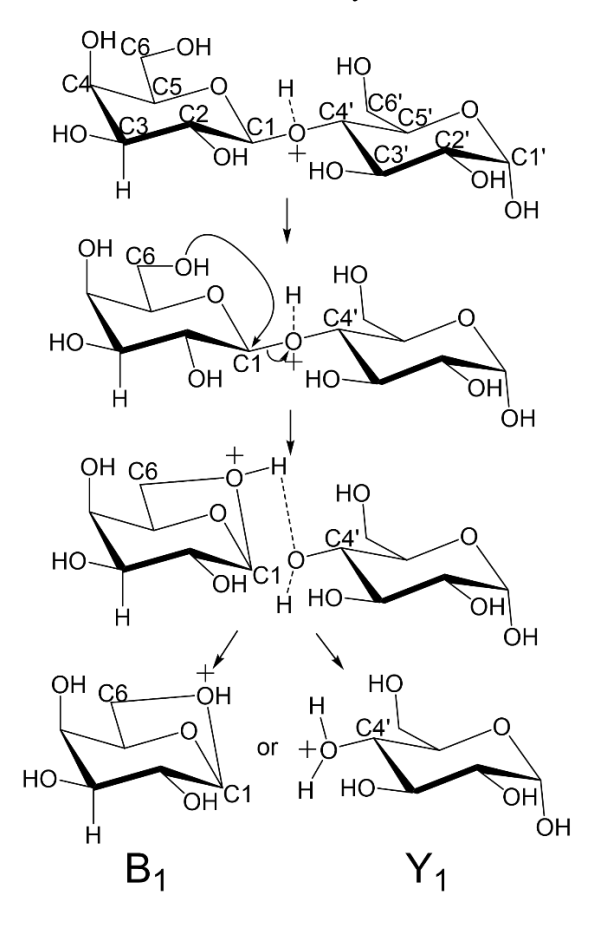
The redistribution of electrons results in cleavage between carbon-2' and carbon-3'. Although it is not well understood mechanistically, the presence of the metal is hypothesized to make these cross-ring cleavages more energetically favorable during CID by stabilizing the complex through coordination with multiple oxygens (Bythell et al., 2017; Rabus et al., 2017).

Scheme 3. Modified from Rabus et al., 2017

The proton charge carrier is a fundamental part of the CID mechanism for protonated carbohydrates. The proton initially migrates to the glycosidic bond for dissociation. Scheme 4 shows the CID dissociation mechanism for protonated lactose. With redistribution of the internal vibrational energy, a hydroxyl oxygen (*e.g.* from carbon-6) attacks carbon-1, cleaving the glycosidic bond and forming an anhydro carbohydrate, similar to the B₁ product in Scheme 2 (Bythell et al., 2017). The proton can remain associated with the glycosidic oxygen or migrate to the anhydro carbohydrate post-cleavage (Scheme 4), which determines whether the charge is

retained on the reducing or non-reducing end. An alternate mechanistic pathway involves the lone pair of electrons attached to the oxygen in the monosaccharide ring forming a double bond with carbon-1, which causes cleavage of the glycosidic bond and formation of an oxocarbenium ion for the B₁ fragment (Bythell et al., 2017). Energetics calculations for both structures are similar. For the oxocarbenium ion formed through the alternate mechanism, a proton can be abstracted from a hydroxyl on the monosaccharide at the non-reducing end after glycosidic cleavage to form a charged Y₁ fragment.

Scheme 4. Modified from Bythell et al., 2017



Dehydration neutral loss fragmentation mechanisms have also been investigated with protonated and metal-adducted carbohydrates. Experimentally, multiple dehydration neutral losses

have been observed for a single monosaccharide (Mookherjee et al., 2018). Mechanistic differences have been described for Na⁺-adducted N-acetylhexosamines (GlcNAc and GalNAc) compared to protonated systems for the first dehydration neutral loss. Na⁺-adducted Nacetylhexosamines have been shown to lose a non-labile hydrogen attached to carbon in addition to the loss of a hydroxyl group (Chiu et al., 2019), while protonated N-acetylhexosamines (GlcNAc and GalNAc) lose two labile hydrogens in addition to oxygen during the dehydration reaction (Mookherjee et al., 2018). This mechanistic difference is hypothesized to be related to charge remote fragmentation with metals as opposed to charge directed fragmentation for protonated Nacetylhexosamines. The metal is predicted to create a more acidic environment, allowing a hydrogen attached to a nearby carbon to transfer to a carbonyl before the hydrogen transfers to a nearby hydroxyl to yield water loss (Chiu et al., 2019). However, the second and third dehydration neutral loss reactions of protonated N-acetylhexosamines lose nonlabile hydrogens in addition to labile hydrogens (Mookherjee et al., 2018). Li⁺- and Na⁺-adducted hexose monosaccharides (glucose, galactose, and mannose) have shown a similar but distinct dehydration mechanism to protonated N-acetylhexosamines, with the loss of two labile hydrogens and oxygen (Chen et al., 2017; Abutokaikah et al., 2018). These mechanistic differences seen with CID indicate that the metal-adduction impacts hexosamines in a distinct manner compared with hexoses.

Although a mechanism has yet to be published for CID fragmentation of carbohydrates adducted to divalent or trivalent metals, the metals are likely to affect fragmentation. For example, for Ca²⁺-adducted carbohydrates, the detected fragments retain the same 2+ charge state (Schaller-Duke et al., 2018). Therefore, the fragmentation mechanism is likely similar to that proposed for Na⁺-adducted carbohydrates in Schemes 2 and 3. However, for some metals, such as Ni²⁺, Co²⁺, and Mg²⁺, a mixture of 2+ and 1+ fragments that have lost a proton are detected (Schaller-Duke et

al., 2018; Wong et al., 2022). The proton loss suggests that a distinct mechanism may occur during dissociation. Furthermore, because the number of cross-ring cleavages is similar to that detected from deprotonated ions in negative-ion mode, the formation of a 1+ ion that has lost a proton may be critical to the formation of cross-ring cleavages (Harvey, 2001; Adamson & Håkansson, 2007a).

Group I metals influence the fragmentation patterns of carbohydrates during CID due to charge density. Studies in the mid-90s from the Lebrilla group compared CID fragmentation patterns of group I metals adducted to carbohydrates (Cancilla et al., 1996). They found that Li⁺ and Na⁺ produced the highest fragmentation efficiency for high-mannose N-linked glycans and HMOs, while the large ionic radii of Rb⁺ and Cs⁺ resulted in almost no fragmentation. In addition, glycosidic-bond cleavages were the dominant fragments detected from K⁺-, Na⁺-, and Li⁺adducted carbohydrates (Cancilla et al., 1996; Harvey, 2001; Przybylski & Bonnet, 2013; Hofmann et al., 2017; Schaller-Duke et al., 2018). These results indicate that the ionic radius is important in carbohydrate fragmentation (Cancilla et al., 1996). The ionic radius (Table 1) influences the bond distance between the carbohydrate oxygens and the cation (Bythell et al., 2017). Additionally, a singly charged metal with a large ionic radius has a low charge density (Table 1) (Cancilla et al., 1996; Harvey, 2000). The lower charge density limits the mobility of protons within the carbohydrate, which is necessary to cause dissociation by CID (Cancilla et al., 1996). The lower charge density also influences the predicted energy barrier for metal loss, which can become energetically favorable compared to covalent bond dissociation, limiting the structural information achievable from CID with very low charge density metals (Chen et al., 2017). However, when low charge density metals such as Na⁺ are adducted to α - and β -glucose anomers, the monosaccharide isomers can be distinguished from one another based on the energetic favorability of dehydration reactions for α -glucose. Na⁺-adducted α -glucose can more accessibly

form 2-ketone or 1,2 anhydroglucose compared to Na $^+$ -adducted β -glucose, allowing for anomeric isomers to be distinguished based on difference in dehydration loss.

The charge density of the carbohydrate-metal ion adduct is likely the influential factor in fragmentation differences between metal-adducted disaccharides and larger oligosaccharides. Na⁺ and Li⁺ adducts of di- and tri-saccharides form more cross-ring cleavages than Na⁺- and Li⁺ adducted heptasaccharides, such as maltoheptaose (Asam & Glish, 1997; Harvey, 2000; da Costa et al., 2012; Azenha et al., 2013). Greater numbers of cross-ring cleavages have been observed for larger carbohydrates adducted to divalent and trivalent metals (König & Leary, 1998; Harvey, 2001; Schaller-Duke et al., 2018; Wong et al., 2022). For larger carbohydrates the low charge density of group I metals limits the yield of cross-ring cleavages in low-energy CID. This suggests that the metal properties and size of the carbohydrate impact the charge density of the gas-phase adduct ion.

The ionization energy is another important metal property affecting fragmentation. Fragments of carbohydrates adducted to either group II or divalent transition metals have been compared to group I metal adducts. Doubly charged transition metals, including Zn²⁺, Ni²⁺, and Co²⁺ with high second ionization energies (Table 1), lead to significant cross-ring cleavages (Sible et al., 1997; Harvey, 2001; Schaller-Duke et al., 2018). The second ionization energy is theorized to impact the affinity for sharing electrons with oxygens in hydroxyl groups, impacting the ion stability. Therefore, a metal with a higher second ionization energy is hypothesized to form a less stable ion, leading to more energetically favorable fragmentation pathways. The higher second ionization energy is also hypothesized to promote the loss of protons, which may explain why CID fragments of Co²⁺-, Zn²⁺-, and Ni²⁺-adducted carbohydrates are detected as 1+ ions following proton loss. Group II and transition metals with lower second ionization energies (Ca²⁺, Mg²⁺, and

Mn²⁺), yield a moderate number of cross-ring fragments (Fura & Leary, 1993; Sible et al., 1997; Harvey, 2001). Research indicates that Ca²⁺ is effective at creating detectable cross-ring cleavages because of its intense precursor signal, which is a factor that benefits group II metals and Mn²⁺ in comparison to other metals and protonation (Harvey, 2001). Monovalent and divalent Ag⁺ and Cu²⁺ influence CID fragmentation in a distinct manner compared to other transition metals. Although most transition metals cause substantial cross-ring cleavages, Cu2+ and Ag+ have displayed results similar to that of group I metals by predominantly forming glycosidic-bond cleavages (Harvey, 2001; Harvey, 2005). The CID fragmentation behavior of Ag⁺ is hypothesized to be due to the similar charge density of Ag⁺ and Na⁺ (Table 1). Furthermore, it is hypothesized that the high second ionization energy and unique electron configuration of Cu²⁺, compared with other divalent transition metals, causes Cu²⁺ to act similarly to group I metals and Ag⁺ (Harvey, 2001; Schaller-Duke et al., 2018). The high second ionization energy of Cu²⁺ causes the ion to be unstable in the 2+ form. Also, it may be favorable for Cu²⁺ to transition to Cu⁺ due to the complete d-orbital shell, which could improve the gas-phase stability of Cu⁺. This likely explains why Cu⁺adducts are often formed from ESI (Harvey, 2001).

For divalent and trivalent metals, a deprotonated precursor, [M + metal - nH]⁺, or anion adduct, [M + metal + anion]⁺, can be fragmented, which affects the resulting CID spectra. Although deprotonated precursors are often detected at lower intensities than divalent metal-adducted carbohydrates, the fragmentation spectra can be diverse, which is valuable for structural analyses of carbohydrates. La³⁺, Cr³⁺, Fe³⁺, and Al³⁺ form [M + metal - 2H]⁺ or [M + metal - H]²⁺ during ionization and yield substantial cross-ring fragmentation, comparable to that seen for Co²⁺ and Ni²⁺ adducts, detected as [M + metal]²⁺ (Schaller-Duke et al., 2018; Schaller-Duke, 2019). When detecting fragments from [M + metal + anion]⁺, the anion (Cl⁻ or Br⁻) is commonly lost

during CID through neutral loss, forming HCl or HBr; yet, the metal is retained, indicating that the anion is likely coordinated to hydrogens as opposed to the retained metal ion (Fura & Leary, 1993). For [M + metal + Cl]⁺, where the metal was Ca²⁺, Co²⁺, or Mn²⁺, cross-ring cleavages could be used to distinguish two linkage isomers of mannotriose (Sible et al., 1997). However, analysis of [M + metal + anion]⁺ and trivalent metal adducts is often challenging due to the weak precursor ion signal compared to [M + divalent metal]²⁺.

Differences in the collision energy required to induce fragmentation when using low-energy CID have been investigated for protonated and group I metal adducts of carbohydrates. For group I metal adducts, the collision energy required to initiate dissociation decreases for K⁺ > Na⁺ > Li⁺ (Cancilla et al., 1996; Harvey, 2000; Bythell et al., 2017). In comparison to group I metal adducts, protonation requires lower collision energies to induce fragmentation (Harvey, 2000). When directly comparing fragmentation of Li⁺- and Ca²⁺-adducted trisaccharides, Ca²⁺adducts required three times less collision energy to induce dissociation (Kim, 2021). It has been suggested that lower charge density metals (Table 1) require more energy to initiate fragmentation when using low collision energies (Bythell et al., 2017). The differences in energy requirements to induce fragmentation are likely due to the differences in the cation binding distance to the hydroxyl oxygens, which impacts the precursor and product ion stability. Protons, being smaller, have closer interaction distances than all group I metals (Cancilla et al., 1996; Bythell et al., 2017).

Metal adduction can stabilize labile carbohydrate modifications and prevent structural rearrangements. For example, fucose and xylose migration can occur during CID of protonated carbohydrates (Brüll et al., 1998; Wuhrer et al., 2006; Hecht et al., 2017; Mucha et al., 2018). Fucose is a critical monosaccharide found in human glycans and HMOs, while xylose is a common monosaccharide found in plant *N*-linked glycans. Fucose and xylose migration lead to

misidentification of precursor ion structures. By utilizing Na⁺ adducts, fucose migration can be minimized (Brüll et al., 1998; Mucha et al., 2018), though it has been hypothesized that other metals would also effectively minimize migration due to the mechanism of charge-remote fragmentation (Mucha et al., 2018). Since the metal is not directly involved in dissociation, it coordinates with multiple oxygens, creating a stable charge location. However, with protonation, since the location of the charge site migrates and can interact with just one oxygen, this allows for fucose migration to occur (Mucha et al., 2018). GAGs have labile sulfate groups that vary in location, making cross-ring cleavages necessary to identify their locations. Na⁺- and Ca²⁺adduction prevent the loss of sulfate groups during CID of GAGs (Zaia & Costello, 2003; Taylor et al., 2009; Kailemia et al., 2012). Unlike other types of carbohydrates, metal adduction minimally affects the number of cross-ring cleavages or glycosidic-bond cleavages for GAGs (Zaia & Costello, 2003; Kailemia et al., 2012). This is likely because with metal adduction, multiple deprotonation sites for GAGs still exist that are involved in the fragmentation mechanism. Finally, HMOs and glycans with labile sialic acid monosaccharides have been stabilized by metal adduction during CID (Leavell & Leary, 2001).

Derivatization can also influence fragment formation when combined with metal adduction or protonation. Recent publications have examined CID fragmentation of metal-adducted (Co²⁺ or Ni²⁺) carbohydrates, which are known to be effective at forming cross-ring cleavages with underivatized carbohydrates (Schaller-Duke et al., 2018). However, when the same metals are used to fragment permethylated glycans, glycosidic-bond cleavages become more predominant (Zhu et al., 2015). When using group I metals of Na⁺ and Li⁺, the formation of cross-ring cleavages decreases and glycosidic-bond cleavages increase during low-energy CID (Brüll et al., 1998; Solouki et al., 1998; Prien et al., 2009). The addition of methyl groups likely inhibits and alters the

movement of protons around the carbohydrate, limiting the formation of cross-ring cleavages at low collision energies. However, cross-ring cleavages have been detected for Na⁺-adducted, permethylated glycans when using high-energy CID (Lemoine et al., 1996). CID of metal-adducted, permethylated and underivatized carbohydrates have also been detected, losing the metal adduct and having a proton as the remaining charge carrier (Han & Costello, 2011; Wong et al., 2022). These results suggest that metal loss from CID may depend on the metal in the precursor, with Mg²⁺-adducted precursors being more likely to lose the metal and become protonated fragments compared to Na⁺-adducted carbohydrates (Wong et al., 2022).

B. Electron-Based Fragmentation

In electron-based fragmentation, an energized electron is transferred to a precursor ion, which results in bond cleavage. Low-energy electron-based fragmentation techniques include electron capture dissociation (ECD) (Zubarev et al., 1998) and electron transfer dissociation (ETD) (Syka et al., 2004). ECD involves creating a low-energy (~1 eV) electron beam that interacts with a trapped precursor ion to induce fragmentation (Zhurov et al., 2013). ECD can also use a higher energy electron beam of ~9 to 10 eV, often called hot-ECD (HECD) (Kjeldsen et al., 2002; Zhurov et al., 2013). The formation of a stable electron beam has previously required high vacuum systems of ~10⁻¹⁰ torr, which are only present in Fourier transform-ion cyclotron resonance (FT-ICR) mass spectrometers (Zhurov et al., 2013). However, recent advances have enabled the use of ECD with mass analyzers with higher pressures than FT-ICRs (Fort et al., 2018; Beckman et al., 2021), though applications to carbohydrates are minimal at this time. Multiply charged precursor ions are required for ECD because adding an electron reduces the charge of the detected fragments; this prevents the analysis of group I metal adducts and protonated carbohydrates because they do not regularly form multiply charged ions (Harvey, 2000; Huang & Dodds, 2013; Mookherjee et al.,

2020). For multiply charged, metal-adducted carbohydrates, ECD has yielded a diverse array of cross-ring and glycosidic-bond cleavages, which are required to distinguish isomers (Adamson & Håkansson, 2007; Yu et al., 2012; Huang et al., 2014).

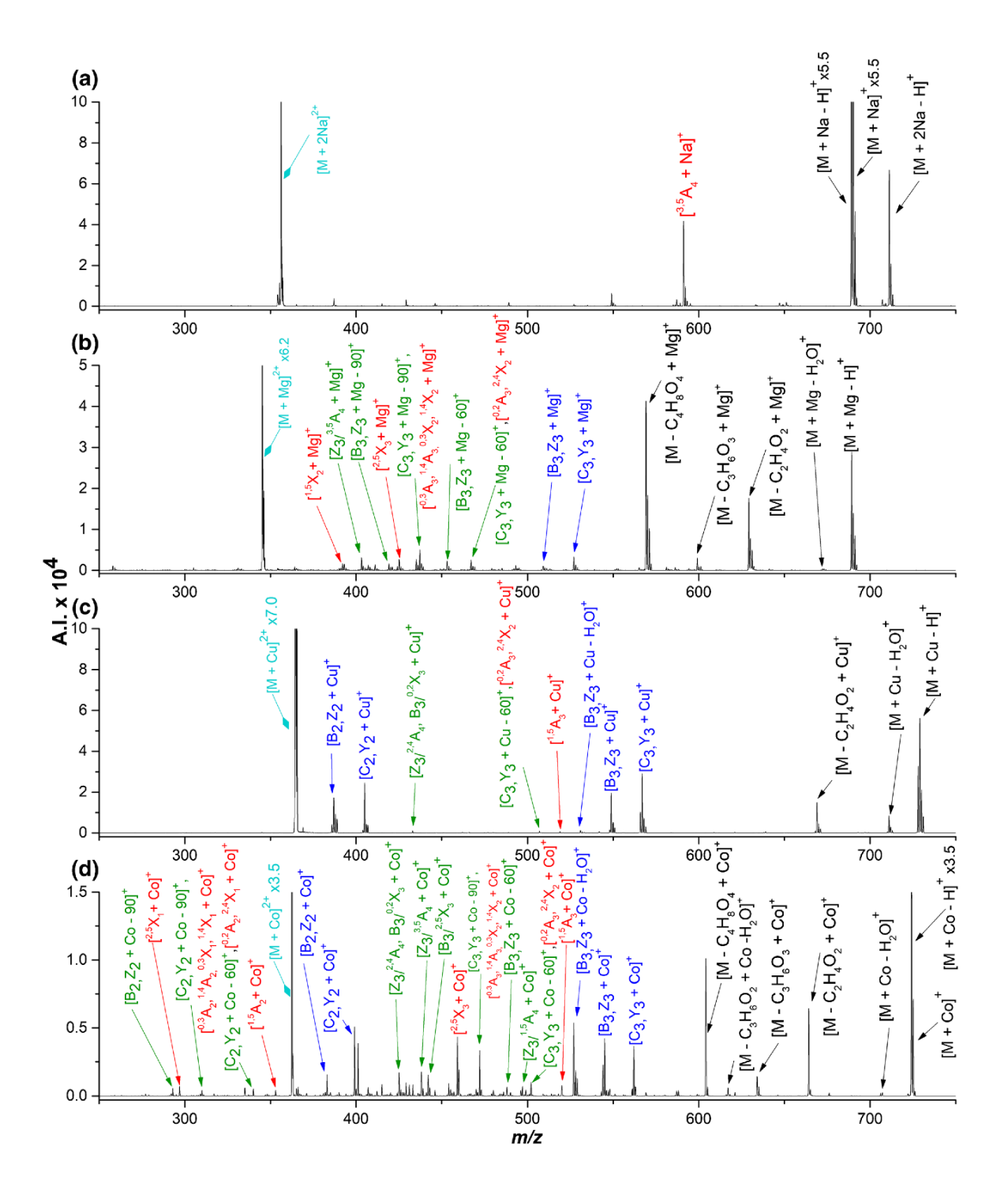
ETD involves the transfer of a low-energy electron from a radical anion reagent to a multiply charged cation to induce fragmentation through an ion/ion reaction (Syka et al., 2004). Therefore, like ECD, ETD requires a multiply charged precursor to analyze glycans. The recombination energy is different for ETD compared to ECD since the electron must overcome the electron affinity of the anion reagent to transfer from the anion to the cation (Mentinova et al., 2013). The difference in recombination energy is hypothesized to be the fundamental difference that separates the available fragmentation pathways in ETD from those in ECD. Additionally, since ETD occurs through ion/ion reactions, proton-transfer-induced fragmentation (PTD) or protontransfer charge reduction (PTCR) can occur and compete with ETD (Gunawardena et al., 2005). Proton transfer involves transferring a proton from the precursor ion to the ETD anion reagent (Stephenson & McLuckey, 1996; Gunawardena et al., 2005). The extent of proton transfer (PT) and electron transfer (ET) are dependent on the molecular properties of the anion reagent, including the electron affinity and Franck-Condon factors (Gunawardena et al., 2005). Fluoranthene, azulene, and azobenzene are the most commonly used ETD reagents because of their ability to induce more electron-based dissociation than proton transfer (Gunawardena et al., 2005; Compton et al., 2012). However, for metal-adducted carbohydrates, fluoranthene and 1,4dicyanobenzene are common reagents because of their commercial availability, though fluoranthene has been more readily utilized because 1,4-dicyanobenzene causes charge reduction or electron transfer no dissociation (ETnoD) (Huang & Dodds, 2015).

The mechanism for low-energy electron fragmentation (e.g., ECD and ETD) is influenced by the charge state and charge density of the precursor ion, making the metal adduct important for dissociation (Liu & McLuckey, 2012). It has been hypothesized that the metal captures the electron, then abstracts a hydroxyl group forming a bond and resulting in a carbon radical within a monosaccharide ring (Han & Costello, 2011; Huang et al., 2014). Scheme 5 shows a fragmentation mechanism for Mg²⁺-adducted cellobiose. Mg^{+•} abstracts the carbon-3' hydroxyl to form a radical on carbon-3'. The electron can then migrate around the ring, generating several different cross-ring cleavages. In Scheme 5, the radical migrates from carbon-3' to carbon-5' to carbon-1' and back to carbon-3', causing bond cleavages and the formation of the ^{2,4}A₂ + H fragment and multiple neutral products. Scheme 5 also shows that a radical hydrogen can be ejected, causing the detected fragment to lose a proton, as shown with the formation of the ^{2,4}A₂ fragment (Yu et al., 2012; Huang et al., 2014). Although in an alternate proposed mechanism, the ^{2,4}A₂ fragment is hypothesized to form from radical hydrogen migration (Huang et al., 2014). Radical hydrogen migration within or between fragments or radical hydrogen ejection from a fragment is hypothesized to be more energetically favorable at low charge states and low charge densities for peptides, which is likely the case for carbohydrates as well (Leymarie et al., 2003; Bythell, 2013; Bythell, 2014).

Scheme 5. Modified from Huang et al., 2014

The charge density, electron configuration, and second ionization energy of the metal adducted to the carbohydrate are critical properties for producing unique fragments during ETD and ECD, which are required for distinguishing isomeric carbohydrates. Significant cross-ring and glycosidic-bond cleavages for disaccharides and larger carbohydrates (11 monosaccharide subunits) can be formed by low-energy electron fragmentation (ETD and ECD). Adducts with Ca²⁺, Sr²⁺, Ba²⁺, 2 Na⁺, and 2 H⁺, result in few cross-ring or glycosidic cleavages, though more fragments are produced with ECD compared to ETD (Adamson & Håkansson, 2007; Yu et al., 2012; Schaller-Duke et al., 2018; Wong et al., 2022), likely due to the slightly higher recombination energy in ECD (Mentinova et al., 2013). Figure 6 shows fragmentation spectra of 2Na⁺-, Mg²⁺-, Cu²⁺-, and Co²⁺-adducted maltotetraose after undergoing a 400 ms ion/ion reaction with fluoranthene. Here, distinct differences in fragmentation can be seen across the four metals, indicating how the unique gas-phase structures of metal-adducted maltotetraose interact with fluoranthene during ion/ion reactions. The metal substantially affects the extent of cross-ring cleavages, with Co²⁺ yielding the most cross-ring cleavages (Schaller-Duke et al., 2018). As previously mentioned in the CID section, it is hypothesized that because of the high second ionization energy of Co²⁺ (Table 1), ions formed through ESI are less stable than group II metal adducts and require the sharing of additional electrons from carbohydrate oxygens. These additional interactions with oxygens can readily induce fragmentation. Mg²⁺ was moderately effective at producing cross-ring cleavages (11 cross-ring cleavages), with slightly less than half the number detected with Co²⁺. Compared with Co²⁺, Cu²⁺ displays predominantly glycosidicbond cleavages. It is hypothesized that because Cu⁺ exists with a stable electron configuration with a full outer d-orbital shell, this limits fragments formed from Cu²⁺ compared to Co²⁺ (SchallerDuke et al., 2018). Finally, Figure 6 shows that few fragments were observed for ETD fragmentation of maltotetraose adducted to two Na⁺. For both ECD and ETD, 2 Na⁺ are less efficient for fragment formation due to the low charge density compared to adducts with 2 Li⁺, Co²⁺, Mg²⁺, Zn²⁺, La³⁺, and Ni²⁺ (Adamson & Håkansson, 2007; Yu et al., 2012; Schaller-Duke et al., 2018; Schaller-Duke, 2019; Wong et al., 2022). Experimental work with 2 K⁺-, 2 Rb⁺-, and 2 Cs⁺-adducted to maltoheptaose result in metal loss during ECD (Yu et al., 2012). These metals have charge densities that are so low that electron fragmentation pathways may not be energetically favorable.

Figure 6. Fragmentation of 2 Na⁺-, Mg²⁺-, Cu²⁺-, and Co²⁺-adducted maltotetraose, using fluoranthene as an ETD reagent. The colors are utilized to distinguish differences in the product ions with black, blue, red, and green representing neutral losses, glycosidic-bond cleavages, cross-ring cleavages, and internal cleavages, respectively. Internal cleavages are a combination of a cross-ring and glycosidic cleavage. The remaining precursor ions are labeled in light blue/cyan. [Color figure can be viewed at wileyonlinelibrary.com] Reprinted with permission from Schaller-Duke, R. M.; Bogala, M. R.; Cassady, C. J. Electron Transfer Dissociation and Collision-Induced Dissociation of Underivatized Metallated Oligosaccharides. *J. Am. Soc. Mass Spectrom.* 2018, 29, 5, 1021-1035. Copyright 2018 American Chemical Society.



ETD and ECD fragmentation of metal-adducted carbohydrates are altered by permethylation. ETD and ECD of permethylated carbohydrates can form both protonated and metal-adducted fragments from metal-adducted precursors (Zhao et al., 2008; Han & Costello, 2011), which has only been observed at low intensities for underivatized carbohydrates (Wong et al., 2022). Therefore, the methyl groups likely alter the fragmentation mechanisms and energetically favorable pathways, affecting the detected fragments (Han & Costello, 2011).

HECD, with electron beam energies of ~9 eV to 10 eV, can improve fragmentation of carbohydrate-metal adducts formed with low charge density, group I metals, such as 2 Na⁺, 2 K⁺, 2 Rb⁺, and 2 Cs⁺. The higher energy is not expected to alter the fragmentation mechanism, as the metal adduct is still expected to accept the electron to induce dissociation (Yu et al., 2012). However, higher energy may allow the electron to migrate within the carbohydrate structure to produce additional cross-ring and glycosidic-bond cleavages that are not observed using ECD with lower electron beam energies. Permethylated carbohydrates adducted to group I metals showed increased cross-ring and glycosidic-bond cleavages, and increased fragmentation efficiency compared to ECD (Yu et al., 2012). Although HECD has several advantages, its use has been limited by instrumental availability.

Electronic excitation dissocation (EED) (Nielsen et al., 2000) developed in parallel to ECD and HECD since all three fragmentation methods utilize an electron beam to cause dissociation. In EED, a high-energy (>10 eV, ~14 eV to 19 eV) electron beam causes an electron within the precursor ion to be ejected and recaptured (Zubarev, 2003). For carbohydrates, the electron can be recaptured by either a carbon or oxygen within a monosaccharide ring, which forms diradicals and induces fragmentation (Huang et al., 2016). Scheme 6 shows the formation of the diradical at carbon-1' and 2'. EED is mechanistically distinct from ECD and HECD, in which the electron is

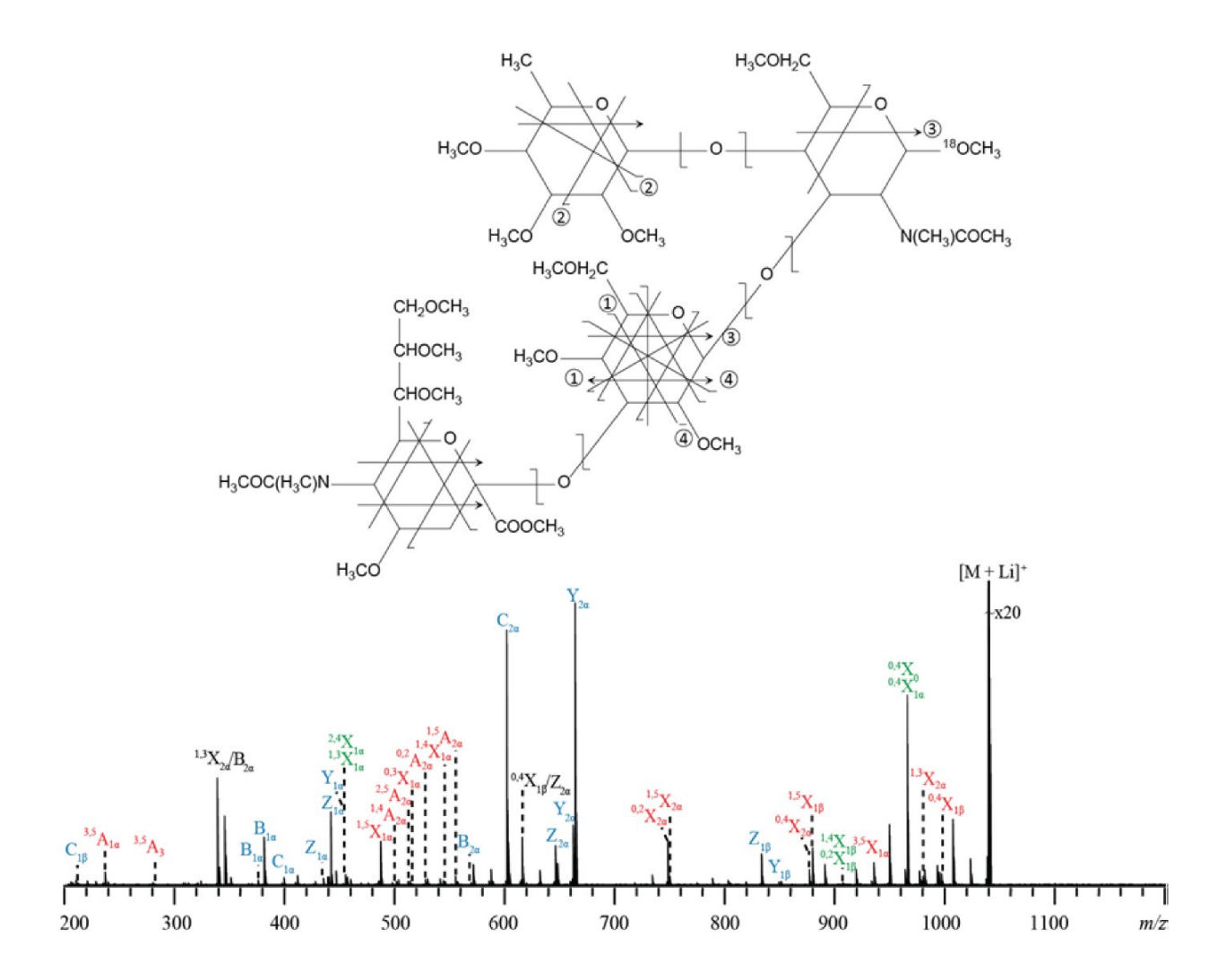
captured at the metal center (Scheme 5). As the diradicals migrate around the monosaccharide, multiple cross-ring cleavages can occur, as shown in Scheme 6 by the formation of Na⁺-adducted ^{1,5}A₂ and ^{3,5}A₂. Scheme 6 shows the formation of the ^{1,5}A₂ fragment from radical migration from carbon-1' to carbon-5' and the formation of formic acid as a neutral loss. Then, ^{3,5}A₂ is formed from radical cleavage of the bond between carbon-3' and carbon-4', forming a double bond between carbon-4' and carbon-5' and a neutral loss of 1,2 ethenediol. Unique to the electron fragmentation techniques, EED allows for the analysis of singly or multiply charged carbohydrates (Yu et al., 2012; Tang et al., 2018). Because the metal is not as influential for initially capturing the electron in EED, it has been hypothesized that EED may be useful for fragmenting carbohydrate-metal adducts that have low fragmentation efficiency in ECD or CID (Huang et al., 2016).

Scheme 6. Modified from Huang et al., 2016

Compared to other fragmentation methods, EED is less effected by the metal forming the adduct with a carbohydrate. Thus, EED has been valuable for fragmenting carbohydrate adducts with low charge density metals (<1.6x10⁻¹⁶ C/nm³), including Na⁺, K⁺, Rb⁺, and Cs⁺. EED has yielded significant cross-ring cleavages for carbohydrate adducts with these metals (Yu et al., 2012; Yu et al., 2013). Carbohydrates adducted to metals with moderately higher charge densities, including Li⁺, Ca²⁺, and Mg²⁺, resulted in similar amounts of cross-ring and glycosidic-bond cleavages by EED when compared to Na⁺-adducted carbohydrates (Yu et al., 2012; Wong et al., 2022). Figure 7 displays fragmentation spectra for Li⁺-adducted sialyl Lewis A (sLe^A), which shows glycosidic-bond and cross-ring cleavages labeled in blue and red, respectively. Figure 7

also displays several isomeric cross-ring cleavages in green and displays fragments that can be identified as either cross-ring cleavages or glycosidic cleavages in black. EED has both a higher fragmentation efficiency and creates more unique fragment products when fragmenting Li⁺-adducted permethylated carbohydrates (Figure 7) compared to ETD and ECD fragmentation (Han & Costello, 2011; Yu et al., 2012; Yu et al., 2013). Therefore, EED is less dependent on the physical properties of the metal charge carrier, making Na⁺ the preferred metal adduct due to its ubiquity in sample preparations.

Figure 7. EED fragmentation for permethylated, Li⁺-adducted sialyl Lewis A (sLe^A). Fragments identified specifically as glycosidic cleavages or cross-ring cleavages are labeled in blue and red, respectively. Isomeric cross-ring cleavages are labeled in green. Fragments that could be either a cross-ring or glycosidic-bond cleavage are labeled in black. The remaining precursor ion is also labeled in black. [Color figure can be viewed at wileyonlinelibrary.com] Reprinted with permission from Yu, X., *et al.* Detailed Glycan Structural Characterization by Electronic Excitation Dissociation. *Anal. Chem.* 2013, 85, 21, 10017-10021. Copyright 2013 American Chemical Society.



EED is also similarly effective for fragmenting underivatized and permethylated glycans (Yu et al., 2012; Huang et al., 2016; Tang et al., 2018; Wong et al., 2022). Thus, EED can be combined with LC, where Na⁺-adducted carbohydrates form during ESI due to Na⁺ contamination (Yu et al., 2013; Tang et al., 2018). When combined with porous graphitic carbon-liquid chromatography (PGC-LC), a mixture of three permethylated, high mannose, *N*-linked glycan isomers were identified, showing the effectiveness of EED (Wei et al., 2020). Unlike results with ETD and ECD, EED of both permethylated and underivatized, metal-adducted carbohydrates have formed protonated fragments at moderate intensities (Yu et al., 2013; Wong et al., 2022). EED,

similar to ECD, is still not broadly accessible to researchers, but as shown in Figure 7, EED can be effective at fragmenting metal-adducted carbohydrates.

Electron detachment dissociation (EDD) (Budnik et al., 2001) and negative electron transfer dissociation (NETD) (Coon et al., 2005), which are the negative ion dissociation analogs of EED and ETD, respectively, have been applied to metal-adducted GAGs. However, with EDD and NETD an electron is lost causing a decrease in the charge state in negative-ion mode (Zhurov et al., 2013). As previously discussed, the addition of Na⁺ can stabilize labile sulfate group, which can also be lost during EDD and NETD for GAG ions that lack metal adducts (Wolff et al., 2010). However, unlike CID, EDD and NETD of Na⁺-adducted GAGs have shown that Na⁺ alters the fragmentation mechanism by decreasing the number of cross-ring and glycosidic-bond cleavages. It is hypothesized that the addition of more Na⁺ adducts decreases the proton mobility within EDD and NETD, limiting fragmentation and sulfate loss (Wolff et al., 2008; Wolff et al., 2010; Leach et al., 2017). Although Na⁺-adduction limits fragmentation for GAGs from NETD, the attachment of multiple Na⁺ adducts has improved localization of sulfate modifications since the Na⁺-adduction selectively minimizes sulfate loss fragmentation pathways (Leach et al., 2017).

C. Photon Fragmentation Methods

Photon absorption is another effective method for carbohydrate dissociation. The two most common methods of photon dissociation are ultraviolet photodissociation (UVPD) (Bowers et al., 1984) and infrared multiphoton dissociation (IRMPD) (Woodin et al., 1978). The number of photons required to cause dissociation is related to the energy of the photon and the structure of the analyte. For UVPD, a pulsed laser delivers the photons over a nanosecond timescale to ions in an ion trap, time-of-flight (TOF), quadrupole time-of-flight (QTOF), or FTICR (Brodbelt et al., 2019). UVPD has utilized three wavelengths to fragment metal-adducted carbohydrates effectively

- 157 nm (F₂ laser), 193 nm (ArF laser), and 355 nm (solid state Nd:YAG laser) corresponding to 7.9 eV, 6.4 eV, and 3.5 eV, respectively, per photon (Thompson et al., 2004; Wilson & Brodbelt, 2008; Shaw et al., 2013; Morrison & Clowers, 2017). This energy allows for bonds to be broken with the absorption of a single photon.

General fragmentation mechanisms have been proposed for UVPD; however, the mechanisms are not as well understood as CID or electron-based fragmentation (Julian, 2017). Two mechanisms have been proposed for UVPD of biomolecules. The first mechanism involves the absorbance of a photon, causing excitation of an electron and bond dissociation on the femtosecond timescale (Zabuga et al., 2014). This dissociation mechanism is similar to that of EED with rapid electron migration, enabling the formation of many cross-ring cleavages, as seen with UVPD using 157 nm excitation. The second mechanism relies on the internal conversion of the photon's energy into vibrational modes (Julian, 2017), which leads to dissociation of the weakest bonds. This mechanism is similar to that observed for low-energy CID and is observed for UVPD with 193 nm and 355 nm excitation. Thus, the photon wavelength affects which mechanism is dominant in producing fragments for UVPD.

Metal adduction and the excitation wavelength influence carbohydrate fragmentation by UVPD. The 157 nm excitation has been more successful at creating carbohydrate fragments than 193 nm (Devakumar et al., 2008; Morrison & Clowers, 2017). Na⁺-adducted trisaccharides form many cross-ring and glycosidic cleavages with 157 nm excitation (Zucker et al., 2011). Using 193 nm, only Co²⁺- and Na⁺-adducted tetrasaccharides have been investigated, with Co²⁺ adducts yielding greater fragmentation efficiency than Na⁺ adducts. Although both Co²⁺ and Na⁺ adducts display predominantly glycosidic-bond cleavages, the fragments were detected at low intensities (Morrison & Clowers, 2017). The Clowers group hypothesized that the limited fragmentation

efficiency is related to metal-adducted carbohydrates having few UV absorbing functional groups at 193 nm (Morrison & Clowers, 2017). For Na⁺-adducted glycans and carbohydrates (unmodified or permethylated), more cross-ring cleavages resulted from UVPD at 157 nm than CID (Devakumar et al., 2007; Devakumar et al., 2008; Zucker et al., 2011; Lee et al., 2012). The attachment of fluorophores, such as 6-aminoquinoline (6-AQ), 2-amino-9(10H)-acridone (AMAC), 7-aminomethylcoumarin (AMC), and 2-aminobenzamide (2-AB), resulted in fragments for Na⁺-adducted carbohydrates with 355 nm excitation (Wilson & Brodbelt, 2008). Modifying carbohydrates with fluorophores adds functional groups that can absorb additional wavelengths of light. For Na⁺-adducted, fluorescently labeled carbohydrates, 355 nm excitation increased the glycosidic-bond cleavages compared to CID, but few cross-ring cleavages were detected (Wilson & Brodbelt, 2008).

In IRMPD, precursor ions absorb multiple infrared photons causing fragmentation. IRMPD requires tens to hundreds of photons to be absorbed by the precursor because each photon's energy is approximately 0.1 eV (Brodbelt & Wilson, 2009). IR photon absorption can coincide with collisional cooling, depending on the pressure of the collision cell, which redistributes the absorbed energy to vibrational degrees of freedom, requiring absorption of many photons to sufficiently increase the internal energy and cause dissociation. IRMPD experiments often utilize lasers with fixed wavelengths, such as the 10.6 μm wavelength from a CO₂ laser (Zhang et al., 2005; Adamson & Håkansson, 2007). However, free-electron lasers (FEL) with wavelengths between 5 μm and 250 μm have been used as well (Lancaster et al., 2006; Polfer et al., 2006). IRMPD analysis of carbohydrates has utilized wavelengths between 7 μm and 11 μm at the Free Electron Laser for Infrared Experiments (FELIX) site (Oepts et al., 1995) because metal-adducted and protonated carbohydrates absorb these wavelengths (Polfer et al., 2006).

Mechanistically, IRMPD is expected to form similar fragments as low-energy CID for metal-adducted and protonated carbohydrates (Schemes 2-4). Therefore, like CID, IRMPD can fragment either singly or multiply charged carbohydrates, allowing many different metals or protons to be used as charge carriers. For IRMPD, the absorbance of every photon causes the vibrational redistribution of energy, which enables dissociation through the mobilization of protons (Zhang et al., 2005). If a metal-adducted carbohydrate is fragmented by IRMPD, charge remote fragmentation occurs; however, protonated carbohydrates initiate charge induced fragmentation. Therefore, the IRMPD fragmentation mechanism is influenced by the charge carrier and metal adduct.

Experimentally, IRMPD fragmentation data of carbohydrates is influenced by the metal adduct. Thus, metals with higher charge density and divalent metals with higher second ionization energy induce more cross-ring cleavages. For maltoheptaose and complex-type *N*-linked glycans, more cross-ring cleavages are detected for Co²⁺ adducts compared to Na⁺, H⁺, Mn²⁺, or Ba²⁺ adducts (Adamson & Håkansson, 2007). These extensive cross-ring cleavages are hypothesized to be due to the higher charge densities and second ionization energies of Co²⁺, which is important for increasing the mobility of protons and creating a less stable precursor. Na⁺, Mn²⁺, Ba²⁺, and protonated carbohydrates primarily form glycosidic-bond cleavages using an IRMPD wavelength of 10.6 μm (Zhang et al., 2005; Adamson & Håkansson, 2007; Li et al., 2011). IRMPD was used to distinguish eight disaccharide linkage and anomeric isomers adducted to Li⁺ based on differences in the relative intensities of 11 fragments monitored at wavelengths between 7 μm and 11 μm (Polfer et al., 2006). Of eight Li⁺-adducted disaccharides, only gentiobiose and isomaltose, which are 1-6 linked disaccharides, formed all 11 fragments. Using a wavelength of 9.0 to 9.6 μm, optimal fragment magnitude differences for all 11 fragments were observed (Polfer et al., 2006).

The effective fragmentation of Li⁺-adducted disaccharides is likely due to the charge density of the overall ion and metal being exploited to create unique fragments. These results indicate that the charge density and ionization energy of metals (Table 1) are critical to fragment formation in IRMPD.

D. Gas-Phase IR Spectroscopy

IRMPD spectroscopy (IRMPDS), causes vibrational excitation and dissociation of metaladducted and protonated carbohydrates through the absorption of tens to hundreds of IR photons. IRMPDS uses a similar experimental technique to IRMPD where IR photon absorption redistributes the absorbed energy to available vibrational degrees of freedom of the carbohydrate or glycoconjugate ion. Absorption of photons increases the internal vibrational energy, which causes dissociation of the lowest energy bonds through intramolecular proton transfer reactions. The main difference to IRMPD is that many wavelengths are examined with IRMPDS, causing wavelength-dependent photofragmentation to occur with carbohydrates based on the vibrational excitation modes for gas-phase structures. This allows for the formation of IRMPDS spectra in terms of wavelength as opposed to IRMPD, which monitors the magnitude of m/z of fragments. IRMPDS uses an optical parametric oscillator (OPO) (Gulyuz et al., 2011) or FEL available at FELIX (Oepts et al., 1995) or "Collaboration pour un Laser Infrarouge à Orsay" (CLIO) (Lemaire et al., 2002). The unique gas-phase structures of metal-adducted or protonated carbohydrates are monitored over a selected wavenumber range, typically between 2700 cm⁻¹ and 3700 cm⁻¹, to examine vibrational stretching modes of C-H (~2840-3000 cm⁻¹), N-H (~3100-3400 cm⁻¹), and O-H (~3400-3700 cm⁻¹) bonds found in carbohydrates (Pearson et al., 2015; Barnes et al., 2020). Experimental data and computational calculations have suggested that the charge carrier significantly influences C-H, N-H, and O-H bond stretching modes (Pearson et al., 2015; Barnes

et al., 2017). C-C stretching (~900-950 cm⁻¹), C-O stretching (~970-1200 cm⁻¹), C-OH bending (~1200-1500 cm⁻¹), and C=O stretching (~1700 cm⁻¹) have also been examined with IRMPDS (Contreras et al., 2012; Gamez et al., 2013). However, examining C-C stretching, C-O stretching, and C-OH bending could not differentiate different group I metals adducted to α-cyclodextrin (CD) (Gamez et al., 2013). Photofragmentation yield, which is based on the fragmentation efficiency of the analyte at different wavelengths, is calculated based on the combined intensity of the fragments and the remaining intensity of the precursor using a modified version of the Beer-Lambert law and is used to generate IRMPDS spectra (Barnes et al., 2017).

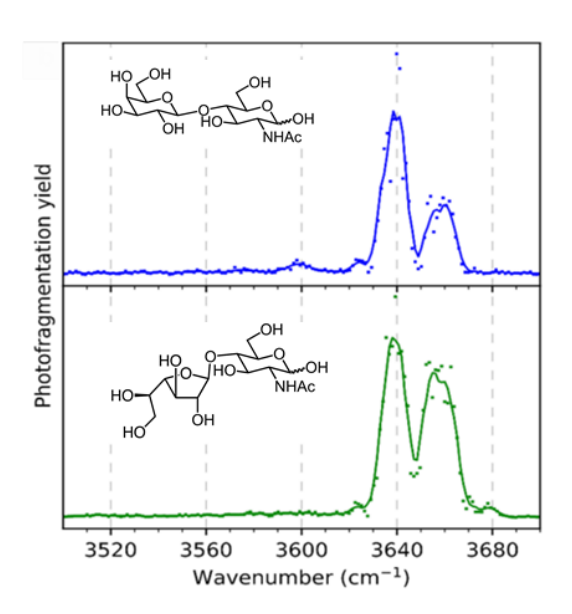
The energy of the laser pulses impacts the charge carriers that can be examined with IRMPDS. IRMPDS spectra have typically used \sim 5 to 10 Hz lasers with \sim 10 to 60 mJ pulses; therefore, recording the spectra can take \sim 40 minutes based on the low repetition rate of the laser pulses (Pearson et al., 2015; Barnes et al., 2017). The energy of these laser pulses has allowed for monitoring the photodissociation of group I metal-adducted carbohydrates (Valle, 2005). Recent developments have used lasers with higher repetition rates (kHz) and lower energy per laser pulse (1 μ J), which still provides detectable dissociation but allows for the same spectrum to be acquired in just 1 minute (Yeni et al., 2022). However, using kHz lasers with 1 μ J of energy per laser pulse has limited these rapid IRMPDS analyses to protonated carbohydrates because of the lower energy requirements to induce detectable fragmentation with protonated carbohydrates compared to metal-adducted carbohydrates (Yeni et al., 2022).

The fragment ions that are monitored with IRMPDS to obtain an IRMPDS spectra are also influenced by the charge carrier. For example, with Rb⁺-adducted monosaccharides, the only fragment detected is the metal ion (Pearson et al., 2015). However, for Li⁺ or protonated species, glycosidic cleavages, cross-ring cleavages, and dehydration products can be detected to monitor

the photofragmentation yield (Tan et al., 2017; Yeni et al., 2022). This data suggests that with larger ionic radii metals, which have a lower charge density, fewer fragment ions can be monitored to determine the photofragmentation efficiency.

IR spectra, collected from IRMPDS, are dependent on the charge carrier for carbohydrate analyses since coordination between the charge carrier and carbohydrate hydroxyls alters the vibrational energy, which changes the vibrational frequencies that cause dissociation. Pyranose and furanose rings of Li⁺-adducted galactose were distinguished based on gas-phase IR spectra (Ho et al., 2021). Figure 8 shows IRMPD spectra between 3500 cm⁻¹ and 3700 cm⁻¹ for Li⁺-adducted disaccharides with differences in OH stretching. The differences in peak intensities are due to differences in metal-adduction changing the photofragmentation efficiency, which relates to the available vibrational modes for photon absorption of the isomers. In comparison, protonated disaccharides containing galactose as pyranose and furanose rings could be differentiated, but the protonated monosaccharides could not be.

Figure 8. This figure displays the IRMPD spectra for Li⁺-adducted disaccharides, βGalp(1-4)-GlcpNAc (top) in blue and βGalf(1-4)-GlcpNAc (bottom) in green. [Color figure can be viewed at wileyonlinelibrary.com] Adapted with permission from Ho, J. S., *et. al.* Distinguishing Galactoside Isomers with Mass Spectrometry and Gas-Phase Infrared Spectroscopy. *J. Am. Chem. Soc.* 2021, 143, 28, 10509-10513. Copyright 2021 American Chemical Society.



IRMPDS is limited by spectral broadening, as seen in Figure 8, which has limited the analysis of metal-adducted and protonated carbohydrate adducts larger than trisaccharides (Tan et al., 2017; Depland et al., 2018; Schindler et al., 2018; Ho et al., 2021). Spectral broadening creates broad Gaussian peaks that make it challenging to attribute bond vibrations to specific IR wavelengths, which in turn limits the ability to distinguish isomers based on differences in gasphase structure. Increased spectral broadening is hypothesized to be due to heterogeneity within the gas-phase ion population (Yalovenko et al., 2020). Spectral broadening also occurs due to the heating of the ions through the acceptance of multiple photons to induce fragmentation, which causes the ion to lose its original gas-phase structure (Valle, 2005). Past work has examined H⁺, Li⁺, Na⁺, K⁺, Rb⁺, and Cs⁺ carbohydrate adducts with IRMPDS (Pearson et al., 2015; Schindler et al., 2017; Depland et al., 2018; Ho et al., 2021). Metals with larger ionic radii coordinate with additional oxygens, as seen with Rb⁺, and require higher energy laser pulses to induce dissociation. Higher energy laser pulses create additional internal energy that can be distributed into accessible vibrational modes, causing peak broadening. Thus, analysis of protonated and Li⁺-adducted

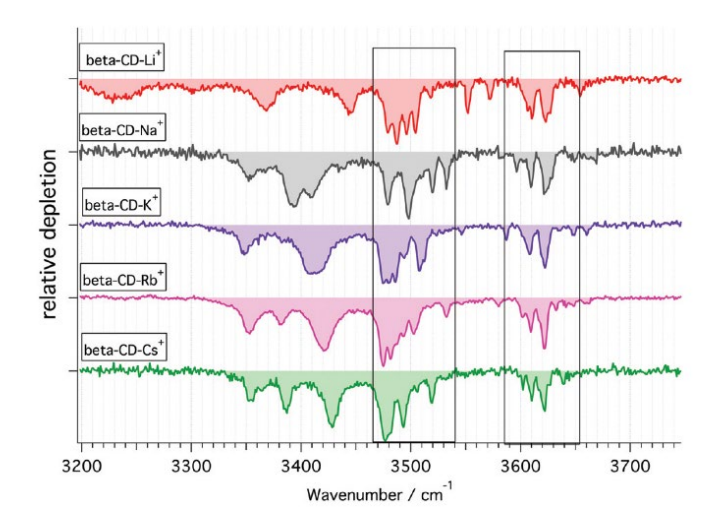
carbohydrates using lower energy pulses that can induce dissociation with limited peak broadening is preferred (Pearson et al., 2015; Tan et al., 2017; Yeni et al., 2022).

With cryogenic IR, spectral broadening can be minimized compared to room-temperature gas-phase IRMPDS, allowing for analysis of glycans with up to 10 monosaccharide subunits (Yalovenko et al., 2020). There are two methods for performing cryogenic IR. Both cryogenic IR spectroscopy techniques can use tunable OPO lasers or FEL. The first technique, known as messenger tagging, involves cooling gas-phase ions to 40 K by tagging them with cold, gaseous N_2 , He, or H_2 , forming a weakly bound complex that is detected by a shift in m/z (Kamrath et al., 2011; Masellis et al., 2017). An IR laser is focused on trapped, weakly complexed ions, causing dissociation of the complex with the absorption of a single photon. Like IRMPDS, the absorption of the photon at a given wavelength using messenger tagging is dependent on the accessible vibrational modes of the gas-phase ion, which causes dissociation of the complex and is minimally impacted by the weakly complexed ions. Dissociation of the tagged complex is observed by an increase in the peak intensity of the untagged ions and a decrease in the peak intensity for the tagged ions (Masellis et al., 2017). The cryogenic IR spectrum is acquired by plotting the ratio of tagged ions versus the sum of the tagged and untagged ions as a function of the laser wavelength. Since similar vibrational modes are investigated with messenger tagging compared to IRMPDS, similar wavenumbers between 2700 cm⁻¹ and 3700 cm⁻¹ are examined to dissociate the tagged complex (Warnke et al., 2021). The second technique encapsulates the ions within helium nanodroplets, which cools the ions to ~0.37 K. The ions are released from the nanodroplets after absorption of multiple IR photons if the photon wavelength is in resonance with the vibrational excitation modes of the ion (Smolarek et al., 2010; Mucha et al., 2017). The ejection of cold ions from helium nanodroplets is monitored by examining the intensity of the m/z of the analyte of interest at varying wavelengths. Analysis of helium nanodroplets utilizes 1000 cm⁻¹ to 2000 cm⁻¹ wavenumbers to monitor vibrational modes that are distinct from those commonly analyzed with either messenger tagging or IRMPDS (Mucha et al., 2017). The wavenumbers examined with helium nanodroplets are related to vibrational modes of C-O and coupled C-O-C-O stretches that are detected from 950 cm⁻¹ to 1200 cm⁻¹. O-H-bending vibrations are also monitored using helium droplets from 1200 cm⁻¹ to 1500 cm⁻¹ (Mucha et al., 2017). The cold temperature of cryogenic IR from the messenger tags or helium droplets causes evaporative cooling and minimizes conformational flexibility when interacting with photons, which increases spectral resolution compared to IRMPDS (Mucha et al., 2017).

Cryogenic IR spectroscopy results are influenced by the charge carrier. Additional gasphase interactions are associated with metals having larger ionic radii, as can be seen in Figure 9 for β-CD adducted to Li⁺, Na⁺, K⁺, Rb⁺, and Cs⁺ (Rabus et al., 2021). Computational data has shown that metals with large ionic radii interact with more oxygen atoms than metals with small ionic radii (Cancilla et al., 1996; Bythell et al., 2017). These additional OH vibrational modes lead to additional IR peaks, as seen with three significant peaks for Rb⁺- and Cs⁺-adducted β-CD compared to just two significant peaks for Li⁺-, Na⁺-, and K⁺-adducted β-CD at wavenumbers between 3350 to 3450 cm⁻¹ (Figure 9). This additional peak is hypothesized to be generated from additional binding interactions between the C6 hydroxyls and the large ionic radii metals. Protonated carbohydrates are often preferred for cryogenic IR spectroscopy when examining large *N*-linked glycans because of the less convoluted IR spectra compared to metal adduction (Dyukova et al., 2020). It is possible that because a proton has a smaller ionic radius than any metal, H⁺ would interact with fewer oxygen atoms, minimizing the number of the vibrational modes compared to the large number possible for larger glycans and HMOs with metal adducts, forming fewer IR

peaks. However, because of the ubiquitous nature and preference of carbohydrates binding Na⁺, as previously discussed, many publications using cryogenic IR have mainly focused on Na⁺-adducted carbohydrates, which have still provided distinct cryogenic IR spectra for distinguishing several isomeric carbohydrates and HMOs (Ben Faleh et al., 2019; Warnke et al., 2019; Abikhodr et al., 2021; Warnke et al., 2021).

Figure 9. The figure shows the cryogenic IR spectra for β-CD adducted to group I metals, including Li⁺ (red, top), Na⁺ (grey), K⁺ (purple), Rb⁺ (pink), and Cs⁺ (green, bottom). [Color figure can be viewed at wileyonlinelibrary.com]. The two marked rectangles display the transitions for carbon-2 (C2) and carbon-3 (C3) hydroxyl (OH) bond stretching. Reproduced from Rabus, J. M., *et. al.* Unravelling the structures of sodiated β-cyclodextrin and its fragments. *Phys. Chem. Chem. Phys.* 2021, 23, 24, 13714-13723, with permission from the Royal Society of Chemistry.



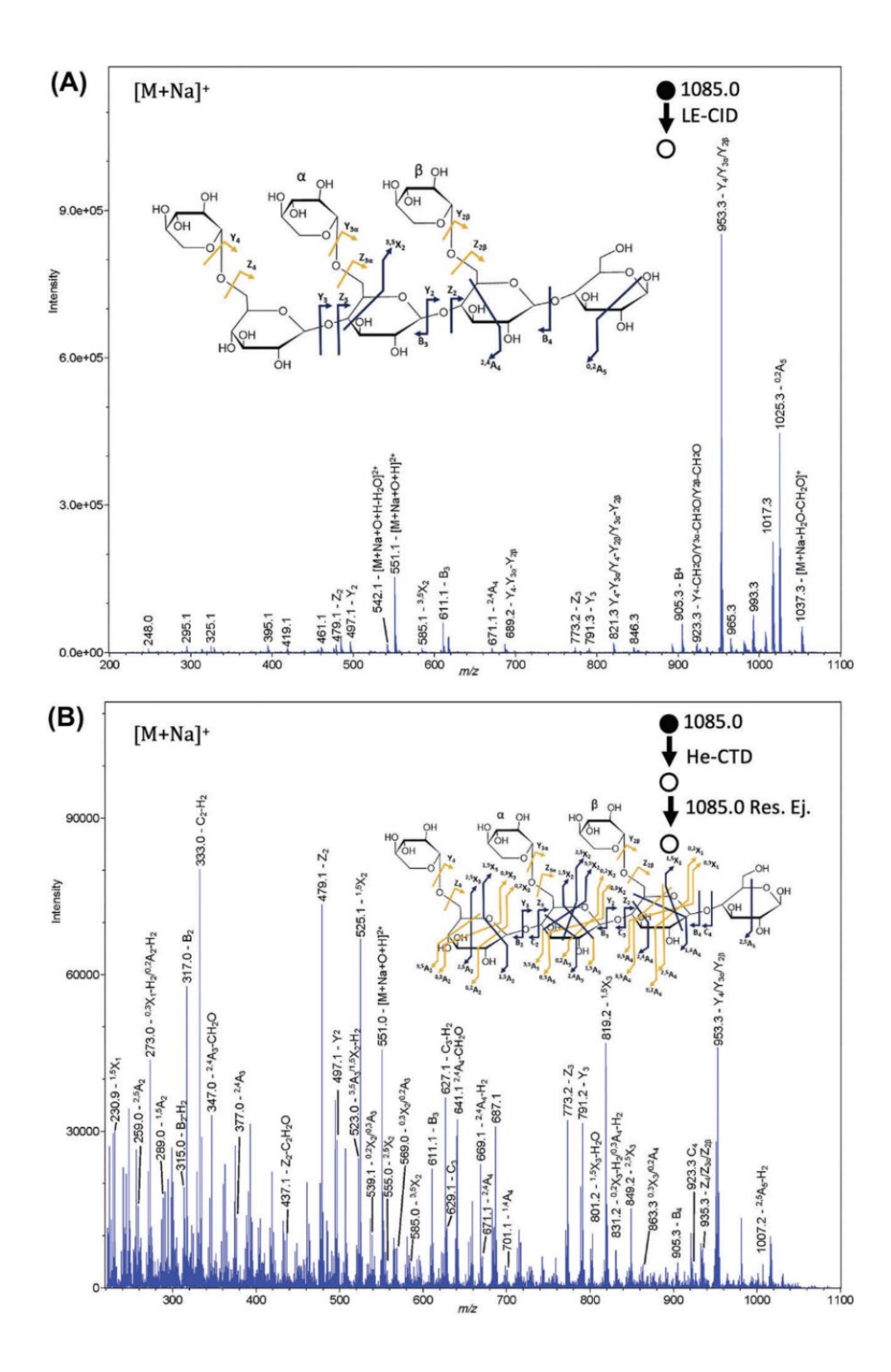
E. Charge Transfer Dissociation

Charge transfer dissociation (CTD) (Chingin et al., 2014) has demonstrated highly effective fragmentation of metal-adducted carbohydrates. In CTD, a plasma is generated by applying microwave energy to a neutral gas (Chingin et al., 2014; Hoffmann & Jackson, 2014).

Electrons are then abstracted from the plasma, forming a cation beam that collides with precursor ions in a trap to induce dissociation. Helium has become the preferred gas for CTD because it has the highest known electron affinity for a singly charged ion (Hoffmann & Jackson, 2014). Therefore, all published data fragmenting carbohydrates has used helium-CTD (He-CTD).

All metal-adducted carbohydrates have shown similar results with extensive cross-ring cleavages (Sasiene et al., 2021), indicating that He-CTD is independent of the metal ion forming the adduct. He-CTD analysis of a branched heptasaccharide with two Na⁺ adducts, one K⁺ and one H⁺, or one Mg²⁺, produced both 2+ and 1+ fragments (Sasiene et al., 2021). These He-CTD results showed similarities to EED since fragments from both techniques are detected with a mixture of charge states (Yu et al., 2012; Sasiene et al., 2021). Figure 10 shows a comparison of the fragments formed from Na⁺-adducted XXXG xyloglucan, which is a polysaccharide found in plant cell walls, from both low-energy CID and He-CTD, respectively. Figure 10 shows that though both He-CTD and low-energy CID have high fragmentation efficiencies for Na⁺-adducted XXXG xyloglucan, many additional cross-ring cleavages are formed with He-CTD. These results indicate that He-CTD is a promising fragmentation technique that can readily produce distinct fragments from carbohydrates with low charge density metals, such as Na⁺. The fragmentation mechanism for He-CTD is not well understood, unlike the previously discussed fragmentation techniques. However, the He-cation beam likely interacts with carbon or oxygen atoms to form diradicals, which may be necessary to form abundant cross-ring cleavages. He-CTD has been hypothesized to occur by initiating radical cleavages at an energy of 6 keV, which can overcome the electrostatic barrier associated with interactions between cationic He and cationic analytes (Hoffmann & Jackson, 2014).

Figure 10. Comparison of (A) low-energy CID and (B) He-CTD fragmentation of Na⁺-adducted XXXG xyloglucan. The precursor ion with 1085.0 *m/z* was fragmented for both methods. Dark blue arrows indicate unambiguous fragment identities; yellow arrows indicate ambiguous fragment identities caused by alternative isomeric product ions. [Color figure can be viewed at wileyonlinelibrary.com] Reprinted with permission from Sasiene, Z. J., *et. al.* Charge transfer dissociation of a branched glycan with alkaliand alkaline earth metal adducts. *J. Mass Spectrom.* 2021, 56, 7, e4774, from John Wiley & Sons. Copyright John Wiley & Sons, Ltd.



He-CTD is promising for differentiating isomeric carbohydrates because fragmentation is independent of the metal adduct used for analysis. He-CTD can fragment singly or multiply charged ions, allowing for the analysis of Na⁺, K⁺, Mg²⁺, and Ca²⁺-adducted carbohydrates. Na⁺-adducted tetra- and penta-saccharides result in significant cross-ring cleavages, which can be used to distinguish 1-3 and 1-4 linkage isomers using CTD (Buck-Wiese et al., 2020). For example, fragmentation of Na⁺-adducted cellulose and lamarin, with five degrees of polymerization or five glucose subunits (DP5) that differ solely in linkage position, produced glycosidic-bond cleavages and diagnostic cross-ring cleavages. Although few publications exist using He-CTD, these results suggest that He-CTD could become a useful tool for distinguishing isomeric, metal-adducted carbohydrates if more broadly accessible to the MS community.

F. Tandem Fragmentation Methods

In tandem fragmentation, two events are combined with the secondary fragmentation event occurring either simultaneously with the primary event or up to several milliseconds afterward. Additionally, the fragmentation events can occur in the same or different mass analyzers (Horn et al., 2000; Ledvina et al., 2009; Frese et al., 2013). Thus, these events can occur simultaneously or be separated by time and/or space in the instrument.

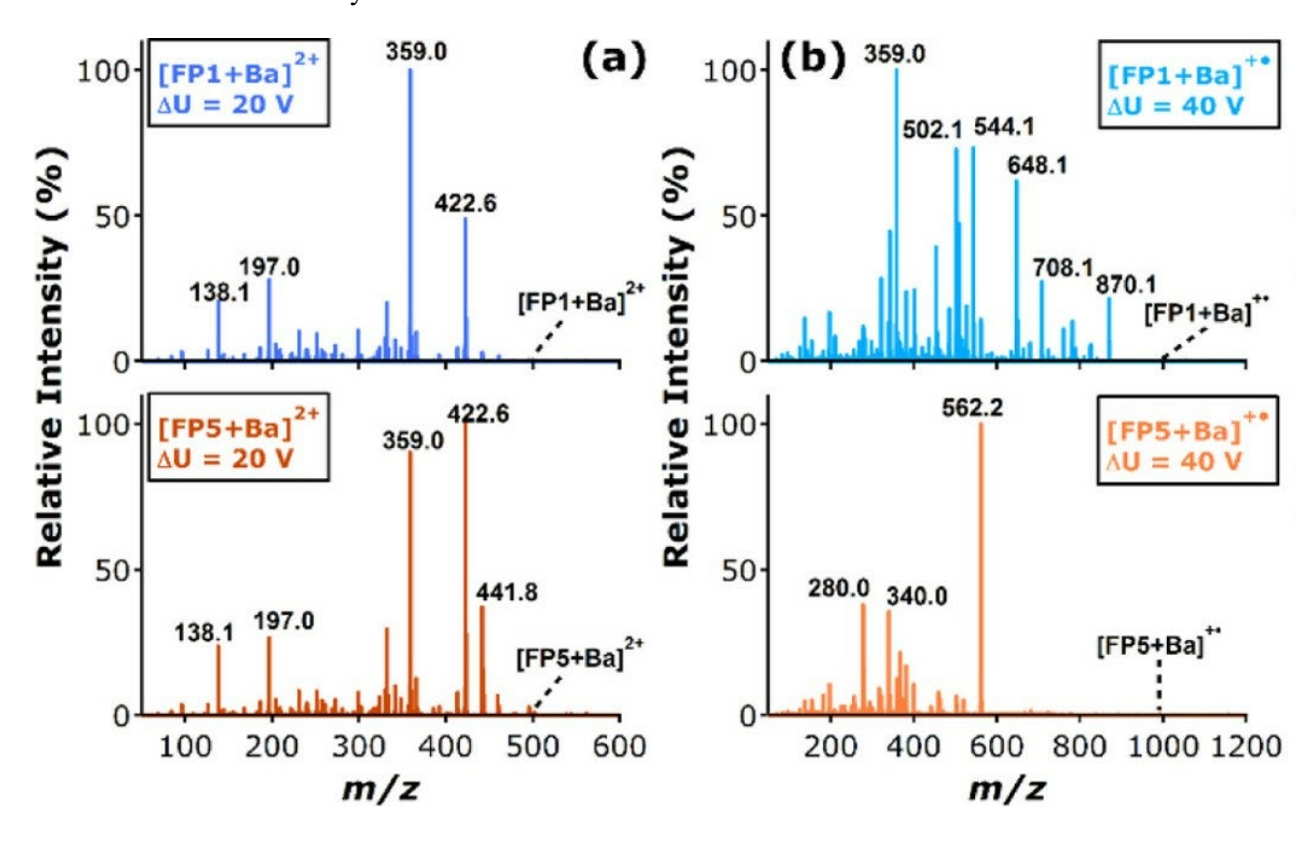
Multi-stage collision-induced dissociation (CIDⁿ) involves using multiple CID events to repeatedly fragment a precursor ion or to selectively fragment products of an initial CID event. CIDⁿ can also be defined as collision-induced dissociation to the 2nd (CID²) or the 3rd (CID³) to specify the number of fragmentation events. CIDⁿ has been highly effective for fragmenting carbohydrate adducts with low charge density metals (Na⁺) and protonated carbohydrates, which have been the primary charge carriers published using CIDⁿ (Sheeley & Reinhold, 1998; Weiskopf et al., 1998; Mookherjee et al., 2018; Mookherjee et al., 2020). Because initial CID fragments are

predominantly glycosidic-bond cleavages, additional cross-ring and glycosidic-bond cleavages have been observed for H⁺- and Na⁺-adducted carbohydrates (underivatized or permethylated) using CID² and CID³, improving the capability to distinguish isomers (Weiskopf et al., 1997; Sheeley & Reinhold, 1998; Mookherjee et al., 2020).

Electron transfer collision-induced dissociation (ETciD) and electron transfer higherenergy collision dissociation (EThcD) (Frese et al., 2012) combine ETD with CID. These techniques involve the initial ion/ion reaction, followed by low-energy collisional activation to fragment ions that do not dissociate due to non-covalent interactions. The electron transfer no dissociation (ETnoD) product can yield an intense signal compared with detected fragments from the initial ion/ion reaction (Huang & Dodds, 2015; Schaller-Duke et al., 2018). Therefore, ETnoD limits the ability to distinguish isomeric carbohydrates. The addition of vibrational energy to ETnoD products can cause charge reduced species to dissociate into distinct fragments. Isomeric HMOs adducted to Ba²⁺ or Ca²⁺ have been distinguished with ETciD (Huang & Dodds, 2015). Ba²⁺ adducts of two pentasaccharide isomers, lacto-N-fucopentaose (LNFP) I and V (see Figure 3), have similar CID spectra, as shown in Figure 11A. However, CID fragmentation of the ET products of the Ba⁺•-adducted isomers yield distinct fragmentation products, allowing for the isomers to be distinguished (Figure 11B). ETciD has shown similar improved fragmentation for Ca²⁺-adducted HMOs (Huang & Dodds, 2015). The supplemental vibrational activation in EThcD and ETciD can increase fragment detection for low charge density, divalent metals (Table 1), such as Ca²⁺ and Ba²⁺. Though it has not been tested, the fragmentation of carbohydrate complexes with divalent transition metals might benefit from EThcD and ETciD as well. Divalent transition metals have higher charge densities, but significant ETnoD is seen for Co²⁺-adducted maltotetraose

(Figure 6). Therefore, EThcD and ETciD are valuable tandem fragmentation techniques that address the problem of ETnoD for specific metal adducts.

Figure 11. Comparison of CID and ETciD fragmentation of Ba²⁺-adducted LNFP I (top) and LNFP V (bottom). **(A)** CID fragmentation spectra for Ba²⁺-adducted carbohydrates. **(B)** ETciD fragmentation spectra for the same Ba²⁺-adducted isomers. ΔU represents the collision voltage applied to the ions to induce fragmentation. Adapted with permission from Huang, Y.; Dodds, E. D. Discrimination of Isomeric Carbohydrates as the Electron Transfer Products of Group II Cation Adducts by Ion Mobility Spectrometry and Tandem Mass Spectrometry. *Anal. Chem.* 2015, 87, 11, 5664-5668. Copyright 2015 American Chemical Society.



G. Fragmentation and IRMPDS/cryogenic IR Spectroscopy

IRMPDS has also been combined with CID to gain additional structural information that cannot be obtained with a single technique. CID has been combined with IRMPDS by performing CID in the same linear ion trap (LIT) as IRMPDS (Schindler et al., 2017). IRMPDS has shown that following CID fragmentation, anomeric linkage information is retained in gas-phase structures. This allows for larger carbohydrate systems to be identified based on consistent IRMPDS spectra of the fragments, which can be reliably confirmed using available monosaccharide standards (Schindler et al., 2017). These standards are often not available for larger carbohydrate systems, which has limited structural validation to fragments. Researchers found that the IR spectra of protonated and Li⁺-adducted fragments could be matched to the IR spectra of protonated and Li⁺-adducted monosaccharides with matching anomeric states. It has yet to be investigated if other metal adducts enable analysis of anomeric memory using IRMPDS.

Combining the techniques of cryogenic IR and CID has enabled the validation of the CID fragmentation mechanisms for Na⁺-adducted carbohydrates by comparing the IR spectra for glycosidic cleavage fragments with disaccharide and monosaccharide standards. Additionally, cryogenic IR spectra have been compared to computational predictions to determine the most probable structures of B₂ - B₄ ions (Rabus et al., 2021). In these experiments, CID has also been implemented with cryogenic IR spectroscopy using a hexapole before the cryogenic IR spectroscopy (Pellegrinelli et al., 2020; Rabus et al., 2021). These examples demonstrate the utility of cryogenic IR spectroscopy and IRMPDS in tandem with CID to effectively examine the mechanisms of glycosidic cleavages for Na⁺-adducted carbohydrates. When used in tandem, these two techniques offer complimentary structural details of metal-adducted carbohydrates, which is valuable for distinguishing carbohydrate isomers.

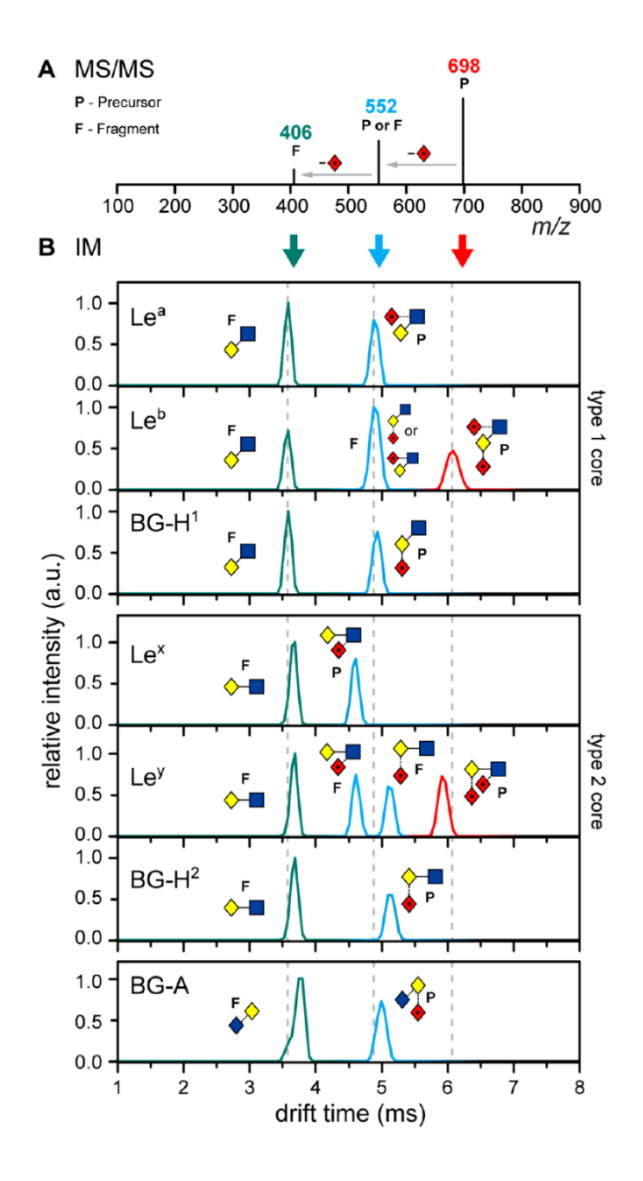
VI. IMS Coupled with Fragmentation

IMS and fragmentation can be combined to acquire structural information that cannot be determined by either technique individually. Fragmentation can occur either before or after IMS. Though multiple fragmentation techniques can be coupled with IMS, CID is the most common (Hofmann et al., 2017; Ujma et al., 2019). Here, we will examine applications of CID, ETD, EED, or UVPD with IMS for structural analysis of carbohydrates.

CID is often applied before IMS because disaccharides are easier to resolve than larger saccharides when using low resolving power IMS (Huang & Dodds, 2013; Hofmann et al., 2017). Na⁺ is the most commonly used metal adduct for tandem CID and IMS experiments because highintensity fragments from glycosidic bond cleavages result, which can be more easily monitored than divalent metal adducts that form more extensive mixtures of moderate-intensity fragments (Schaller-Duke et al., 2018). Blood group tri- and tetra-saccharides, HMOs, and parotid gland Nlinked glycans adducted to Na⁺ have been distinguished using CID before TWIMS (Hofmann et al., 2017). Figure 12 shows the drift times of Na⁺-adducted tri- and tetra-saccharide precursors and glycosidic-bond cleavage fragments. The drift times and CCS values for glycosidic cleavage fragments are the same when the same type 1 or type 2 core-structure fragments are formed from different fucose-linked isomeric precursors (Hofmann et al., 2017). Evaluating and distinguishing the drift times and CCS values for core structures allows for the formation of diagnostic drift times and CCS values that can be used to differentiate larger and complex isomeric N-linked glycans and HMOs. Li⁺-adducted carbohydrates have been fragmented by CID, resulting in both glycosidicbond and cross-ring cleavage fragments that can be monitored by high-resolution cIMS (Ollivier et al., 2021; Ollivier et al., 2021a). Using Li⁺-adducted carbohydrates has enabled cIMS separation of both cross-ring and glycosidic cleavage fragments, enabling differentiation of isomeric

carbohydrates within a set of 33 carbohydrates (Ollivier et al., 2021a). Similar to results with Na⁺, Li⁺-adducted fragments formed diagnostic CCS values for certain fragments allowing for differentiating anomeric pentasaccharide isomers. Although publications have shown that drift times of protonated fragments can be used to distinguish disaccharide linkage isomers (Mookherjee et al., 2020), tandem CID with IMS is challenging for protonated carbohydrates because fucose migration can occur (Harvey et al., 2002). Recent experiments using TWIMS after CID have also shown that linkage memory exists for protonated carbohydrates (Mookherjee et al., 2020). Here, linkage memory describes the retention of the precursor linkage position and/or stereochemistry, following glycosidic-bond dissociation by CID. The Guttman group determined that 1-6 linkages of protonated disaccharides could be differentiated from 1-3 and 1-4 linkages based on the ATD of protonated Y₁ fragments. This work was done with low resolution TWIMS and could not differentiate the 1-3 and 1-4 linkage based on the ATD of the protonated Y₁ fragments.

Figure 12. CID fragmentation spectra and drift times of eight Na⁺-adducted Lewis and blood group carbohydrates. (A) CID spectra of the Na⁺-adducted precursor (P) and fragment (F) ions. Fragments ions (F) are the result of fucose loss from precursor ions at 698 *m/z* (red) or 552 *m/z* (blue). (B) IMS arrival time distributions of Na⁺-adducted Lewis and blood group precursor (P) and fragment (F) ions resulting from CID. Colors in the IMS distributions (B) correlate with the *m/z* values presented in the MS/MS spectrum (A). [Color figure can be viewed at wileyonlinelibrary.com] Reprinted with permission from Hofmann, J., *et. al.* Identification of Lewis and Blood Group Carbohydrate Epitopes by Ion Mobility-Tandem-Mass Spectrometry Fingerprinting. *Anal. Chem.* 2017, 89, 4, 2318-2325. Copyright 2017 American Chemical Society.



When CID is applied after IMS, the structures of different gas-phase conformations can be analyzed (Ujma et al., 2019). With the development of high-resolution cIMS, three gas-phase conformations of three different Na $^+$ -adducted pentasaccharides could be detected, though only a single conformation was observed with lower resolution IMS. The three gas-phase conformations correlate to an open ring reducing end monosaccharide and two closed rings representing the α and β anomeric configuration of the reducing end monosaccharide for each analyzed

pentasaccharide. These structures were supported by detecting unique cross-ring cleavages for the open-ring conformation, which were not detected for either closed-ring conformation of cello- or malto-pentaose (Ujma et al., 2019). The third pentasaccharide (mannopentaose) is branched, which limited the ability to create unique cross-ring cleavages by CID for validating the open-ring conformation, as seen with the Na⁺-adducted linear pentasaccharides (cello- and malto-pentasse). High-resolution cIMS has been used to examine Na⁺-adducted HMO di- and tri-saccharides (Peterson & Nagy, 2021). CID was conducted post-IM to distinguish Na⁺-adducted linkage isomers, resulting in different fragments with varying intensities (Peterson & Nagy, 2021). CID fragmentation after IMS can also distinguish mixtures of Co²⁺-adducted tetrasaccharide homo- and hetero-dimers of the form [2M + Co]²⁺, where M is identical glycans or isomers, respectively (Morrison et al., 2018). Co²⁺ produced unique fragments, allowing for six tetrasaccharide heteroand homo-dimers to be separated. Although IMS could separate the monomers from the dimers based on drift times, the homo- and hetero-dimers could not be distinguished without CID. Overall, IMS combined with CID can improve the structural analysis of isomeric carbohydrates from complex mixtures using different metal-ion adducts.

Electron transfer reactions generate unique gas-phase structures that can be analyzed by IMS. As previously stated, ET does not always cause dissociation (ETnoD), and the charge reduced products can be separated from other charge reduced isomers via IMS. Carbohydrate isomers were adducted to group I metals, group II metals, or charge reduced group II metals formed by ETnoD, and CCS values were measured using TWIMS (Huang & Dodds, 2015a). Charge reduced Ca^{+•}, Mg^{+•}, and Ba^{+•} allowed for better separation of ETnoD products of tri-, penta- and hexa-saccharides compared to Ca²⁺, Mg²⁺, and Ba²⁺ adducts. As a general trend, Group I metal adducts of Na⁺, Li⁺, and K⁺ without ET were more effective for separating trisaccharides and

hexasaccharides than charge reduced group II metals (Huang & Dodds, 2015a), although, Ba^{+•} was more effective at separating the pentasaccharides than Na⁺, Li⁺, and K⁺ based on the CCS values. These results highlight the effects of the metal ionic radius and charge density changes after the ion/ion reaction. Specifically, different metals have unique interactions with the anion reagent, forming distinct gas-phase structures compared to the 2+ or 1+ metal adducts, as seen by differences in CCS values (Huang & Dodds, 2015a).

Although EED is minimally influenced by the metal ion, when EED is applied post-IMS, isomeric carbohydrates can be distinguished (Pu et al., 2016). As previously mentioned, EED is beneficial for detecting fragments from carbohydrate adducts with low charge density metals (Table 1), such as Na⁺ (Yu et al., 2012). TIMS allowed for quick baseline separation of Na⁺-adducted HMOs, LNT and LNnT, followed by the generation of unique cross-ring cleavages using EED, which were not generated by CID, ECD, or ETD (Pu et al., 2016).

UVPD has also been utilized post-IMS to fragment individual, Na⁺-adducted di- and trisaccharides (Zucker et al., 2011; Lee et al., 2012). Though low resolution IMS could not resolve a mixture of seven isomeric Na⁺-adducted disaccharides, UVPD yielded fragments with unique cross-ring cleavages of the Na⁺-adducted gas-phase precursor ions, allowing for all seven disaccharides to be distinguished (Lee et al., 2012).

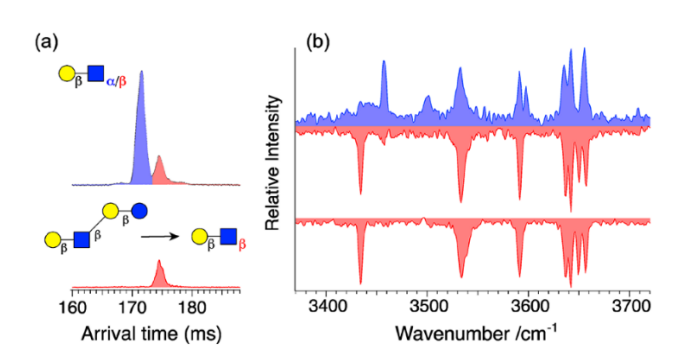
Cryogenic IR-spectroscopy has been combined with CID and/or IMS, providing complementary information regarding carbohydrate structure (Bansal et al., 2020; Rabus et al., 2021). CID has been combined with cryogenic IR spectroscopy and IMS using a module allowing CID to occur in an isolated portion of a SLIM device after precursor IMS separation of all ions, but before recording a cryogenic IR spectrum (Bansal et al., 2020). Since CID is done within the SLIM device, IMS can also be used to separate the fragments before recording the cryogenic IR

spectra. CID occurs by constructing a quadrupole ion trap-like structure along the SLIM path to trap the ions by applying a DC voltage at the front and back of the trap. Then by increasing the RF and DC voltage of all electrodes in the trap, the ions accelerate as the ions move out of the trap and back onto the main SLIM separation path, increasing the occurrence of collisions with the nitrogen buffer gas and yielding fragmentation (Webb et al., 2016; Bansal et al., 2020).

Combining CID, IMS, and cryogenic IR spectroscopy can further enhance the ability to distinguish isomeric metal-adducted carbohydrates, which cannot be distinguished using CID or low resolution IMS. Evidence of consistent IR fingerprints and anomeric memory of Na⁺-adducted fragments was shown using cryogenic IR spectroscopy after IMS separation of the precursor followed by CID and finally IMS separation of the fragments (Bansal et al., 2020). Here, anomeric memory was shown by examining the cryogenic IR spectra and IMS arrival times from the Na⁺-adducted C_2 fragment of LNnT and comparing the spectra and arrival times for standards of Gal β 1-4GlcNAc with α or β reducing ends. A consistent IR spectral fingerprint with a unique peak at \sim 3435 cm⁻¹ and arrival time of \sim 175 ms for both the Na⁺-adducted C_2 fragment of LNnT and the β -reducing end standard of Gal β 1-4GlcNAc validated the anomericity of the glycosidic bond, as shown in Figures 13 (Bansal et al., 2020).

Figure 13. (A, top) Arrival times are shown for the Na⁺-adducted Gal β 1-4GlcNac with α (blue) or β (red) anomeric conformations at the reducing end of the carbohydrate. (A, bottom) Arrival times of the Na⁺-adducted Gal β 1-4GlcNac fragment (red), resulting from fragmentation of LNnT. The disaccharide with the β configuration at the reducing end (A, bottom in red) has the same arrival time as that of the standard (A, top in red). (B, top) Cryogenic IR spectra for Na⁺-adducted Gal β 1-4GlcNac standard with either the α (blue) and β (red) anomeric conformation at the disaccharide reducing end. (B, bottom in red) The cryogenic IR spectra of the Na⁺-adducted Gal β 1-4GlcNac fragment from LNnT matches the spectra for

the disaccharide standard with the β configuration at the reducing end (B, top in red). [Color figure can be viewed at wileyonlinelibrary.com] Reprinted with the permission from Bansal, P., *et. al.* Using SLIM-based IMS-IMS Together with Cryogenic Infrared Spectroscopy for Glycan Analysis. *Anal. Chem.* 2020, 92, 13, 9079-9085 (https://pubs.acs.org/doi/10.1021/acs.analchem.0c01265). Further permission related to the material excerpted should be directed to the American Chemical Society.



VII. Hydrogen/deuterium exchange mass spectrometry

Hydrogen/deuterium exchange (HDX) experiments have been used to determine the number of labile hydrogens within molecules and to characterize molecular conformations (Bai et al., 1993; Katta & Chait, 1993; Wales & Engen, 2006; Konermann et al., 2011; Gallagher & Hudgens, 2016). Labile hydrogen atoms attached to oxygen, nitrogen, and sulfur can exchange with deuterium from deuterating reagents (*e.g.*, deuterated ammonia (ND₃), deuterium oxide (D₂O), deuterated methanol (CH₃OD), *etc.*) in either solution or the gas phase. Integrating HDX with MS allows the quantity of deuterium exchange to be measured due to the mass difference of the labeled and unlabeled analytes. Molecular conformations can be monitored by HDX because exchange rates are dependent not only on the exchanging functional group, but also on their accessibility to the deuterating reagent. Thus, three-dimensional conformations can be

characterized and molecular regions that are highly structured will take longer to exchange in comparison to less structured regions (Linderstrom-Lang, 1958).

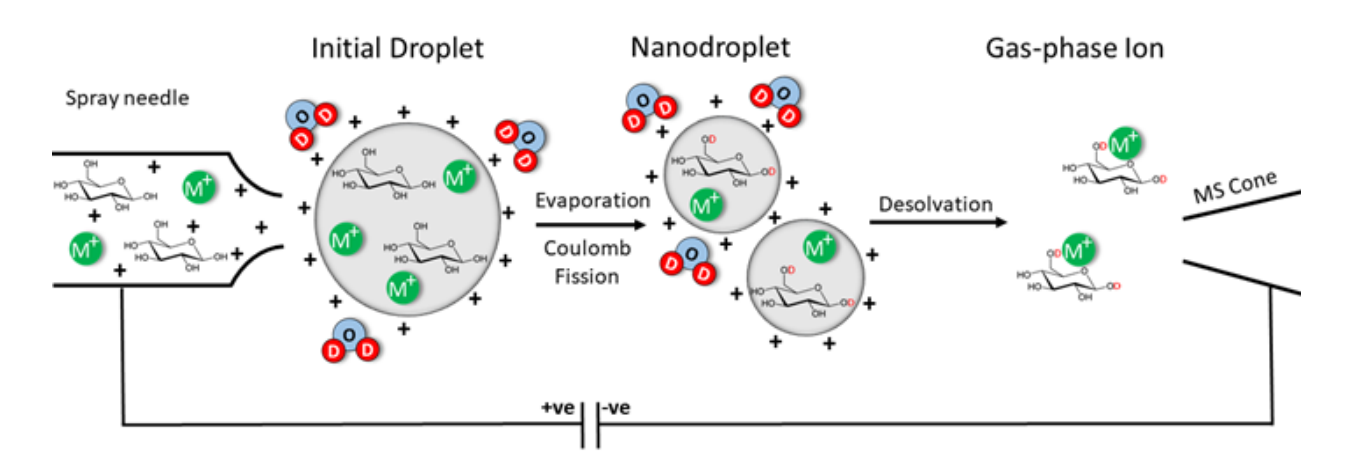
Solution-phase HDX is commonly utilized to examine protein structure and dynamics. Proteins are diluted into a D₂O-based buffer to initiate exchange. Due to the chemical exchange rates, these methods focus on detecting HDX at backbone amides within proteins. Following exchange, samples are quenched in acidic buffer (pH 2.5) to minimize the loss of deuterium labels, or back exchange, at backbone amides (Konermann et al., 2011). Traditional solution-phase HDX is of limited applicability for carbohydrates since hydroxyl groups are prone to rapid exchange and back exchange, on the order of microseconds to milliseconds (Kostyukevich et al., 2014; Liyanage et al., 2019; Kim & Gallagher, 2020). Carbohydrates containing acetamido functional groups have been labeled using solution-phase HDX; however, this functional group is only present in certain classes of monosaccharides, limiting widespread carbohydrate analyses (Guttman et al., 2011).

Solution-phase HDX labeling of carbohydrate hydroxyls has generated valuable information regarding the CID fragmentation pathways for Li⁺- and Na⁺-adducted mono- and disaccharides (Hofmeister et al., 1991; Abutokaikah et al., 2018). For these experiments, carbohydrates are incubated in D_2O solvent prior to ionization, causing all labile hydrogens to exchange with deuterium. Deuterium labeling showed that Na⁺-adducted monosaccharides undergo a retro-aldol mechanism to form cross-ring cleavages by CID (Scheme 3) (Bythell et al., 2017; Rabus et al., 2017; Chiu et al., 2019). Additionally, D_2O loss during fragmentation of Li⁺-adducted monosaccharides was observed from hydroxyls, rather than loss of C_α protons (Abutokaikah et al., 2018). In both instances, labeling the hydroxyls with deuterium enabled the C_α protons and the hydroxyl protons to be distinguished, allowing for mechanistic insights.

Gas-phase HDX methods introduce gaseous deuterating reagents, typically ND₃ or D₂O, into different vacuum regions of the mass spectrometer, such as the LIT (Kaltashov et al., 1997; Evans et al., 2003), transfer cell (Uppal et al., 2017), or FT-ICR cell (Gard et al., 1993; Campbell et al., 1995; Liyanage et al., 2019). In contrast to solution-phase HDX, gas-phase HDX occurs after an ion is formed, so labels are not indicative of solvated conformations but rather gas-phase conformations (Uppal et al., 2017). Gas-phase HDX has been effective for labeling protonated-oxonium ions that are generated after carbohydrate fragmentation (Uppal et al., 2017). However, carbohydrate-metal adducts do not exchange in the gas phase to an appreciable extent (Zhang & Brodbelt, 2004; Uppal et al., 2017; Liyanage et al., 2019).

Recently, HDX has been performed during ESI as analytes transition from solvated species to gas-phase ions (Figure 14) (Kostyukevich et al., 2013; Zherebker et al., 2016; Liyanage et al., 2019; DeBastiani et al., 2021). For these in-ESI HDX methods, deuterating reagents, such as D₂O or CH₃OD, are introduced as liquid or gas during ionization. Because exchange is negligible for carbohydrate-metal adducts in the gas phase, these methods monitor deuterium incorporation for solvated carbohydrates with the exchange reaction being quenched upon metal adduction and ESI droplet desolvation (Kostyukevich et al., 2015; Kim et al., 2018; Liyanage et al., 2019). Initial in-ESI HDX analyses of carbohydrates showed different *m/z* distributions depending on spray solvent (acetonitrile, H₂O, methanol, and ethanol) for both a Na⁺- and K⁺-adducted pentasaccharide (Kostyukevich et al., 2015). Recent MD simulations have shown that the solvent surrounding a Na⁺-adducted carbohydrate alters the inter- and intra-molecular hydrogen bonding, which could lead to populations with different structures, e.g., dihedral angles (Calixte et al., 2021). These simulations support the data with different HDX distributions, which show that different carbohydrate conformations are present in different solvents.

Figure 14. Schematic of in-ESI HDX. A plume of charged droplets is emitted from the spray needle, which shrink through desolvation and coulombic fission, resulting in nanodroplets. Analytes are exposed to deuterated reagent (*e.g.*, D₂O) whilst in the solvated droplets and as desolvated, gaseous ions prior to entering the vacuum region of the MS. Carbohydrates form metal adducts as they transition from solvated nanodroplets to gaseous ions, with metal-adduction quenching HDX and preventing gas-phase exchange. Therefore, carbohydrates undergo HDX while solvated within the initial droplets and nanodroplets. [Color figure can be viewed online at wileyonlinelibrary.com]



For HDX analyses that aim to monitor conformations, exchange is measured at multiple timepoints to examine how molecular dynamics affect HDX. To alter the HDX labeling time, methods have been developed to change the lifetime of ESI droplets, including changing the tip size from which samples are sprayed and altering the spray solvent conductivity, both of which alter the initial size of ESI droplets (Kim & Gallagher, 2020; Liyanage et al., 2021). Three Na⁺-adducted trisaccharide isomers were detected following in-ESI HDX (Liyanage et al., 2021). These isomers, including melezitose, maltotriose, and isomaltotriose, could be distinguished based on differences in HDX. This work shows potential to further distinguish carbohydrate isomers in a

MS workflow as well as provide a unique insight into solvated carbohydrate structures that is not readily available through other MS-based techniques.

VIII. Conclusion

Metal-ion adduction is a valuable tool for mass spectrometric analyses of carbohydrates and glycoconjugates. The metal ion properties, specifically the size of the ionic radius, charge density, and ionization energies, have significant impacts on carbohydrate analyses by MS-based techniques. Metal adduction improves ionization efficiency for carbohydrates in both ESI and MALDI. Fragmentation of metal-adducted carbohydrates provides unique fragments, which are often required to distinguish isomeric carbohydrates. Metal adduction also stabilizes glycoconjugates with labile modifications, allowing for additional structural information to be acquired from fragmentation. IMS-MS measures differences in the three-dimensional structures of metal-adducted carbohydrates. The use of different metals for these analyses has enabled more thorough characterizations of carbohydrates by yielding diagnostic fragments, CCS values, and arrival time distributions. Metal-adduction also serves as a quenching mechanism, in tandem with desolvation, for in-ESI HDX of carbohydrates, providing a unique capability to characterize solvated glycan structures by MS.

Na⁺ is the most common metal, charge carrier for carbohydrate analyses; however, experimental results have indicated that other metals yield superior results for MS-based analyses of carbohydrates. Li⁺, Ca²⁺, Mg²⁺, and Co²⁺ have favorable physical properties, such as the charge density and second ionization energy, for characterizing carbohydrate-metal-ion adducts. Specifically, adducts with Ca²⁺, Mg²⁺, and Co²⁺ have improved ion signals compared with Na⁺- and proton-adduction when ionized by ESI. Ca²⁺, Mg²⁺, and Co²⁺ also form a diverse array of

fragments with multiple fragmentation techniques. Recently CTD and EED have been shown to be highly effective at forming unique dissociation products, regardless of the charge carrier, though these fragmentation techniques are not yet broadly accessible to the MS community. Finally, Li⁺ adducts appear to be the best metal ion for IRMPDS and cryogenic IR spectroscopy due to the minimal band broadening compared to other metal ions.

Although metal adduction has enabled carbohydrate analyses, the structural complexity of naturally occurring carbohydrate and glycoconjugate systems drives the need for continued development of analytical methods. High-resolution IMS, ECD, EED, CTD, IRMPDS, and cryogenic IR spectroscopy have yet to be commonly integrated into commercial MS instruments and analytical workflows. Yet, all of these methods are promising for their abilities to analyze glycans. IRMPDS and cryogenic IR spectroscopy have enabled structural analyses of carbohydrates since spectra can be compared to computational predictions, which enables structural validation when standards are not available. High-resolution IMS has shown the ability to resolve linkage and stereoisomers, though additional studies are needed to test the limits of these separations. However, the widespread adoption of gas-phase IMS separations could increase the use of metals by enabling rapid direct injection methods that allow metal salts to be added directly to the sample before MS analysis. Post-LC column addition of Na⁺, Li⁺, and Co²⁺ has been utilized to improve identification of carbohydrates since the mid-90s (Kohler & Leary, 1995), but the technique has yet to become widespread. Finally, a large amount of work has focused on using Na⁺ as the metal adduct of choice because it is a common contaminant and LC separations are incompatible with the addition of high metal-salt concentrations. Thus, most available fragment identification software focuses on identifying H⁺- or Na⁺-adducted carbohydrates and glycans. This has required manual identification for data utilizing other metals, which is time consuming.

Development of improved software for fragment identification for multiple metal adducts could extend the applications of metal adducts for carbohydrate analyses in the MS community because implementing metal-adduction has already improved experimental results and will continue providing additional structural details and insight into complex, biological carbohydrate structures.

IX.Abbreviation List

α	alpha
β	beta
μ	reduced mass of the ion and buffer gas
Ω	collisional cross section
Δx	full width of peak at half its maximum height
AMAC	2-amino-9(10H)-acridone
AMC	7-aminomethylcoumarin
6-AQ	6-aminoquinoline
2-AB	2-aminobenzamide
Asn	asparagine
ATD	arrival time distribution
CCS	collisional cross section
DTCCS	CCS values measured by DTIMS, often utilized as standards

CD	cyclodextrin
CID	collision-induced dissociation
CID^n	multi-stage collision-induced dissociation
CID^2	collision-induced dissociation to the 2 nd
CID ³	collision-induced dissociation to the 3 rd
cIMS	cyclic ion mobility spectrometry
CLIO	Collaboration pour un Laser Infrarouge à Orsay
CPCD	chemical physics and chemical dynamics
CRM	charged residue model
CTD	charge transfer dissociation
DC	direct current
DHB	2,5-dihydroxybenzoic acid
DHN	1,4-dihydroxynaphthalene-2-carboxylic acid
DP5	five degrees of polymerization or five glucose subunits
DTIMS	drift tube ion mobility spectrometry
E	electric field
e	charge of an electron
ECD	electron capture dissociation

EDD electron detachment dissociation **EED** electron excitation dissociation **ESI** electrospray ionization ET electron transfer **ETD** electron transfer dissociation **ETciD** electron transfer collision induced dissociation electron transfer high-energy collision dissociation **EThcD ETnoD** electron transfer no dissociation eV electron volts F fragment **FEL** free-electron laser **FELIX** Free-Electron Lasers for Infrared Experiments Fourier transform-ion cyclotron resonance FT-ICR full width of peak at half its maximum height **FWHM** GalNAc N-acetylgalactosamine glycosaminoglycan **GAG** Galβ1-4GlcNAc N-acetyl-D-lactosamine galactofuranose Galf Glcpgalactopyranose

N-acetylglucosamine GlcNAc Gly glycine hot electron capture dissociation **HECD** helium-charge transfer dissociation He-CTD human milk oligosaccharide HMO hydrogen/deuterium exchange **HDX IEM** ion evaporation method ion mobility spectrometry **IMS** IR infrared infrared multiphoton dissociation **IRMPD** infrared multiphoton dissociation spectroscopy **IRMPDS** mobility K k_B Boltzmann constant length Lliquid chromatography LC Lacto-N-fucopentaose **LNFP** LNH lacto-N-hexaose

LNnH

lacto-N-neohexaose

LNnT lacto-N-neotetraose LNT lacto-N-tetraose linear ion trap LIT carbohydrate analyte M matrix-assisted laser desorption/ionization **MALDI** molecular dynamics MD melezitose Mel MS mass spectrometry MS/MS tandem mass spectrometry mass-to-charge ratio m/zgas number density Nnano-elecrospray ionization nano-ESI negative electron transfer dissociation **NETD** nuclear magnetic resonance **NMR** optical parametric oscillator OPO P precursor printed circuit board PCB

Phe-Gly

phenylalanine-glycine

PGC porous graphitic carbon PT proton transfer proton-transfer charge reduction **PTCR** proton-transfer-induced fragmentation PTD QTOF quadrupole time-of-flight Rresolution RF radio frequency resolving power R_p sLe^A sialyl Lewis A structures for lossless ion manipulations **SLIM** Ser serine serpentine ultralong path with extended routing **SUPER** Ttemperature arrival time t_a time-of-flight TOF trapped ion mobility spectrometry **TIMS** traveling wave ion mobility spectrometry **TWIMS** ultraviolet photodissociation **UVPD**

 $egin{align*} V & & ext{voltage} \ & v_a & & ext{velocity} \ & z & & ext{ion charge} \ \end{aligned}$

X. Acknowledgements

D.T.G. was supported by the Welch Foundation (AA-1899). A.V.Q. and J.B.H. were supported by the National Science Foundation (CHE-1945078). We thank Alexis N. Edwards for discussions on ion mobility.

XI. References

Abikhodr, A. H., Yatsyna, V., Ben Faleh, A., Warnke, S. and Rizzo, T. R. 2021. Identifying mixtures of isomeric human milk oligosaccharides by the decomposition of IR spectral fingerprints. *Anal Chem 93* (44): 14730-14736.

Abutokaikah, M. T., Frye, J. W., Tschampel, J., Rabus, J. M. and Bythell, B. J. 2018. Fragmentation pathways of lithiated hexose monosaccharides. *J Am Soc Mass Spectrom* 29 (8): 1627-1637.

Adamson, J. T. and Håkansson, K. 2007. Electron capture dissociation of oligosaccharides ionized with alkali, alkaline earth, and transition metals. *Anal Chem* 79 (7): 2901-2910.

Adamson, J. T. and Håkansson, K. 2007a. Electron detachment dissociation of neutral and sialylated oligosaccharides. *J Am Soc Mass Spectrom* 18 (12): 2162-2172.

Angyal, S. J. (1989). Complexes of metal cations with carbohydrates in solution. In: *Adv Carbohydr Chem Biochem*. (ed. R. S. Tipson), 1-43. San Diego, CA: Elsevier Inc.

Asam, M. R. and Glish, G. L. 1997. Tandem mass spectrometry of alkali cationized polysaccharides in a quadrupole ion trap. *J Am Soc Mass Spectrom* 8 (9): 987-995.

Attah, I. K., Nagy, G., Garimella, S. V. B., Norheim, R. V., Anderson, G. A., Ibrahim, Y. M. and Smith, R. D. 2019. Traveling-wave-based electrodynamic switch for concurrent dual-polarity ion manipulations in structures for lossless ion manipulations. *Anal Chem 91* (22): 14712-14718.

Azenha, C. S., Coimbra, M. A., Moreira, A. S., Domingues, P. and Domingues, M. R. 2013. Differentiation of isomeric β-(1-4) hexose disaccharides by positive electrospray tandem mass spectrometry. *J Mass Spectrom* 48 (5): 548-552.

Bahr, U., Pfenninger, A., Karas, M. and Stahl, B. 1997. High-sensitivity analysis of neutral underivatized oligosaccharides by nanoelectrospray mass spectrometry. *Anal Chem* 69 (22): 4530-4535.

Bai, Y., Milne, J. S., Mayne, L. and Englander, S. W. 1993. Primary structure effects on peptide group hydrogen exchange. *Proteins: Struct Funct Genet* 17 (1): 75-86.

Bansal, P., Yatsyna, V., AbiKhodr, A. H., Warnke, S., Ben Faleh, A., Yalovenko, N., Wysocki, V. H. and Rizzo, T. R. 2020. Using SLIM-based IMS-IMS together with cryogenic infrared spectroscopy for glycan analysis. *Anal Chem* 92 (13): 9079–9085.

Barnes, L., Allouche, A.-R., Chambert, S., Schindler, B. and Compagnon, I. 2020. Ion spectroscopy of heterogeneous mixtures: IRMPD and DFT analysis of anomers and conformers of monosaccharides. *Int J Mass Spectrom* 447: 116235.

Barnes, L., Schindler, B., Chambert, S., Allouche, A.-R. and Compagnon, I. 2017. Conformational preferences of protonated *N*-acetylated hexosamines probed by InfraRed Multiple Photon Dissociation (IRMPD) spectroscopy and ab initio calculations. *Int J Mass Spectrom* 421: 116-123.

Beckman, J. S., Voinov, V. G., Hare, M., Sturgeon, D., Vasil'ev, Y., Oppenheimer, D., Shaw, J. B., Wu, S., Glaskin, R., Klein, C., Schwarzer, C. and Stafford, G. 2021. Improved protein and PTM characterization with a practical electron-based fragmentation on Q-TOF instruments. *J Am Soc Mass Spectrom* 32 (8): 2081–2091.

Ben Faleh, A., Warnke, S. and Rizzo, T. R. 2019. Combining ultrahigh-resolution ion-mobility spectrometry with cryogenic infrared spectroscopy for the analysis of glycan mixtures. *Anal Chem 91* (7): 4876-4882.

Berkenkamp, S., Menzel, C., Karas, M. and Hillenkamp, F. 1997. Performance of infrared matrix-assisted laser desorption/ionization mass spectrometry with lasers emitting in the 3 μm wavelength range. *Rapid Commun Mass Spectrom* 11 (13): 1399-1406.

Bertozzi, C. R. and Rabuka, D. (2009). Structural basis of glycan diversity. In: *Essentials of Glycobiology*. (ed. A. Varki, R. D. Cummings, J. D. Esko, H. H. Freeze, P. Stanley, C. R. Bertozzi, G. W. Hart and M. E. Etzler), New York: Cold Spring Harbor Laboratory Press.

Bohnhorst, A., Hitzemann, M., Lippmann, M., Kirk, A. T. and Zimmermann, S. 2020. Enhanced resolving power by moving field ion mobility spectrometry. *Anal Chem* 92 (19): 12967-12974.

Börnsen, K. O., Mohr, M. D. and Widmer, H. M. 1995. Ion exchange and purification of carbohydrates on a Nafion® membrane as a new sample pretreatment for matrix-assisted laser desorption/ionization mass spectrometry. *Rapid Commun Mass Spectrom* 9 (11): 1031-1034.

Botek, E., Debrun, J. L., Hakim, B. and Morin-Allory, L. 2001. Attachment of alkali cations on β-D-glucopyranose: matrix-assisted laser desorption/ionization time-of-flight studies and ab initio calculations. *Rapid Commun Mass Spectrom* 15 (4): 273-276.

Bowers, W. D., Delbert, S. S., Hunter, R. L. and McIver Jr, R. T. 1984. Fragmentation of oligopeptide ions using ultraviolet laser radiation and Fourier transform mass spectrometry. *J Am Chem Soc* 106 (23): 7288-7289.

Brodbelt, J. S., Morrison, L. J. and Santos, I. 2019. Ultraviolet photodissociation mass spectrometry for analysis of biological molecules. *Chem Rev* 120 (7): 3328-3380.

Brodbelt, J. S. and Wilson, J. J. 2009. Infrared multiphoton dissociation in quadrupole ion traps. *Mass Spectrom Rev* 28 (3): 390-424.

Brüll, L. P., Kovácik, V., Thomas-Oates, J. E., Heerma, W. and Haverkamp, J. 1998. Sodium-cationized oligosaccharides do not appear to undergo 'internal residue loss' rearrangement processes on tandem mass spectrometry. *Rapid Commun Mass Spectrom* 12 (20): 1520-1532.

Bubb, W. A. 2003. NMR spectroscopy in the study of carbohydrates: Characterizing the structural complexity. *Concepts Magn Reson A: Bridg Educ Res* 19A (1): 1-19.

Bucior, I., Scheuring, S., Engel, A. and Burger, M. M. 2004. Carbohydrate–carbohydrate interaction provides adhesion force and specificity for cellular recognition. *J Cell Biol* 165 (4): 529-537.

Buck-Wiese, H., Fanuel, M., Liebeke, M., Le Mai Hoang, K., Pardo-Vargas, A., Seeberger, P. H., Hehemann, J. H., Rogniaux, H., Jackson, G. P. and Ropartz, D. 2020. Discrimination of β-1,4- and β-1,3-linkages in native oligosaccharides via charge transfer dissociation mass spectrometry. *J Am Soc Mass Spectrom* 31 (6): 1249-1259.

Budnik, B. A., Haselmann, K. F. and Zubarev, R. A. 2001. Electron detachment dissociation of peptide di-anions: an electron–hole recombination phenomenon. *Chem Phys Lett* 342 (3): 299-302.

Bythell, B. J. 2013. To jump or not to jump? C_{α} hydrogen atom transfer in post-cleavage radical-cation complexes. *J Phys Chem A* 117 (6): 1189-1196.

Bythell, B. J. 2014. C_{α} hydrogen atom transfer in post-cleavage radical-cation complexes: short and steep versus long winding road. *J Phys Chem A* 118 (45): 10797-10803.

Bythell, B. J., Abutokaikah, M. T., Wagoner, A. R., Guan, S. and Rabus, J. M. 2017. Cationized carbohydrate gas-phase fragmentation chemistry. *J Am Soc Mass Spectrom* 28 (4): 688-703.

Calixte, E. I., Liyanage, O. T., Gass, D. T. and Gallagher, E. S. 2021. Formation of carbohydrate-metal adducts from solvent mixtures during electrospray: a molecular dynamics and ESI-MS study. *J Am Soc Mass Spectrom* 32 (12): 2738–2745.

Calixte, E. I., Liyanage, O. T., Kim, H. J., Ziperman, E. D., Pearson, A. J. and Gallagher, E. S. 2020. Release of carbohydrate-metal adducts from electrospray droplets: insight into glycan ionization by electrospray. *J Phys Chem B* 124 (3): 479-486.

Campbell, S., Rodgers, M. T., Marzluff, E. M. and Beauchamp, J. L. 1995. Deuterium exchange reactions as a probe of biomolecule structure. Fundamental studies of gas phase H/D exchange reactions of protonated glycine oligomers with D2O, CD3OD, CD3CO2D, and ND3. *J Am Chem Soc* 117 (51): 12840-12854.

Cancilla, M. T., Penn, S. G., Carroll, J. A. and Lebrilla, C. B. 1996. Coordination of alkali metals to oligosaccharides dictates fragmentation behavior in matrix assisted laser desorption ionization/fourier transform mass spectrometry. *J Am Chem Soc* 118 (28): 6736-6745.

Castillo, J. J., Galermo, A. G., Amicucci, M. J., Nandita, E., Couture, G., Bacalzo, N., Chen, Y. and Lebrilla, C. B. 2021. A multidimensional mass spectrometry-based workflow for de novo structural elucidation of oligosaccharides from polysaccharides. *J Am Soc Mass Spectrom 32* (8): 2175–2185. Chao, H. C. and McLuckey, S. A. 2021. In-Depth Structural Characterization and Quantification of Cerebrosides and Glycosphingosines with Gas-Phase Ion Chemistry. *Anal Chem 93* (19): 7332-7340. Chao, H. C. and McLuckey, S. A. 2021. Manipulation of ion types via gas-phase ion/ion chemistry for the structural characterization of the glycan moiety on gangliosides. *Anal Chem 93* (47): 15752–15760. Chen, J. L., Lee, C., Lu, I. C., Chien, C. L., Lee, Y. T., Hu, W. P. and Ni, C. K. 2016. Theoretical investigation of low detection sensitivity for underivatized carbohydrates in ESI and MALDI. *J Mass Spectrom 51* (12): 1180-1186.

Chen, J. L., Nguan, H. S., Hsu, P. J., Tsai, S. T., Liew, C. Y., Kuo, J. L., Hu, W. P. and Ni, C. K. 2017. Collision-induced dissociation of sodiated glucose and identification of anomeric configuration. *Phys Chem Chem Phys* 19 (23): 15454-15462.

Chen, Z., Glover, M. S. and Li, L. 2018. Recent advances in ion mobility–mass spectrometry for improved structural characterization of glycans and glycoconjugates. *Curr Opin Chem Biol* 42: 1-8. Chingin, K., Makarov, A., Denisov, E., Rebrov, O. and Zubarev, R. A. 2014. Fragmentation of positively-charged biological ions activated with a beam of high-energy cations. *Anal Chem* 86 (1): 372-379. Chiu, C. C., Tsai, S. T., Hsu, P. J., Huynh, H. T., Chen, J. L., Phan, H. T., Huang, S. P., Lin, H. Y., Kuo, J. L. and Ni, C. K. 2019. Unexpected dissociation mechanism of sodiated *N*-acetylglucosamine and *N*-acetylgalactosamine. *J Phys Chem A* 123 (16): 3441-3453.

Chu, K. Y., Lee, S., Tsai, M. T., Lu, I. C., Dyakov, Y. A., Lai, Y. H., Lee, Y. T. and Ni, C. K. 2014. Thermal proton transfer reactions in ultraviolet matrix-assisted laser desorption/ionization. *J Am Soc Mass Spectrom* 25 (3): 310-318.

Clowers, B. H., Dwivedi, P., Steiner, W. E., Hill, H. H., Jr. and Bendiak, B. 2005. Separation of sodiated isobaric disaccharides and trisaccharides using electrospray ionization-atmospheric pressure ion mobility-time of flight mass spectrometry. *J Am Soc Mass Spectrom* 16 (5): 660-669.

Compton, P. D., Strukl, J. V., Bai, D. L., Shabanowitz, J. and Hunt, D. F. 2012. Optimization of electron transfer dissociation via informed selection of reagents and operating parameters. *Anal Chem* 84 (3): 1781-1785.

Contreras, C. S., Polfer, N. C., Oomens, J., Steill, J. D., Bendiak, B. and Eyler, J. R. 2012. On the path to glycan conformer identification: Gas-phase study of the anomers of methyl glycosides of *N*-acetyl-D-glucosamine and *N*-acetyl-D-galactosamine. *Int J Mass Spectrom 330-332*: 285-294.

Coon, J. J., Shabanowitz, J., Hunt, D. F. and Syka, J. E. P. 2005. Electron transfer dissociation of peptide anions. *J Am Soc Mass Spectrom* 16 (6): 880-882.

Cumeras, R., Figueras, E., Davis, C. E., Baumbach, J. I. and Gracia, I. 2015. Review on ion mobility spectrometry. Part 1: current instrumentation. *Analyst* 140 (5): 1376-1390.

da Costa, E. V., Moreira, A. S., Nunes, F. M., Coimbra, M. A., Evtuguin, D. V. and Domingues, M. R. 2012. Differentiation of isomeric pentose disaccharides by electrospray ionization tandem mass spectrometry and discriminant analysis. *Rapid Commun Mass Spectrom* 26 (24): 2897-2904.

DeBastiani, A., Majuta, S. N., Sharif, D., Attanayake, K., Li, C., Li, P. and Valentine, S. J. 2021.

Characterizing multidevice capillary vibrating sharp-edge spray ionization for in-droplet

hydrogen/deuterium exchange to enhance compound identification. ACS Omega 6 (28): 18370-18382.

Dell, A. (1990). Preparation and desorption mass spectrometry of permethyl and peracetyl derivatives of

oligosaccharides. In: *Methods Enzymol*. (ed. J. A. McCloskey), 647-660. San Diego, CA: Elsevier Inc.

Deng, L., Ibrahim, Y. M., Baker, E. S., Aly, N. A., Hamid, A. M., Zhang, X., Zheng, X., Garimella, S. V.

B., Webb, I. K., Prost, S. A., Sandoval, J. A., Norheim, R. V., Anderson, G. A., Tolmachev, A. V. and

Smith, R. D. 2016. Ion mobility separations of isomers based upon long path length structures for lossless

ion manipulations combined with mass spectrometry. ChemistrySelect 1 (10): 2396-2399.

Deng, L., Webb, I. K., Garimella, S. V. B., Hamid, A. M., Zheng, X., Norheim, R. V., Prost, S. A., Anderson, G. A., Sandoval, J. A., Baker, E. S., Ibrahim, Y. M. and Smith, R. D. 2017. Serpentine ultralong path with extended routing (SUPER) high resolution traveling wave ion mobility-MS using structures for lossless ion manipulations. *Anal Chem.* 89 (8): 4628-4634.

Depland, A. D., Renois-Predelus, G., Schindler, B. and Compagnon, I. 2018. Identification of sialic acid linkage isomers in glycans using coupled InfraRed Multiple Photon Dissociation (IRMPD) spectroscopy and mass spectrometry. *Int J Mass Spectrom* 434: 65-69.

Devakumar, A., Mechref, Y., Kang, P., Novotny, M. V. and Reilly, J. P. 2007. Laser-induced photofragmentation of neutral and acidic glycans inside an ion-trap mass spectrometer. *Rapid Commun Mass Spectrom* 21 (8): 1452-1460.

Devakumar, A., Mechref, Y., Kang, P., Novotny, M. V. and Reilly, J. P. 2008. Identification of isomeric N-glycan structures by mass spectrometry with 157 nm laser-induced photofragmentation. *J Am Soc Mass Spectrom* 19 (7): 1027-1040.

Dodds, J. N. and Baker, E. S. 2019. Ion mobility spectrometry: fundamental concepts, instrumentation, applications, and the road ahead. *J Am Soc Mass Spectrom* 30 (11): 2185-2195.

Dodds, J. N., May, J. C. and McLean, J. A. 2017. Correlating resolving power, resolution, and collision cross section: unifying cross-platform assessment of separation efficiency in ion mobility spectrometry. *Anal Chem 89* (22): 12176-12184.

Domon, B. and Costello, C. E. 1988. A systematic nomenclature for carbohydrate fragmentations in FAB-MS/MS spectra of glycoconjugates. *Glycoconj J* 5 (4): 397-409.

Drake, R. R., West, C. A., Mehta, A. S. and Angel, P. M. (2018). MALDI mass spectrometry imaging of N-linked glycans in tissues. In: *Advances in Experimental Medicine and Biology*. (ed. Y. Yamaguchi and K. Kato), 59-76. Singapore: Springer.

Dube, D. H. and Bertozzi, C. R. 2005. Glycans in cancer and inflammation--potential for therapeutics and diagnostics. *Nat Rev Drug Discov* 4 (6): 477-488.

Dyukova, I., Carrascosa, E., Pellegrinelli, R. P. and Rizzo, T. R. 2020. Combining cryogenic infrared spectroscopy with selective enzymatic cleavage for determining glycan primary structure. *Anal Chem 92* (2): 1658-1662.

Edwards, A. N., Tran, H. M. and Gallagher, E. S. 2021. Propagating error through traveling-wave ion mobility calibration. *J Am Soc Mass Spectrom* 32 (11): 2621-2630.

Evans, S. E., Lueck, N. and Marzluff, E. M. 2003. Gas phase hydrogen/deuterium exchange of proteins in an ion trap mass spectrometer. *Int J Mass Spectrom* 222 (1): 175-187.

Eyler, J. R. 2009. Infrared multiple photon dissociation spectroscopy of ions in Penning traps. *Mass Spectrom Rev* 28 (3): 448-467.

Fabian, W. M. F. 2007. Metal binding induced conformational interconversions in methyl β-D-xylopyranoside. *Theor Chem Acc* 117 (2): 223-229.

Fenn, L. S. and McLean, J. A. 2011. Structural resolution of carbohydrate positional and structural isomers based on gas-phase ion mobility-mass spectrometry. *Phys Chem Chem Phys* 13 (6): 2196-2205. Fort, K. L., Cramer, C. N., Voinov, V. G., Vasil'ev, Y. V., Lopez, N. I., Beckman, J. S. and Heck, A. J. R. 2018. Exploring ECD on a benchtop Q exactive orbitrap mass spectrometer. *J Proteome Res* 17 (2): 926-933.

Frese, C. K., Altelaar, A. F., van den Toorn, H., Nolting, D., Griep-Raming, J., Heck, A. J. and Mohammed, S. 2012. Toward full peptide sequence coverage by dual fragmentation combining electron-transfer and higher-energy collision dissociation tandem mass spectrometry. *Anal Chem* 84 (22): 9668-9673.

Frese, C. K., Nolting, D., Altelaar, A. F., Griep-Raming, J., Mohammed, S. and Heck, A. J. 2013. Characterization of electron transfer dissociation in the Orbitrap Velos HCD cell. *J Am Soc Mass Spectrom* 24 (11): 1663-1670.

Fura, A. and Leary, J. A. 1993. Differentiation of calcium(2+)- and magnesium(2+)-coordinated branched trisaccharide isomers: An electrospray ionization and tandem mass spectrometry study. *Anal Chem 65* (20): 2805-2811.

Gabelica, V., Shvartsburg, A. A., Afonso, C., Barran, P., Benesch, J. L. P., Bleiholder, C., Bowers, M. T., Bilbao, A., Bush, M. F., Campbell, J. L., Campuzano, I. D. G., Causon, T., Clowers, B. H., Creaser, C. S., De Pauw, E., Far, J., Fernandez-Lima, F., Fjeldsted, J. C., Giles, K., Groessl, M., Hogan, C. J., Jr., Hann, S., Kim, H. I., Kurulugama, R. T., May, J. C., McLean, J. A., Pagel, K., Richardson, K., Ridgeway, M. E., Rosu, F., Sobott, F., Thalassinos, K., Valentine, S. J. and Wyttenbach, T. 2019. Recommendations for reporting ion mobility mass spectrometry measurements. *Mass Spectrom Rev* 38 (3): 291-320. Gallagher, E. S. and Hudgens, J. W. (2016). Mapping protein-ligand interactions with proteolytic fragmentation, hydrogen/deuterium exchange-mass spectrometry. In: *Methods Enzymol*. (ed. Z. Kelman), 357-404. San Diego, CA: Elsevier Inc.

Gamez, F., Hurtado, P., Hortal, A. R., Martinez-Haya, B., Berden, G. and Oomens, J. 2013. Cations in a molecular funnel: vibrational spectroscopy of isolated cyclodextrin complexes with alkali metals.

*ChemPhysChem 14 (2): 400-407.

Gard, E., Willard, D., Bregar, J., Green, M. K. and Lebrilla, C. B. 1993. Site specificity in the H–D exchange reactions of gas-phase protonated amino acids with CH3OD. *J Mass Spectrom* 28 (12): 1632-1639.

Gaye, M. M., Nagy, G., Clemmer, D. E. and Pohl, N. L. 2016. Multidimensional analysis of 16 glucose isomers by ion mobility spectrometry. *Anal Chem* 88 (4): 2335-2344.

Gelb, A. S., Jarratt, R. E., Huang, Y. and Dodds, E. D. 2014. A study of calibrant selection in measurement of carbohydrate and peptide ion-neutral collision cross sections by traveling wave ion mobility spectrometry. *Anal Chem* 86 (22): 11396-11402.

Giles, K., Ujma, J., Wildgoose, J., Pringle, S., Richardson, K., Langridge, D. and Green, M. 2019. A cyclic ion mobility-mass spectrometry system. *Anal Chem 91* (13): 8564-8573.

Grabarics, M., Lettow, M., Kirschbaum, C., Greis, K., Manz, C. and Pagel, K. 2021. Mass spectrometry-based techniques to elucidate the sugar code. *Chem Rev* 122 (8): 7840-7908.

Gulyuz, K., Stedwell, C. N., Wang, D. and Polfer, N. C. 2011. Hybrid quadrupole mass filter/quadrupole ion trap/time-of-flight-mass spectrometer for infrared multiple photon dissociation spectroscopy of mass-selected ions. *Rev Sci Instrum* 82 (5): 054101.

Gunawardena, H. P., He, M., Chrisman, P. A., Pitteri, S. J., Hogan, J. M., Hodges, B. D. M. and McLuckey, S. A. 2005. Electron transfer versus proton transfer in gas-phase ion/ion reactions of polyprotonated peptides. *J Am Chem Soc* 127 (36): 12627-12639.

Guttman, M., Scian, M. and Lee, K. K. 2011. Tracking hydrogen/deuterium exchange at glycan sites in glycoproteins by mass spectrometry. *Anal Chem* 83 (19): 7492-7499.

Gyurcsik, B. and Nagy, L. 2000. Carbohydrates as ligands: coordination equilibria and structure of the metal complexes. *Coord Chem Rev* 203 (1): 81-149.

Han, L. and Costello, C. E. 2011. Electron transfer dissociation of milk oligosaccharides. *J Am Soc Mass Spectrom* 22 (6): 997-1013.

Harvey, D. J. 1999. Matrix-assisted laser desorption/ionization mass spectrometry of carbohydrates. *Mass Spectrom Rev* 18 (6): 349-450.

Harvey, D. J. 2000. Collision-induced fragmentation of underivatized *N*-linked carbohydrates ionized by electrospray. *J Mass Spectrom* 35 (10): 1178-1190.

Harvey, D. J. 2001. Ionization and collision-induced fragmentation of N-linked and related carbohydrates using divalent cations. *J Am Soc Mass Spectrom* 12 (8): 926-937.

Harvey, D. J. 2005. Ionization and fragmentation of *N*-linked glycans as silver adducts by electrospray mass spectrometry. *Rapid Commun Mass Spectrom* 19 (4): 484-492.

Harvey, D. J. 2005a. Structural determination of *N*-linked glycans by matrix-assisted laser desorption/ionization and electrospray ionization mass spectrometry. *Proteomics* 5 (7): 1774-1786. Harvey, D. J. 2021. Analysis of carbohydrates and glycoconjugates by matrix-assisted laser desorption/ionization mass spectrometry: an update for 2015–2016. *Mass Spectrom Rev* 40 (4): 408-565.

Harvey, D. J., Bateman, R. H. and Green, M. R. 1997. High-energy collision-induced fragmentation of complex oligosaccharides ionized by matrix-assisted laser desorption/ionization mass spectrometry. *J Mass Spectrom* 32 (2): 167-187.

Harvey, D. J., Hunter, A. P., Bateman, R. H., Brown, J. and Critchley, G. 1999a. Relationship between insource and post-source fragment ions in the matrix-assisted laser desorption (ionization) mass spectra of carbohydrates recorded with reflectron time-of-flight mass spectrometers. *Int J Mass Spectrom* 188 (1): 131-146.

Harvey, D. J., Mattu, T. S., Wormald, M. R., Royle, L., Dwek, R. A. and Rudd, P. M. 2002. "Internal residue loss": rearrangements occurring during the fragmentation of carbohydrates derivatized at the reducing terminus. *Anal Chem.* 74 (4): 734-740.

Haynes, W. M., Lide, D. R. and Bruno, T. J. (2016). *CRC handbook of chemistry and physics*. Boca Raton, FL, CRC press.

Heaton, A. L. and Armentrout, P. B. 2008. Experimental and theoretical studies of sodium cation interactions with D-arabinose, xylose, glucose, and galactose. *J Phys Chem A* 112 (41): 10156-10167. Hecht, E. S., Loziuk, P. L. and Muddiman, D. C. 2017. Xylose migration during tandem mass spectrometry of *N*-linked glycans. *J Am Soc Mass Spectrom* 28 (4): 729-732.

Ho, J. S., Gharbi, A., Schindler, B., Yeni, O., Bredy, R., Legentil, L., Ferrieres, V., Kiessling, L. L. and Compagnon, I. 2021. Distinguishing galactoside isomers with mass spectrometry and gas-phase infrared spectroscopy. *J Am Chem Soc* 143 (28): 10509-10513

Hoffmann, W. D. and Jackson, G. P. 2014. Charge transfer dissociation (CTD) mass spectrometry of peptide cations using kiloelectronvolt helium cations. *J Am Soc Mass Spectrom* 25 (11): 1939-1943. Hofmann, J., Stuckmann, A., Crispin, M., Harvey, D. J., Pagel, K. and Struwe, W. B. 2017. Identification of lewis and blood group carbohydrate epitopes by ion mobility-tandem-mass spectrometry fingerprinting. *Anal Chem* 89 (4): 2318-2325.

Hofmeister, G. E., Zhou, Z. and Leary, J. A. 1991. Linkage position determination in lithium-cationized disaccharides: tandem mass spectrometry and semiempirical calculations. *J Am Chem Soc* 113 (16): 5964-5970.

Hollerbach, A. L., Li, A., Prabhakaran, A., Nagy, G., Harrilal, C. P., Conant, C. R., Norheim, R. V., Schimelfenig, C. E., Anderson, G. A., Garimella, S. V. B., Smith, R. D. and Ibrahim, Y. M. 2020. Ultrahigh-resolution ion mobility separations over extended path lengths and mobility ranges achieved using a multilevel structures for lossless ion manipulations module. *Anal Chem* 92 (11): 7972-7979.

Horn, D. M., Ge, Y. and McLafferty, F. W. 2000. Activated ion electron capture dissociation for mass spectral sequencing of larger (42 kDa) proteins. *Anal Chem* 72 (20): 4778-4784.

Huang, Y. and Dodds, E. D. 2013. Ion mobility studies of carbohydrates as group I adducts: isomer specific collisional cross section dependence on metal ion radius. *Anal Chem* 85 (20): 9728-9735.

Huang, Y. and Dodds, E. D. 2015. Discrimination of isomeric carbohydrates as the electron transfer products of group II cation adducts by ion mobility spectrometry and tandem mass spectrometry. *Anal Chem* 87 (11): 5664-5668.

Huang, Y. and Dodds, E. D. 2015a. Ion-neutral collisional cross sections of carbohydrate isomers as divalent cation adducts and their electron transfer products. *Analyst* 140 (20): 6912-6921.

Huang, Y., Pu, Y., Yu, X., Costello, C. E. and Lin, C. 2014. Mechanistic study on electron capture dissociation of the oligosaccharide-Mg²⁺ complex. *J Am Soc Mass Spectrom* 25 (8): 1451-1460.

Huang, Y., Pu, Y., Yu, X., Costello, C. E. and Lin, C. 2016. Mechanistic study on electronic excitation dissociation of the cellobiose-Na⁺ complex. *J Am Soc Mass Spectrom* 27 (2): 319-328.

Ibrahim, Y. M., Hamid, A. M., Cox, J. T., Garimella, S. V. and Smith, R. D. 2017. Ion elevators and escalators in multilevel structures for lossless ion manipulations. *Anal Chem* 89 (3): 1972-1977.

Jennings, K. R. 1968. Collision-induced decompositions of aromatic molecular ions. *Int J Mass Spectrom* 1 (3): 227-235.

Julian, R. R. 2017. The mechanism behind top-down UVPD xxperiments: making sense of apparent contradictions. *J Am Soc Mass Spectrom* 28 (9): 1823-1826.

Kailemia, M. J., Li, L., Ly, M., Linhardt, R. J. and Amster, I. J. 2012. Complete mass spectral characterization of a synthetic ultralow-molecular-weight heparin using collision-induced dissociation. *Anal Chem 84* (13): 5475-5478.

Kailemia, M. J., Park, D. and Lebrilla, C. B. 2017. Glycans and glycoproteins as specific biomarkers for cancer. *Anal Bioanal Chem* 409 (2): 395-410.

Kailemia, M. J., Ruhaak, L. R., Lebrilla, C. B. and Amster, I. J. 2014. Oligosaccharide analysis by mass spectrometry: a review of recent developments. *Anal Chem* 86 (1): 196-212.

Kaltashov, I. A., Doroshenko, V. M. and Cotter, R. J. 1997. Gas phase hydrogen/deuterium exchange reactions of peptide ions in a quadrupole ion trap mass spectrometer. *Proteins: Struct Funct Genet* 28 (1): 53-58.

Kamrath, M. Z., Garand, E., Jordan, P. A., Leavitt, C. M., Wolk, A. B., Van Stipdonk, M. J., Miller, S. J. and Johnson, M. A. 2011. Vibrational characterization of simple peptides using cryogenic infrared photodissociation of H₂-tagged, mass-selected ions. *J Am Chem Soc* 133 (16): 6440-6448.

Kang, P., Mechref, Y., Klouckova, I. and Novotny, M. V. 2005. Solid-phase permethylation of glycans for mass spectrometric analysis. *Rapid Commun Mass Spectrom* 19 (23): 3421-3428.

Kanu, A. B., Gribb, M. M. and Hill, H. H. 2008. Predicting optimal resolving power for ambient pressure ion mobility spectrometry. *Anal Chem 80* (17): 6610-6619.

Karas, M., Bachmann, D. and Hillenkamp, F. 1985. Influence of the wavelength in high-irradiance ultraviolet laser desorption mass spectrometry of organic molecules. *Anal Chem* 57 (14): 2935-2939.

Karas, M., Bahr, U. and Dülcks, T. 2000. Nano-electrospray ionization mass spectrometry: addressing analytical problems beyond routine. *Fresenius J Anal Chem* 366 (6): 669-676.

Katta, V. and Chait, B. T. 1993. Hydrogen/deuterium exchange electrospray ionization mass spectrometry: a method for probing protein conformational changes in solution. *J Am Chem Soc* 115 (14): 6317-6321.

Kawasaki, N., Ohta, M., Hyuga, S., Hashimoto, O. and Hayakawa, T. 1999. Analysis of carbohydrate heterogeneity in a glycoprotein using liquid chromatography/mass spectrometry and liquid chromatography with tandem mass spectrometry. *Anal Bioanal Chem* 269 (2): 297-303.

Kim, H. J. (2021). Rapid deuterium labeling and localization for structural elucidation of carbohydrates. Doctor of Philosophy Dissertation. Baylor University.

Kim, H. J. and Gallagher, E. S. 2020. Achieving multiple hydrogen/deuterium exchange timepoints of carbohydrate hydroxyls using theta-electrospray emitters. *Analyst* 145 (8): 3056-3063.

Kim, H. J., Liyanage, O. T., Mulenos, M. R. and Gallagher, E. S. 2018. Mass spectral detection of forward- and reverse-hydrogen/deuterium exchange resulting from residual solvent vapors in electrospray sources. *J Am Soc Mass Spectrom* 29 (10): 2030-2040.

Kjeldsen, F., Haselmann, K. F., Budnik, B. A., Jensen, F. and Zubarev, R. A. 2002. Dissociative capture of hot (3–13 eV) electrons by polypeptide polycations: an efficient process accompanied by secondary fragmentation. *Chem Phys Lett* 356 (3): 201-206.

Kleckner, I. R. and Foster, M. P. 2011. An introduction to NMR-based approaches for measuring protein dynamics. *Biochim Biophys Acta* 1814 (8): 942-968.

Knochenmuss, R. 2002. A quantitative model of ultraviolet matrix-assisted laser desorption/ionization. *J Mass Spectrom* 37 (8): 867-877.

Knochenmuss, R. 2003. A quantitative model of ultraviolet matrix-assisted laser desorption/ionization including analyte ion generation. *Anal Chem* 75 (10): 2199-2207.

Knochenmuss, R. 2016. The coupled chemical and physical dynamics model of MALDI. *Annu Rev Anal Chem (Palo Alto Calif)* 9 (1): 365-385.

Kohler, M. and Leary, J. A. 1995. LC/MS/MS of carbohydrates with postcolumn addition of metal chlorides using triaxial electrospray probe. *Anal Chem* 67 (19): 3501-3508.

Konermann, L., Ahadi, E., Rodriguez, A. D. and Vahidi, S. 2013. Unraveling the mechanism of electrospray ionization. *Anal Chem* 85 (1): 2-9.

Konermann, L., Pan, J. and Liu, Y. H. 2011. Hydrogen exchange mass spectrometry for studying protein structure and dynamics. *Chem Soc Rev* 40 (3): 1224-1234.

König, S. and Leary, J. A. 1998. Evidence for linkage position determination in cobalt coordinated pentasaccharides using ion trap mass spectrometry. *J Am Soc Mass Spectrom 9* (11): 1125-1134.

Kostyukevich, Y., Kononikhin, A., Popov, I. and Nikolaev, E. 2013. Simple atmospheric hydrogen/deuterium exchange method for enumeration of labile hydrogens by electrospray ionization mass spectrometry. *Anal Chem 85* (11): 5330-5334.

Kostyukevich, Y., Kononikhin, A., Popov, I. and Nikolaev, E. 2014. In-ESI source hydrogen/deuterium exchange of carbohydrate ions. *Anal Chem* 86 (5): 2595-2600.

Kostyukevich, Y., Kononikhin, A., Popov, I. and Nikolaev, E. 2015. Conformations of cationized linear oligosaccharides revealed by FTMS combined with in-ESI H/D exchange. *J Mass Spectrom* 50 (10): 1150-1156.

Lai, Y. H. and Wang, Y. S. 2017. Matrix-assisted laser desorption/ionization mass spectrometry: mechanistic studies and methods for improving the structural identification of carbohydrates. *Mass Spectrom (Tokyo)* 6 (Spec Iss 2): S0072.

Laine, R. A. 1994. Invited Commentary: A calculation of all possible oligosaccharide isomers both branched and linear yields 1.05×1012 structures for a reducing hexasaccharide: the Isomer Barrier to development of single-method saccharide sequencing or synthesis systems. *Glycobiology* 4 (6): 759-767. Lancaster, K. S., An, H. J., Li, B. and Lebrilla, C. B. 2006. Interrogation of N-linked oligosaccharides using infrared multiphoton dissociation in FT-ICR mass spectrometry. *Anal Chem* 78 (14): 4990-4997. Le Pendu, J., Nystrom, K. and Ruvoen-Clouet, N. 2014. Host-pathogen co-evolution and glycan interactions. *Curr Opin Virol* 7: 88-94.

Leach, F. E., 3rd, Riley, N. M., Westphall, M. S., Coon, J. J. and Amster, I. J. 2017. Negative electron transfer dissociation sequencing of increasingly sulfated glycosaminoglycan oligosaccharides on an orbitrap mass spectrometer. *J Am Soc Mass Spectrom* 28 (9): 1844-1854.

Leach, F. E., 3rd, Wolff, J. J., Xiao, Z., Ly, M., Laremore, T. N., Arungundram, S., Al-Mafraji, K., Venot, A., Boons, G. J., Linhardt, R. J. and Amster, I. J. 2011. Negative electron transfer dissociation Fourier transform mass spectrometry of glycosaminoglycan carbohydrates. *Eur J Mass Spectrom* (Chichester) 17 (2): 167-176.

Leavell, M. D. and Leary, J. A. 2001. Stabilization and linkage analysis of metal-ligated sialic acid containing oligosaccharides. *J Am Soc Mass Spectrom* 12 (5): 528-536.

Ledvina, A. R., McAlister, G. C., Gardner, M. W., Smith, S. I., Madsen, J. A., Schwartz, J. C., Stafford, G. C., Jr., Syka, J. E., Brodbelt, J. S. and Coon, J. J. 2009. Infrared photoactivation reduces peptide folding and hydrogen-atom migration following ETD tandem mass spectrometry. *Angew Chem Int Ed Engl* 48 (45): 8526-8528.

Lee, C., Lu, I. C., Hsu, H. C., Lin, H. Y., Liang, S. P., Lee, Y. T. and Ni, C. K. 2016. Formation of metal-related ions in matrix-assisted laser desorption ionization. *J Am Soc Mass Spectrom* 27 (9): 1491-1498. Lee, S., Valentine, S. J., Reilly, J. P. and Clemmer, D. E. 2012. Analyzing a mixture of disaccharides by IMS-VUVPD-MS. *Int J Mass Spectrom* 309: 161-167.

Lemaire, J., Boissel, P., Heninger, M., Mauclaire, G., Bellec, G., Mestdagh, H., Simon, A., Caer, S. L., Ortega, J. M., Glotin, F. and Maitre, P. 2002. Gas phase infrared spectroscopy of selectively prepared ions. *Phys Rev Lett* 89 (27): 273002.

Lemoine, J., Chirat, F. and Domon, B. 1996. Structural analysis of derivatized oligosaccharides using post-source decay matrix-assisted laser desorption/ionization mass spectrometry. *J Mass Spectrom* 31 (8): 908-912.

Leymarie, N., Costello, C. E. and O'Connor, P. B. 2003. Electron capture dissociation initiates a free radical reaction cascade. *J Am Chem Soc* 125 (29): 8949-8958.

Li, B., Russell, S. C., Zhang, J., Hedrick, J. L. and Lebrilla, C. B. 2011. Structure determination by MALDI-IRMPD mass spectrometry and exoglycosidase digestions of *O*-linked oligosaccharides from *Xenopus borealis* egg jelly. *Glycobiology* 21 (7): 877-894.

Linderstrom-Lang, K. 1958. Deuterium exchange and protein structure. *Symposium on Protein Structure* (Albert Neuberger, editor, Methuen & Co. Ltd.), Paris, 1957–9: 23-34.

Liu, H. and Håkansson, K. 2011. Electron capture dissociation of divalent metal-adducted sulfated oligosaccharides. *Int J Mass Spectrom* 305 (2-3): 170-177.

Liu, J. and McLuckey, S. A. 2012. Electron transfer dissociation: effects of cation charge state on product partitioning in ion/ion electron transfer to multiply protonated polypeptides. *Int J Mass Spectrom* 330-332: 174-181.

Liyanage, O. T., Brantley, M. R., Calixte, E. I., Solouki, T., Shuford, K. L. and Gallagher, E. S. 2019. Characterization of electrospray ionization (ESI) parameters on in-ESI hydrogen/deuterium exchange of carbohydrate-metal ion adducts. *J Am Soc Mass Spectrom* 30 (2): 235-247.

Liyanage, O. T., Quintero, A. V., Hatvany, J. B. and Gallagher, E. S. 2021. Distinguishing carbohydrate isomers with rapid hydrogen/deuterium exchange-mass spectrometry. *J Am Soc Mass Spectrom* 32 (1): 152-156.

Lord Rayleigh 1882. XX. On the equilibrium of liquid conducting masses charged with electricity. *Philos Mag 14* (87): 184-186.

Marchand, A., Livet, S., Rosu, F. and Gabelica, V. 2017. Drift tube ion mobility: how to reconstruct collision cross section distributions from arrival time distributions? *Anal Chem 89* (23): 12674-12681. Masellis, C., Khanal, N., Kamrath, M. Z., Clemmer, D. E. and Rizzo, T. R. 2017. Cryogenic vibrational spectroscopy provides unique fingerprints for glycan identification. *J Am Soc Mass Spectrom 28* (10): 2217-2222.

May, J. C., Leaptrot, K. L., Rose, B. S., Moser, K. L. W., Deng, L., Maxon, L., DeBord, D. and McLean, J. A. 2021. Resolving power and collision cross section measurement accuracy of a prototype high-resolution ion mobility platform incorporating structures for lossless ion manipulation. *J Am Soc Mass Spectrom* 32 (4): 1126–1137.

McLafferty, F. W., Bente, P. F., Kornfeld, R., Tsai, S.-C. and Howe, I. 1973. Metastable ion characteristics. XXII. Collisional activation spectra of organic ions. *J Am Chem Soc* 95 (7): 2120-2129.

McLafferty, F. W. and Schuddemage, H. D. R. 1969. Minimization of rearrangement reactions in mass spectra by use of collisional activation. *J Am Chem Soc* 91 (7): 1866-1868.

McLuckey, S. A. and Goeringer, D. E. 1997. Slow heating methods in tandem mass spectrometry. *J Mass Spectrom* 32 (5): 461-474.

Mechref, Y. and Novotny, M. V. 2002. Structural Investigations of Glycoconjugates at High Sensitivity. *Chem Rev* 102 (2): 321-370.

Mentinova, M., Crizer, D. M., Baba, T., McGee, W. M., Glish, G. L. and McLuckey, S. A. 2013. Cation recombination energy/coulomb repulsion effects in ETD/ECD as revealed by variation of charge per residue at fixed total charge. *J Am Soc Mass Spectrom* 24 (11): 1676-1689.

Michelmann, K., Silveira, J. A., Ridgeway, M. E. and Park, M. A. 2015. Fundamentals of trapped ion mobility spectrometry. *J Am Soc Mass Spectrom* 26 (1): 14-24.

Mitchell Wells, J. and McLuckey, S. A. (2005). Collision-induced dissociation (CID) of peptides and proteins. In: *Methods Enzymol*. (ed. A. L. Burlingame), 148-185. San Diego, CA: Elsevier Inc.

Mohr, M. D., Börnsen, K. O. and Widmer, H. M. 1995. Matrix-assisted laser desorption/ionization mass spectrometry: Improved matrix for oligosaccharides. *Rapid Commun Mass Spectrom* 9 (9): 809-814.

Mookherjee, A., Uppal, S. S. and Guttman, M. 2018. Dissection of fragmentation pathways in protonated *N*-acetylhexosamines. *Anal Chem 90* (20): 11883-11891.

Mookherjee, A., Uppal, S. S., Murphree, T. A. and Guttman, M. 2020. Linkage memory in underivatized protonated carbohydrates. *J Am Soc Mass Spectrom* 32 (2): 581–589.

Morelle, W., Slomianny, M. C., Diemer, H., Schaeffer, C., van Dorsselaer, A. and Michalski, J. C. 2004. Fragmentation characteristics of permethylated oligosaccharides using a matrix-assisted laser desorption/ionization two-stage time-of-flight (TOF/TOF) tandem mass spectrometer. *Rapid Commun Mass Spectrom* 18 (22): 2637-2649.

Morrison, K. A., Bendiak, B. K. and Clowers, B. H. 2017a. Enhanced mixture separations of metal adducted tetrasaccharides using frequency encoded ion mobility separations and tandem mass Spectrometry. *J Am Soc Mass Spectrom* 28 (4): 664-677.

Morrison, K. A., Bendiak, B. K. and Clowers, B. H. 2018. Assessment of dimeric metal-glycan adducts via isotopic labeling and ion mobility-mass spectrometry. *J Am Soc Mass Spectrom* 29 (8): 1638-1649. Morrison, K. A. and Clowers, B. H. 2017. Differential fragmentation of mobility-selected glycans via ultraviolet photodissociation and ion mobility-mass spectrometry. *J Am Soc Mass Spectrom* 28 (6): 1236-1241.

Mucha, E., Gonzalez Florez, A. I., Marianski, M., Thomas, D. A., Hoffmann, W., Struwe, W. B., Hahm, H. S., Gewinner, S., Schollkopf, W., Seeberger, P. H., von Helden, G. and Pagel, K. 2017. Glycan fingerprinting via cold-ion infrared spectroscopy. *Angew Chem Int Ed Engl 56* (37): 11248-11251.

Mucha, E., Lettow, M., Marianski, M., Thomas, D. A., Struwe, W. B., Harvey, D. J., Meijer, G., Seeberger, P. H., von Helden, G. and Pagel, K. 2018. Fucose migration in intact protonated glycan ions: a universal phenomenon in mass spectrometry. *Angew Chem Int Ed Engl 57* (25): 7440-7443.

Mucha, E., Stuckmann, A., Marianski, M., Struwe, W. B., Meijer, G. and Pagel, K. 2019. In-depth structural analysis of glycans in the gas phase. *Chem Sci 10* (5): 1272-1284.

Nagy, G., Attah, I. K., Garimella, S. V. B., Tang, K., Ibrahim, Y. M., Baker, E. S. and Smith, R. D. 2018. Unraveling the isomeric heterogeneity of glycans: ion mobility separations in structures for lossless ion manipulations. *Chem Commun (Camb)* 54 (83): 11701-11704.

Naven, T. J. P. and Harvey, D. J. 1996. Effect of structure on the signal strength of oligosaccharides in matrix-assisted laser desorption/ionization mass spectrometry on time-of-flight and magnetic sector instruments. *Rapid Commun Mass Spectrom* 10 (11): 1361-1366.

Nicolardi, S., Joseph, A. A., Zhu, Q., Shen, Z., Pardo-Vargas, A., Chiodo, F., Molinaro, A., Silipo, A., van der Burgt, Y. E. M., Yu, B., Seeberger, P. H. and Wuhrer, M. 2021. Analysis of synthetic monodisperse polysaccharides by wide mass range ultrahigh-resolution MALDI mass spectrometry. *Anal Chem* 93 (10): 4666-4675.

Nielsen, M. L., Budnik, B. A., Haselmann, K. F., Olsen, J. V. and Zubarev, R. A. 2000. Intramolecular hydrogen atom transfer in hydrogen-deficient polypeptide radical cations. *Chem Phys Lett* 330 (5): 558-562.

Nishikaze, T. 2019. Sialic acid derivatization for glycan analysis by mass spectrometry. *Proc Jpn Acad Ser B Phys Biol Sci* 95 (9): 523-537.

Oepts, D., Van Der Meer, A. F. G. and Van Amersfoort, P. W. 1995. The free-electron-laser user facility FELIX. *Infrared Phys Technol* 36 (1): 297-308.

Okamoto, M., Takahashi, K.-i., Doi, T. and Takimoto, Y. 1997. High-sensitivity detection and postsource decay of 2-aminopyridine-derivatized oligosaccharides with matrix-assisted laser desorption/ionization mass spectrometry. *Anal Chem.* 69 (15): 2919-2926.

Ollivier, S., Fanuel, M., Rogniaux, H. and Ropartz, D. 2021a. Molecular networking of high-resolution tandem ion mobility spectra: a structurally relevant way of organizing data in glycomics? *Anal Chem 93* (31): 10871–10878.

Ollivier, S., Tarquis, L., Fanuel, M., Li, A., Durand, J., Laville, E., Potocki-Veronese, G., Ropartz, D. and Rogniaux, H. 2021. Anomeric retention of carbohydrates in multistage cyclic ion mobility (IMSⁿ): de novo structural elucidation of enzymatically produced mannosides. *Anal Chem 93* (15): 6254-6261. Pearson, W. L., 3rd, Contreras, C., Powell, D., Berden, G., Oomens, J., Bendiak, B. and Eyler, J. R. 2015. Differentiation of rubidiated methyl-D-glycoside stereoisomers by infrared multiple-photon dissociation spectroscopy in the O-H and C-H stretching regions. *J Phys Chem B 119* (41): 12970-12981. Pellegrinelli, R. P., Yue, L., Carrascosa, E., Warnke, S., Ben Faleh, A. and Rizzo, T. R. 2020. How general is anomeric retention during collision-induced dissociation of glycans? *J Am Chem Soc 142* (13): 5948–5951.

Peng, W., Gutierrez Reyes, C. D., Gautam, S., Yu, A., Cho, B. G., Goli, M., Donohoo, K., Mondello, S., Kobeissy, F. and Mechref, Y. (accepted for publication). MS-based glycomics and glycoproteomics methods enabling isomeric characterization. *Mass Spectrom Rev*.

Peterson, T. L. and Nagy, G. 2021. Toward sequencing the human milk glycome: high-resolution cyclic ion mobility separations of core human milk oligosaccharide building blocks. *Anal Chem 93* (27): 9397–9407.

Polfer, N. C., Valle, J. J., Moore, D. T., Oomens, J., Eyler, J. R. and Bendiak, B. 2006. Differentiation of isomers by wavelength-tunable infrared multiple-photon dissociation-mass spectrometry: application to glucose-containing disaccharides. *Anal Chem* 78 (3): 670-679.

Powell, A. K. and Harvey, D. J. 1996. Stabilization of sialic acids in *N*-linked oligosaccharides and gangliosides for analysis by positive ion matrix-assisted laser desorption/ionization mass spectrometry. *Rapid Commun Mass Spectrom* 10 (9): 1027-1032.

Prien, J. M., Ashline, D. J., Lapadula, A. J., Zhang, H. and Reinhold, V. N. 2009. The high mannose glycans from bovine ribonuclease B isomer characterization by ion trap MS. *J Am Soc Mass Spectrom* 20 (4): 539-556.

Przybylski, C. and Bonnet, V. 2013. Discrimination of cyclic and linear oligosaccharides by tandem mass spectrometry using collision-induced dissociation (CID), pulsed-Q-dissociation (PQD) and the higher-energy C-trap dissociation modes. *Rapid Commun Mass Spectrom* 27 (1): 75-87.

Pu, Y., Ridgeway, M. E., Glaskin, R. S., Park, M. A., Costello, C. E. and Lin, C. 2016. Separation and identification of isomeric glycans by selected accumulation-trapped ion mobility spectrometry-electron activated dissociation tandem mass spectrometry. *Anal Chem* 88 (7): 3440-3443.

Rabus, J. M., Abutokaikah, M. T., Ross, R. T. and Bythell, B. J. 2017. Sodium-cationized carbohydrate gas-phase fragmentation chemistry: influence of glycosidic linkage position. *Phys Chem Chem Phys* 19 (37): 25643-25652.

Rabus, J. M., Pellegrinelli, R. P., Khodr, A. H. A., Bythell, B. J., Rizzo, T. R. and Carrascosa, E. 2021. Unravelling the structures of sodiated β-cyclodextrin and its fragments. *Phys Chem Chem Phys* 23 (24): 13714-13723.

Revercomb, H. E. and Mason, E. A. 1975. Theory of plasma chromatography/gaseous electrophoresis. *Anal Chem* 47 (7): 970-983.

Richardson, K., Langridge, D., Dixit, S. M. and Ruotolo, B. T. 2021. An improved calibration approach for traveling wave ion mobility spectrometry: robust, high-precision collision cross sections. *Anal Chem 93* (7): 3542-3550.

Richardson, K., Langridge, D. and Giles, K. 2018. Fundamentals of travelling wave ion mobility revisited: I. Smoothly moving waves. *Int J Mass Spectrom* 428: 71-80.

Ridgeway, M. E., Lubeck, M., Jordens, J., Mann, M. and Park, M. A. 2018. Trapped ion mobility spectrometry: A short review. *Int J Mass Spectrom* 425: 22-35.

Rondeau, P., Sers, S., Jhurry, D. and Cadet, F. 2003. Sugar interaction with metals in aqueous solution: indirect determination from infrared and direct determination from nuclear magnetic resonance spectroscopy. *Appl Spectrosc* 57 (4): 466-472.

Sans, M., Feider, C. L. and Eberlin, L. S. 2018. Advances in mass spectrometry imaging coupled to ion mobility spectrometry for enhanced imaging of biological tissues. *Curr Opin Chem Biol* 42: 138-146. Sasiene, Z. J., Ropartz, D., Rogniaux, H. and Jackson, G. P. 2021. Charge transfer dissociation of a branched glycan with alkali- and alkaline earth metal adducts. *J Mass Spectrom* 56 (7): e4774. Schaller-Duke, R. M. (2019). Electron transfer dissociation and collision-induced dissociation mass spectrometry of metallated oligosaccharides. Doctor of Philosophy Dissertation. The University of Alabama.

Schaller-Duke, R. M., Bogala, M. R. and Cassady, C. J. 2018. Electron transfer dissociation and collision-induced dissociation of underivatized metallated oligosaccharides. *J Am Soc Mass Spectrom* 29 (5): 1021-1035.

Schindler, B., Barnes, L., Renois, G., Gray, C., Chambert, S., Fort, S., Flitsch, S., Loison, C., Allouche, A. R. and Compagnon, I. 2017. Anomeric memory of the glycosidic bond upon fragmentation and its consequences for carbohydrate sequencing. *Nat Commun* 8 (1): 973.

Schindler, B., Laloy-Borgna, G., Barnes, L., Allouche, A. R., Bouju, E., Dugas, V., Demesmay, C. and Compagnon, I. 2018. Online separation and identification of isomers using infrared multiple photon dissociation ion spectroscopy coupled to liquid chromatography: application to the analysis of disaccharides regio-isomers and monosaccharide anomers. *Anal Chem 90* (20): 11741-11745. Shannon, R. D. 1976. Revised effective ionic radii and systematic studies of interatomic distances in

halides and chalcogenides. Acta Crystallogr A 32 (5): 751-767.

Shaw, J. B., Li, W., Holden, D. D., Zhang, Y., Griep-Raming, J., Fellers, R. T., Early, B. P., Thomas, P. M., Kelleher, N. L. and Brodbelt, J. S. 2013. Complete protein characterization using top-down mass spectrometry and ultraviolet photodissociation. *J Am Chem Soc* 135 (34): 12646-12651.

Sheeley, D. M. and Reinhold, V. N. 1998. Structural characterization of carbohydrate sequence, linkage, and branching in a quadrupole ion trap mass spectrometer: neutral oligosaccharides and N-linked glycans. *Anal Chem* 70 (14): 3053-3059.

Shvartsburg, A. A. and Smith, R. D. 2008. Fundamentals of traveling wave ion mobility spectrometry. *Anal Chem* 80 (24): 9689-9699.

Sible, E. M., Brimmer, S. P. and Leary, J. A. 1997. Interaction of first row transition metals with α1-3, α1-6 mannotriose and conserved trimannosyl core oligosaccharides: A comparative electrospray ionization study of doubly and singly charged complexes. *J Am Soc Mass Spectrom* 8 (1): 32-42.

Siems, W. F., Wu, C., Tarver, E. E., Hill, H. H., Jr., Larsen, P. R. and McMinn, D. G. 1994. Measuring the resolving power of ion mobility spectrometers. *Anal Chem* 66 (23): 4195-4201.

Smolarek, S., Brauer, N. B., Buma, W. J. and Drabbels, M. 2010. IR spectroscopy of molecular ions by nonthermal ion ejection from helium nanodroplets. *J Am Chem Soc* 132 (40): 14086-14091.

Solouki, T., Reinhold, B. B., Costello, C. E., O'Malley, M., Guan, S. and Marshall, A. G. 1998.

Electrospray ionization and matrix-assisted laser desorption/ionization fourier transform ion cyclotron resonance mass spectrometry of permethylated oligosaccharides. *Anal Chem* 70 (5): 857-864.

Spengler, B., Kirsch, D., Kaufmann, R. and Lemoine, J. 1994. Structure analysis of branched oligosaccharides using post-source decay in matrix-assisted laser desorption ionization mass spectrometry. *J Mass Spectrom* 29 (12): 782-787.

Stahl, B., Steup, M., Karas, M. and Hillenkamp, F. 1991. Analysis of neutral oligosaccharides by matrix-assisted laser desorption ionization mass spectrometry. *Anal Chem* 63 (14): 1463-1466.

Stephenson, J. L. and McLuckey, S. A. 1996. Ion/ion reactions in the gas phase: proton transfer reactions involving multiply-charged proteins. *J Am Chem Soc* 118 (31): 7390-7397.

Struwe, W. B., Baldauf, C., Hofmann, J., Rudd, P. M. and Pagel, K. 2016. Ion mobility separation of deprotonated oligosaccharide isomers - evidence for gas-phase charge migration. *Chem Commun (Camb)* 52 (83): 12353-12356.

Swanson, K. D., Spencer, S. E. and Glish, G. L. 2017. Metal cationization extractive electrospray ionization mass spectrometry of compounds containing multiple oxygens. *J Am Soc Mass Spectrom* 28 (6): 1030-1035.

Syka, J. E. P., Coon, J. J., Schroeder, M. J., Shabanowitz, J. and Hunt, D. F. 2004. Peptide and protein sequence analysis by electron transfer dissociation mass spectrometry. *PNAS* 101 (26): 9528-9533.

Tan, Y., Zhao, N., Liu, J., Li, P., Stedwell, C. N., Yu, L. and Polfer, N. C. 2017. Vibrational signatures of isomeric lithiated N-acetyl-D-hexosamines by gas-phase infrared multiple-photon dissociation (IRMPD) spectroscopy. *J Am Soc Mass Spectrom* 28 (3): 539-550.

Tanaka, K., Waki, H., Ido, Y., Akita, S., Yoshida, Y., Yoshida, T. and Matsuo, T. 1988. Protein and polymer analyses up to m/z 100 000 by laser ionization time-of-flight mass spectrometry. *Rapid Commun Mass Spectrom* 2 (8): 151-153.

Tang, Y., Wei, J., Costello, C. E. and Lin, C. 2018. Characterization of isomeric glycans by reversed phase liquid chromatography-electronic excitation dissociation tandem mass spectrometry. *J Am Soc Mass Spectrom* 29 (6): 1295-1307.

Taylor, C. J., Burke, R. M., Wu, B., Panja, S., Nielsen, S. B. and Dessent, C. E. H. 2009. Structural characterization of negatively charged glycosaminoglycans using high-energy (50–150keV) collisional activation. *Int J Mass Spectrom* 285 (1-2): 70-77.

Thompson, M. S., Cui, W. and Reilly, J. P. 2004. Fragmentation of singly charged peptide ions by photodissociation at λ =157 nm. *Angew Chem Int Ed Engl 43* (36): 4791-4794.

Tolmachev, A. V., Webb, I. K., Ibrahim, Y. M., Garimella, S. V. B., Zhang, X., Anderson, G. A. and Smith, R. D. 2014. Characterization of ion dynamics in structures for lossless ion manipulations. *Anal Chem* 86 (18): 9162-9168.

Ujma, J., Ropartz, D., Giles, K., Richardson, K., Langridge, D., Wildgoose, J., Green, M. and Pringle, S. 2019. Cyclic ion mobility mass spectrometry distinguishes anomers and open-ring forms of pentasaccharides. *J Am Soc Mass Spectrom* 30 (6): 1028-1037.

Uppal, S. S., Beasley, S. E., Scian, M. and Guttman, M. 2017. Gas-phase hydrogen/deuterium exchange for distinguishing isomeric carbohydrate Ions. *Anal Chem* 89 (8): 4737-4742.

Valle, J. J. (2005). Differentiation of carbohydrate stereoisomers by infrared multiple photon dissociation using a free electron laser and a Fourier transform ion cyclotron resonance mass spectrometer. Doctor of Philosophy Dissertation. University of Florida.

Varki, A., Kannagi, R., Toole, B. and Stanley, P. (2015). Glycosylation changes in cancer. In: *Essentials of Glycobiology*. (ed. A. Varki, R. D. Cummings, J. D. Esko, P. Stanley, G. W. Hart, M. Aebi, A. G. Darvill, T. Kinoshita, N. H. Packer, J. H. Prestegard, R. L. Schnaar and P. H. Seeberger), New York: Cold Spring Harbor Laboratory Press.

Vliegenthart, J. F. G., Dorland, L. and van Halbeek, H. 1983. High-resolution, ¹H-nuclear magnetic resonance spectroscopy as a tool in the structural analysis of carbohydrates related to glycoproteins. *Adv Carbohydr Chem Biochem* 41: 209-374.

Wales, T. E. and Engen, J. R. 2006. Hydrogen exchange mass spectrometry for the analysis of protein dynamics. *Mass Spectrom Rev* 25 (1): 158-170.

Warnke, S., Ben Faleh, A. and Rizzo, T. R. 2021. Toward high-throughput cryogenic IR fingerprinting of mobility-separated glycan isomers. *ACS Meas Sci Au* 1 (3): 157–164.

Warnke, S., Ben Faleh, A., Scutelnic, V. and Rizzo, T. R. 2019. Separation and identification of glycan anomers using ultrahigh-resolution ion-mobility spectrometry and cryogenic ion spectroscopy. *J Am Soc Mass Spectrom* 30 (11): 2204-2211.

Webb, I. K., Garimella, S. V., Norheim, R. V., Baker, E. S., Ibrahim, Y. M. and Smith, R. D. 2016. A structures for lossless ion manipulations (SLIM) module for collision induced dissociation. *J Am Soc Mass Spectrom* 27 (7): 1285-1288.

Wei, J., Tang, Y., Bai, Y., Zaia, J., Costello, C. E., Hong, P. and Lin, C. 2020. Toward automatic and comprehensive glycan characterization by online PGC-LC-EED MS/MS. *Anal Chem 92* (1): 782-791. Weiskopf, A. S., Vouros, P. and Harvey, D. J. 1997. Characterization of oligosaccharide composition and structure by quadrupole ion trap mass spectrometry. *Rapid Commun Mass Spectrom 11* (14): 1493-1504. Weiskopf, A. S., Vouros, P. and Harvey, D. J. 1998. Electrospray ionization-ion trap mass spectrometry for structural analysis of complex N-linked glycoprotein oligosaccharides. *Anal Chem 70* (20): 4441-4447.

Williams, J. P., Grabenauer, M., Holland, R. J., Carpenter, C. J., Wormald, M. R., Giles, K., Harvey, D. J., Bateman, R. H., Scrivens, J. H. and Bowers, M. T. 2010. Characterization of simple isomeric oligosaccharides and the rapid separation of glycan mixtures by ion mobility mass spectrometry. *Int J Mass Spectrom* 298 (1): 119-127.

Williamson, D. L., Bergman, A. E. and Nagy, G. 2021. Investigating the structure of alpha/beta carbohydrate linkage isomers as a function of group I metal adduction and degree of polymerization as revealed by cyclic ion mobility separations. *J Am Soc Mass Spectrom* 32 (10): 2573–2582.

Wilson, J. J. and Brodbelt, J. S. 2008. Ultraviolet photodissociation at 355 nm of fluorescently labeled oligosaccharides. *Anal Chem* 80 (13): 5186-5196.

Wolff, J. J., Laremore, T. N., Busch, A. M., Linhardt, R. J. and Amster, I. J. 2008. Influence of charge state and sodium cationization on the electron detachment dissociation and infrared multiphoton dissociation of glycosaminoglycan oligosaccharides. *J Am Soc Mass Spectrom* 19 (6): 790-798.

Wolff, J. J., Leach, F. E., Laremore, T. N., Kaplan, D. A., Easterling, M. L., Linhardt, R. J. and Amster, I.

Wong, H. K., Chen, X., Wu, R., Wong, Y. E., Hung, Y. W. and Chan, T. D. 2022. Dissociation of mannose-rich glycans using collision-based and electron-based ion activation methods. *J Am Soc Mass Spectrom* 33 (5): 803-812.

J. 2010. Negative electron transfer dissociation of glycosaminoglycans. Anal Chem 82 (9): 3460-3466.

Woodin, R. L., Bomse, D. S. and Beauchamp, J. L. 1978. Multiphoton dissociation of molecules with low power continuous wave infrared laser radiation. *J Am Chem Soc* 100 (10): 3248-3250.

Woods, R. J. 2018. Predicting the structures of glycans, glycoproteins, and their complexes. *Chem Rev* 118 (17): 8005-8024.

Wormald, M. R., Petrescu, A. J., Pao, Y.-L., Glithero, A., Elliott, T. and Dwek, R. A. 2002. Conformational studies of oligosaccharides and glycopeptides: complementarity of NMR, X-ray crystallography, and molecular modelling. *Chem Rev* 102 (2): 371-386.

Wuhrer, M., Koeleman, C. A. M., Hokke, C. H. and Deelder, A. M. 2006. Mass spectrometry of proton adducts of fucosylated N-glycans: fucose transfer between antennae gives rise to misleading fragments. *Rapid Commun Mass Spectrom* 20 (11): 1747-1754.

Xie, C., Li, L., Wu, Q., Guan, P., Wang, C., Yu, J. and Tang, K. 2021. Effective separation of carbohydrate isomers using metal cation and halogen anion complexes in trapped ion mobility spectrometry. *Talanta* 225: 121903.

Xie, C., Wu, Q., Zhang, S., Wang, C., Gao, W., Yu, J. and Tang, K. 2020. Improving glycan isomeric separation via metal ion incorporation for drift tube ion mobility-mass spectrometry. *Talanta 211*: 120719.

Yalovenko, N., Yatsyna, V., Bansal, P., AbiKhodr, A. H. and Rizzo, T. R. 2020. Analyzing glycans cleaved from a biotherapeutic protein using ultrahigh-resolution ion mobility spectrometry together with cryogenic ion spectroscopy. *Analyst* 145 (20): 6493-6499.

Yamashita, M. and Fenn, J. B. 1984. Electrospray ion source. Another variation on the free-jet theme. *J Phys Chem* 88 (20): 4451-4459.

Yeni, O., Schindler, B., Moge, B. and Compagnon, I. 2022. Rapid IRMPD (InfraRed multiple photon dissociation) analysis for glycomics. *Analyst* 147 (2): 312-317.

Yu, X., Huang, Y., Lin, C. and Costello, C. E. 2012. Energy-dependent electron activated dissociation of metal-adducted permethylated oligosaccharides. *Anal Chem* 84 (17): 7487-7494.

Yu, X., Jiang, Y., Chen, Y., Huang, Y., Costello, C. E. and Lin, C. 2013. Detailed glycan structural characterization by electronic excitation dissociation. *Anal Chem* 85 (21): 10017-10021.

Zabuga, A. V., Kamrath, M. Z., Boyarkin, O. V. and Rizzo, T. R. 2014. Fragmentation mechanism of UV-excited peptides in the gas phase. *J Chem Phys* 141 (15): 154309.

Zaia, J. 2004. Mass spectrometry of oligosaccharides. Mass Spectrom Rev 23 (3): 161-227.

Zaia, J. 2005. Principles of mass spectrometry of glycosaminoglycans. *J Biomacromol Mass Spectrom 1* (1): 3-36.

Zaia, J. and Costello, C. E. 2003. Tandem mass spectrometry of sulfated heparin-like glycosaminoglycan oligosaccharides. *Anal Chem* 75 (10): 2445-2455.

Zenobi, R. and Knochenmuss, R. 1998. Ion formation in MALDI mass spectrometry. *Mass Spectrom Rev* 17 (5): 337-366.

Zhang, J. and Brodbelt, J. S. 2004. Gas-phase hydrogen/deuterium exchange and conformations of deprotonated flavonoids and gas-phase acidities of flavonoids. *J Am Chem Soc* 126 (18): 5906-5919. Zhang, J., Schubothe, K., Li, B., Russell, S. and Lebrilla, C. B. 2005. Infrared multiphoton dissociation of

O-linked mucin-type oligosaccharides. *Anal Chem* 77 (1): 208-214.

Zhao, C., Xie, B., Chan, S.-Y., Costello, C. E. and O'Connor, P. B. 2008. Collisionally activated dissociation and electron capture dissociation provide complementary structural information for branched permethylated oligosaccharides. *J Am Soc Mass Spectrom* 19 (1): 138-150.

Zheng, X., Zhang, X., Schocker, N. S., Renslow, R. S., Orton, D. J., Khamsi, J., Ashmus, R. A., Almeida, I. C., Tang, K., Costello, C. E., Smith, R. D., Michael, K. and Baker, E. S. 2017. Enhancing glycan isomer separations with metal ions and positive and negative polarity ion mobility spectrometry-mass spectrometry analyses. *Anal Bioanal Chem* 409 (2): 467-476.

Zherebker, A., Kostyukevich, Y., Kononikhin, A., Roznyatovsky, V. A., Popov, I., Grishin, Y. K., Perminova, I. V. and Nikolaev, E. 2016. High desolvation temperature facilitates the ESI-source H/D exchange at non-labile sites of hydroxybenzoic acids and aromatic amino acids. *Analyst (Cambridge, U. K.)* 141 (8): 2426-2434.

Zhu, F., Glover, M. S., Shi, H., Trinidad, J. C. and Clemmer, D. E. 2015. Populations of metal-glycan structures influence MS fragmentation patterns. *J Am Soc Mass Spectrom* 26 (1): 25-35.

Zhurov, K. O., Fornelli, L., Wodrich, M. D., Laskay, U. A. and Tsybin, Y. O. 2013. Principles of electron capture and transfer dissociation mass spectrometry applied to peptide and protein structure analysis.

Chem Soc Rev. 42 (12): 5014-5030.

Zubarev, R. A. 2003. Reactions of polypeptide ions with electrons in the gas phase. *Mass Spectrom Rev* 22 (1): 57-77.

Zubarev, R. A., Kelleher, N. L. and McLafferty, F. W. 1998. Electron capture dissociation of multiply charged protein cations. a nonergodic process. *J Am Chem Soc* 120 (13): 3265-3266.

Zucker, S. M., Lee, S., Webber, N., Valentine, S. J., Reilly, J. P. and Clemmer, D. E. 2011. An ion mobility/ion trap/photodissociation instrument for characterization of ion structure. *J Am Soc Mass Spectrom* 22 (9): 1477-1485.